

Wood Composites Production with Epoxy Resin Substituted Liquefied Lignocellulosic Biomass, and Polymeric Diphenylmethane Diisocyanate Substituted Defatted Soy Flour as Wood Adhesives

by

Osei Asibe Asafu-Adjaye

A dissertation submitted to the Graduate Faculty of
Auburn University
in partial fulfillment of the
requirements for the Degree of

Doctor of Philosophy

Auburn, Alabama
August 8, 2020

Keywords: Fast pyrolysis, hydrothermal liquefaction, Bio-oil, Soy flour, Epoxy resin, Polymeric diphenylmethane diisocyanate, particleboard, oriented strand board, medium density fiberboard

Copyright 2020 by Osei Asibe Asafu-Adjaye

Approved by

Brian K. Via, Chair, Professor, School of Forestry and Wildlife Sciences
Maria L. Auad, Professor, Department of Chemical Engineering
Maria P. Soledad, Associate Professor, School of Forestry and Wildlife Sciences
Sushil Adhikari, Professor, Department of Biosystem Engineering
Terry Liles, PhD, Director of Raw Materials, Huber Engineered Wood, LLC

Abstract

Wood composites such as oriented strand board (OSB), particleboard and medium density fiberboard (MDF) have contributed significantly towards efficient wood utilization. Wood composites are engineered wood products from reconstituted wood materials bonded with thermosetting adhesives under heat and pressure. Currently, synthetic adhesives dominate the wood composites industry. Recent environmental health concerns, sustainability, and price uncertainties of these synthetic adhesives, which are petroleum derived, have engendered efforts to more environmentally friendly, sustainable, and cost-effective bio-based adhesive alternatives. In this study, synthetic adhesives were modified with renewable components to form composite panels taking advantage of the individual binder components.

The first section of this work, chapters 3 and 4, focused on the utilization of bio-oil in epoxy resin modification for binding wood composites. In chapters 3, bio-oil was obtained from fast pyrolysis (FP), and hydrothermal liquefaction (HTL) of loblolly pine biomass. Water/ethanol mixture (1/1, wt/wt) was used as the solvent. The FTIR results revealed that the FP and HTL bio-oils had similar chemical functional groups. However, the gas chromatography–mass spectrometry (GC-MS) analysis indicated variations in the composition of the bio-oils. The study found low ash content of 0.01 wt % and pH of 2.3 ± 0.5 for both FP and HTL bio-oils. The ^{31}P -NMR spectroscopy analysis revealed that the FP and HTL bio-oils were rich in phenolic OH and aliphatic OH functionalities, which could serve as a potential bio-polyol. OSB was manufactured utilizing epoxy, and epoxy modified pyrolysis bio-oil as an adhesive binder in Chapter 4. The results showed that epoxy resin with bio-oil content of 20% showed comparable bonding properties to

that of polymeric diphenylmethane diisocyanate (PMDI). Bio-oil substitution of 20% improved the hydrophobicity of the OSB. The TGA and DSC analysis of the epoxy resins showed improved thermal stability at lower bio-oil substitution levels. It was concluded that epoxy resin amended bio-oil could be a potential adhesive to produce OSB.

The second section delved into the utilization of PMDI and defatted soy flour. In chapter 5 the chemical functionalities of PMDI amended soy was studied via FTIR and the acceptable range of soy flour substitution in PMDI for OSB applications was discussed. Heating PMDI to approximately 40 °C eliminate soy aggregation and reduces viscosity. The production of particle boards to ascertain the contribution of soy flour in increasing the Cold Tack of pMDI resin was discussed in chapter 6. PDMI resin has low tack which limits its application. The soy flour increases the tack of pMDI resin, which increases the surface coverage and the relative bonded area at the glue line. 20% substitution level of soy is a practical maximum because higher levels could lead to excessive cold tack as well as to higher resin viscosity. In chapter 7, CO₂ evolution was used to understand the kinetics of the soy and PMDI during mixing and how different mixing techniques affect the resulting wood composites. It was found that soy chemically interacts with the isocyanate groups of PMDI during mixing. As a result, CO₂ is evolved. Results of partial substitution of pMDI resin by 10-15% soy flour for the manufacture of OSB, improved board properties. For MDF the soy-substituted resin performed as well as the control pMDI. The reaction of soy flour with pMDI occurs over several hours as tracked by CO₂ evolution. Uniform mixing of soy flour with pMDI is critical because unreacted soy flour tends to retain water, which degrades the wet properties of the board.

Acknowledgments

I am indebted to my research advisor, Dr. Brian K. Via, for giving me the opportunity to pursue a doctorate degree. Your industrial experience, help, encouragement, comradeship, and criticism have shaped this work and my career aspirations. Thank you, Dr. Via. I cannot gainsay the invaluable mentorship, encouragement, and insightful experiential contributions of my committee members: Dr. Soledad Peresin, Dr. Sushil Adhikari, Dr. Maria Auad and Dr. Terry Lilies. Thank you all for the reposed confidence you extended to me at my fledgling stage as a research student and uplifting me when I was crestfallen. Dr. Sujit Banerjee, I am grateful for the advice and help provided during this work. Your tutelage helped me analyzed phenomena on varying levels fundamentally and practically, thank you. I am thankful to Dr. Iris Vega Erramuspe, Dr. Jason Street, Dr. Yusuf Celikbag, Dr. George Cheng, and Dr. Farag Ramsis, for their noteworthy assistance, contributions, and submissions in the furtherance of this work.

I would like to express my profound appreciation to all my course tutors, who contributed to the fountain of knowledge I acquired during my classes. I would like to recognize the help I received from my friends, (Alejandro Cardozo; Archana Bensode; Alonso Jose; Celeste Iglesias; Diego Maldonado; Sunjita Wasti; Tawsif Rahman), during this research work and making Auburn a second home. I am exceptionally thankful to Dr. Timothy McDonald for serving as the University Reader for this current dissertation.

Finally, I wish to dedicate this dissertation to Nana Abena Abrafi Gyasi – my best friend, life partner and wife – for her love, support, prayers and encouragement before, during and after this research study. You deserve the most acknowledgment. Thank you for believing in me.

Table of Contents

Abstract	ii
Acknowledgments.....	iv
Table of Contents	v
List of Tables	xii
List of Figures	xiv
List of Abbreviations	xix
Chapter 1 Introduction	1
1.1 Research Plan	3
1.2 Motivation	4
1.3 Dissertation Organization.....	4
1.4 References	6
Chapter 2 Literature Review.....	8
2.1 Oriented Strand Board (OSB)	8
2.2 Manufacturing Process of Oriented strand Board	9
2.3 Particleboard.....	11
2.4 Particle board Classification.....	12
2.5 Particle board Production Process	13
2.6 Medium Density Fiber Board (MDF).....	15
2.7 Medium Density Board Manufacturing.....	16
2.8 Epoxy Resin.....	17
2.8.1 Synthesis of Epoxy Resin	19

2.8.2 Epoxy Resin Application	20
2.9 Bio-oil.....	22
2.9.1 Hydrothermal Liquefaction (HTL)	22
2.9.1.1 Fast pyrolysis.....	26
2.9.1.2 Fast Pyrolysis Mechanisms.....	27
2.10 ³¹ P-NMR	28
2.11 Polymeric diphenyl-methane diisocyanate (pMDI)	30
2.11.1 Polymeric diphenyl-methane diisocyanate (pMDI) Synthesis.....	32
2.11.1.1 Water reaction with PMDI.....	34
2.11.1.2 Hydroxyl reaction with pMDI	35
2.11.1.3 Carboxylic acid.....	36
2.11.1.4 Isocyanate reaction with Phenol	37
2.12 Soy Products.....	37
2.13 Adhesion Theory	42
2.14 Press Theory	46
2.15 References	48
 Chapter 3 Elucidation of the effect of Fast Pyrolysis and Hydrothermal Liquefaction on the Physico-chemical properties of Bio-oil from Loblolly Pine Biomass	 56
3.1 Abstract.....	56
3.2 Introduction	56
3.3 Materials and Methods	59
3.3.1 Materials.....	59
3.3.2 Hydrothermal liquefaction Process.....	60

3.3.3 Separation of HTL Products and Yield Calculation	62
3.3.4 Fast Pyrolysis Process	63
3.3.5 Distillation.....	63
3.3.6 Physical properties analysis of the HTL and FP Bio-oils	65
3.3.7 GC-MS analysis of HTL and FP Bio-oils	65
3.3.8 Thermogravimetric Analysis (TGA).....	66
3.3.9 Hydroxyl (OH) group analysis of HTL and FP bio-oils: 31P-NMR	66
3.3.10 FTIR Analysis of the bio-oils of HTL, and FP Bio-oils	67
3.4 Results and Discussion.....	67
3.4.1 Biomass Characterization.....	67
3.4.2 Fast Pyrolysis and Hydrothermal Liquefaction Product Yield and Characteristics..	68
3.4.3 Bulk properties of fast pyrolysis and hydrothermal liquefaction bio-oil.	70
3.4.4 Viscosity Analysis.....	71
3.4.5 Chemical characteristic of FP and HTL of bio-oils.	73
3.4.6 Thermogravimetric Analysis.....	74
3.4.7 FTIR Analysis	76
3.4.8 Hydroxyl (OH) group analysis of HTL and FP bio-oils: 31P-NMR	78
3.5 Conclusions	80
3.6 Acknowledgements	81
3.7 References	82
Chapter 4 Development and Characterization Oriented Strand Board (OSB) with Epoxy and Partially Substituted Epoxy Resins with Fast Pyrolysis Bio-oil as Adhesive	89
4.1 Abstract.....	89

4.2 Introduction	90
4.3 Materials and Methods	92
4.3.1 Materials.....	92
4.3.2 Fast Pyrolysis Bio-oil Production	92
4.3.3 ATR-FT-IR	93
4.3.4 Epoxy/Pyrolysis Bio-oil Resin Formulation	93
4.3.5 Fabrication of Oriented Strand Board.....	94
4.3.6 Characterization of board properties.....	95
4.3.7 Bending test (Modulus of Elasticity (MOE) and Modulus of Rupture (MOR)).....	95
4.3.8 Internal Bond Strength	96
4.3.9 Thickness Swelling (TS) and Water Absorption (WA)	97
4.3.10 Thermogravimetric Analysis.....	97
4.3.11 Differential Scanning Calorimetry (DSC) Analysis	97
4.3.12 Solvent Resistance of cured Epoxy and Epoxy Substituted Bio-oil	98
4.3.13 Scanning Electron Microscopy Analysis of cured Epoxy and Epoxy/bio-oil Resin	98
4.3.14 Data Analysis.....	98
4.4 Results and Discussion.....	99
4.4.1 Viscosity.....	99
4.4.2 ATR-FT-IR	100
4.4.3 Bending properties	103
4.4.4 Internal Bond Strength (IB)	106
4.4.5 Thickness Swell (TS) and Water Absorption (WA).....	107

4.4.6 Thermogravimetric Measurements of Epoxy and Epoxy substituted Bio-oil.....	109
4.4.7 DSC analysis	111
4.4.8 Solvent Resistance of Epoxy and Epoxy substituted Bio-oil.....	112
4.4.9 Epoxy and Epoxy substituted with Bio-oil Morphology	114
4.5 Conclusion.....	116
4.6 Acknowledgements	116
4.7 References	118
Chapter 5 Bond Durability of Polymeric Diphenylmethane Diisocyanate (PMDI) Substituted with Defatted Soy Flour in Oriented Strand Board Production.....	121
5.1 Abstract.....	121
5.2 Introduction	121
5.3 Materials	122
5.3.1 Attenuated Total Reflection -Fourier Transform-Infrared (ATR-FT- IR).....	122
5.3.2 Viscosity.....	122
5.3.3 OSB Production	122
5.3.4 Moisture Cycle Test for Board Delamination (Adhesive Bond Performance) and Strength Retention Test.....	123
5.4 Results and Discussion.....	124
5.4.1 FT-IR Analysis of PMDI substituted Soy Flour	124
5.4.2 5.3.2. Effect of Soy Flour substitution on Adhesive Viscosity.....	126
5.4.3 5.3.3. Soy flour substitution effect on OSB properties	127
5.4.3.1 2% Adhesive loading.....	128
5.4.3.2 4% Adhesive loading.....	129

5.4.4 Six cycle water-vacuum soak test and strength retention test.....	131
5.5 Conclusions	133
5.6 Acknowledgements	133
5.7 References.....	140
Chapter 6 Increasing Cold Tack of pMDI resin with Partial Soy Flour Substitution.....	136
6.1 Abstract.....	136
6.2 Introduction	136
6.3 Materials and Methods	137
6.3.1 Materials.....	137
6.3.2 Cold Tack of PMDI substituted soy.....	137
6.3.3 Particle Board Production	137
6.3.4 Soy flour substitution in MDI mitigates platen sticking	138
6.4 Results and Discussion.....	138
6.4.1 Cold Tack.....	138
6.4.2 Particleboard Applications	140
6.4.3 Soy flour substitution in MDI mitigates platen sticking	142
6.5 Conclusions	144
6.6 Acknowledgment.....	144
6.7 References	145
Chapter 7 Soy Flour Substitution in pMDI Resin for Composite Panel Applications	146
7.1 Abstract.....	146
7.2 Introduction	146
7.3 Materials and Methods	147

7.3.1 Methods.....	147
7.4 Results and Discussion.....	150
7.4.1 Mixing Soy Flour and MDI resin: CO2 evolution.....	150
7.4.2 Strand Board Applications.....	152
7.4.3 Soy Flour in MDF Application.....	155
7.4.4 Mechanism.....	155
7.5 Conclusions.....	156
7.6 Acknowledgment.....	156
7.7 References.....	157
Chapter 8 General Conclusions and Recommendations.....	159
8.1 General Conclusions.....	159
8.1.1 Future Work.....	163
8.2 Appendix A.....	165
GC-MS Analysis.....	165
8.3 Appendix B.....	168

List of Tables

Table 2.1 Property Requirements Specified by the American National Standards Institute A208.1 (ANSI/A208.1, 1999) for Various Classes of Particleboard Products.....	12
Table 2.2 Property Requirements Specified by the American National Standards Institute A208.1 (ANSI/A208.1, 1999) for Various Grades of Particleboard Flooring Products.	13
Table 2.3 Types of pyrolysis (Wang et al., 2017).....	25
Table 2.4 Chemical shifts and integration regions of bio-oil phosphilated by TMDP (Pu et al. 2011).	30
Table 2.5: Amino acids in soy protein with high reactivity (Bjorksten, 1951)	40
Table 2.6: Relative contributions (kcal/mol) of van der Waals, hydrogen bonds, and electrostatic secondary forces to the adhesion of species from a PF resin to wood cellulose (Pizzi 2003).....	45
Table 3.1: Biomass Composition, Proximate, Ultimate, and Heating value analyses (dry basis as wt. %) room temperature.	68
Table 3.2 : Product yields for fast pyrolysis and hydrothermal liquefaction.....	70
Table 3.3: Ultimate analysis and physical properties of fast pyrolysis bio-oil and hydrothermal liquefaction bio-oil (dry wt % basis).	71
Table 4.1: OSB manufacturing parameters.....	95
Table 4.2 : Adhesive formulations with associated viscosities, panel density and mat moisture content (MC).....	99
Table 4.3: FTIR band assignment of pyrolysis bio-oil, EPON 828 (unmodified commercial grade) and Epoxy substituted bio-oil (EP-bio-oil).....	102
Table 4.4: TGA data of the cured epoxy resins and epoxy bio-oil resins.....	111
Table 5.1: (a) Soy substitution only in face adhesive	128

Table 7.1: Edge swell results of MDI and substituted with 12% and 15% soy flour with different blending techniques 153

Table 7.2: Properties of boards made from flakes prepared immediately after resination and after 3 and 6 hours..... 154

List of Figures

Figure 2.1 U.S OSB market size (USD Billion), by application, from 2014 – 2025 (Grand View Research, 2019).....	9
Figure 2.2 A) Oriented strand board panel manufacturing process; B) OSB panels	11
Figure 2.3: A) Particle board production process; B) Particle board panel	14
Figure 2.4: Medium Density Fiber Board production process (Chapman, 2004.....	17
Figure 2.5 : Diglycidyl ether of bisphenol A (DGEBA).....	18
Figure 2.6:Reaction mechanisms of Epoxy resin	20
Figure 2.7: U.S. Epoxy resin market revenue by application, 2014 – 2024 ((USD) (Research and Market, 2016).....	21
Figure 2.8: Schematic representation of residue formation in the presence and absence of hydrogen donor solvent.Pyrolysis.....	24
Figure 2.9: Phosphitylation of free OH group with TMDP in the solvent system of CDCl ₃ /Pyridine/DMF.....	28
Figure 2.10: 2.10. N-hydroxy compounds used as an internal standard in ³¹ P-NMR analysis: (a) N-hydroxyphthalimide, (b) 1-hydroxy-7-azabenzotriazole, (c) N-hydroxy-5-norbornene-2,3-dicarboximide, and (d) N-hydroxy-1,8-naphthalimide. Table 2.2 shows ³¹ P-NMR chemical...	29
Figure 2.11: Reaction of aniline with formaldehyde	32
Figure 2.12: Phosgenation of the methylenedianiline diamine.....	33
Figure 2.13: 3 possible MDI isomers.....	33
Figure 2.14: Polyisocyanate structure found in polymeric MDI	33

Figure 2.15: The reaction of isocyanate and water producing a primary amine and carbon dioxide.	34
Figure 2.16: Reaction between an isocyanate group and urea producing biuret linkage	34
Figure 2.17: The reaction of urea with an isocyanate group to form biuret linkage.....	35
Figure 2.18: Reaction between a hydroxyl group from bio-oil and isocyanate group to produce urethane linkage	35
Figure 2.19: The reaction of an isocyanate and urethane to form an allophanate bridge	36
Figure 2.20: Hydrogen bonding between urethane groups	36
Figure 2.21: Hydrogen bonding between urea groups.....	36
Figure 2.22: Reaction of carboxylic acid with isocyanate	37
Figure 2.23: Reaction of phenol with isocyanate	37
Figure 2.24: Denaturation of the protein structure (Frihart et. al., 2010).	41
Figure 2.25: Chain link analogy for an adhesive bond in wood proposed by (Marra 1992)	43
Figure 3.1: Schematic diagram of reactor for hydrothermal liquefaction.	61
Figure 3.2: Temperature – pressure profile of HTL process at 300 °C.....	61
Figure 3.3: Schematic of the auger pyrolysis reactor at MSU used to produce bio-oil.....	64
Figure 3.4: Variation of viscosity of bio-oil with temperature and shear rate produced by FP (A) and HTL (B).....	72
Figure 3.5: Chemical composition of FP and HTL bio-oil by GC-MS.	74
Figure 3.6: Thermogravimetric analysis (TGA) - A and derivative weight loss (DTG) - B curves of fast pyrolysis and hydrothermal liquefaction bio-oils.	76
Figure 3.7: FTIR spectra of bio-oil samples from loblolly pine biomass obtained from hydrothermal liquefaction (HTL) and pyrolysis processes (FP).....	77

Figure 3.8: ³¹ P-NMR spectra for the FP and HTL bio-oils phosphitylated with TMDP.	79
Figure 4.1: Reaction of hydroxyl groups of the bio-oil with the epoxide of Epoxy resin.....	100
Figure 4.2: FTIR spectra of fast pyrolysis bio-oil, EPON 828 (unmodified commercial grade) and epoxy substituted bio-oil at different bio-oil content (EP-bio-oil).....	101
Figure 4.3: Reaction of carbonyl groups of the bio-oil with the epoxide of Epoxy resin.....	102
Figure 4.4: Modulus of Rupture of OSB bonded with the epoxy and epoxy substituted bio-oil adhesives with different bio-oil contents. B (20%) = 80% epoxy resin substituted with 20% bio- oil; B (30%) = 70% epoxy resin substituted with 30% bio-oil; B (40%) = 60% epoxy.....	104
Figure 4.5: Modulus of Rupture of OSB bonded with the epoxy and epoxy substituted bio-oil adhesives with different bio-oil contents. B (20%) = 80% epoxy resin substituted with 20% bio- oil; B (30%) = 70% epoxy resin substituted with 30% bio-oil; B (40%) = 60% epoxy.....	105
Figure 4.6: Internal bond strength of OSB bonded with the epoxy and epoxy substituted bio-oil adhesives with different bio-oil contents. B (20%) = 80% epoxy resin substituted with 20% bio- oil; B (30%) = 70% epoxy resin substituted with 30% bio-oil; B (40%) = 60%.....	107
Figure 4.7: Thickness swell (TS) and water absorption (WA) bonded with the epoxy and epoxy substituted bio-oil adhesives with different bio-oil contents. B (20%) = 80% epoxy resin substituted with 20% bio-oil; B (30%) = 70% epoxy resin substituted with 30% bio-oil.....	108
Figure 4.8: Thermogravimetric (TGA) and (B) Derivative weight loss (DTG) thermograms of Epon 828 (commercial neat epoxy), and epoxy substituted bio-oil at different bio-oil content.	111
Figure 4.9: Thermal transitions differential scanning calorimetry (DSC) of Epon 828 (commercial neat epoxy), and epoxy substituted bio-oil at different bio-oil content.	112

Figure 4.10: Mass loss (wt %) of Epon 828 (commercial neat epoxy), and epoxy substituted bio-oil resins system under acetone for 6 h. EP_B = epoxy resin substituted bio-oil; B (20%) = 80% epoxy resin substituted with 20% bio-oil; B (30%) = 70% epoxy resin substitution.....	113
Figure 4.11: Morphology by scanning electron microscopy (a) neat Epoxy (EPON 828); (b) Epoxy/Bio-oil (80:20); (c) Epoxy/Bio-oil (780:30).....	115
Figure 5.1: FTIR spectra for PMDI, Soy and cured PMDI (90%)/Soy (10%)	126
Figure 5.2: Viscosity of PMDI and PMDI/soy mixture (9:1) at 5 minutes of mixing.....	127
Figure 5.3: Internal bond strength of PMDI and PMDI substituted with soy flour.....	129
Figure 5.4: Effect of soy flour substitution on the modulus of elasticity and modulus of rupture and edge swell of OSB panels at 1.5 minutes and 1.75 minutes of hot pressing.	130
Figure 5.5: Delaminated OSB panel pressed for 1.5 minutes.....	131
Figure 5.6: Delaminated OSB panel pressed for 1.5 minutes.....	132
Figure 6.1: Images of bolts after rolling down inclined resinated plates. B= is schematic setup of the tack test.	139
Figure 6.2: Effect of soy flour substitution on distance down an inclined surface.....	140
Figure 6.3: Effect of soy substitution on particleboard properties; n (number of samples tested per treatment) =12; ES =Edge swell; TS= thickness swell; WA= water absorption and IB = Internal bond strength.....	141
Figure 6.4: Platens coded B was placed on MDI resinated particles, and A and C were placed on either MDI substituted with soy or soy powder sprinkled on top of MDI coated particles.....	142
Figure 6.5: Surface appearance of particle boards with MDI (A) only and MDI (either mixed with soy (B) or surface sprinkled with soy (C))......	143

Figure 7.1: 1 Medium density fiber board mat (A); hot press with MDF mat (B); trimmed MDF panels (C); Tested specimen for MOR and MOE (wet from left (dark colored) and dry) (D)... 148

Figure 7.2: CO2 measurement set up with a thermometer and CO2 sensor housed in the cover.
 149

Figure 7.3: CO2 evolution from the reaction of MDI resin with soy flour or water. 151

Figure 7.4: Effect of soy substitution on strand board properties. The hatched bars represent wet properties; n=8. 154

Figure 7.5: Effect of soy substitution on MDF properties at two different densities; n=8. 155

List of Abbreviations

FP	Fast Pyrolysis
HTL	Hydrothermal Liquefaction
PMDI	Polymeric Methylene Diphenyl Diisocyanate
OSB	Oriented Strand Board
MDF	Medium Density Fiber Board
MOR	Modulus of Rupture
MOE	Modulus of Elasticity
IB	Internal Bond
TS	Thickness Swell
WA	Water Absorption
TGA	Thermogravimetric Analysis
DTG	Derivative Thermogravimetric Analysis
DSC	Differential Scanning Calorimetry
FT-IR	Fourier Transform-Infrared

Chapter 1

Introduction

Wood composite defines engineered wood materials bonded together with adhesive. Usually, the wood materials are brought into adhesion with the adhesive under pressure and depending on the type of adhesive, heat may be applied to accelerate curing. Wood composites are engineered to utilize the synergetic properties of wood and adhesive use to bond them to enhance strength, fire resistance, biological degradation and the in situ anisotropic properties of solid wood. Wood composites are uniform in design and properties in comparison to solid wood, affording wood defects to be uniformly distributed to reduce variability found in the natural wood. Wood composites also promote the utilization of small diameter trees, underutilized wood species, saw mill wastes like sawdust, shavings and chip. Wood composite products are recently used to substitute solid wood in contemporary building structures (Barnes 2012). Wood composites such as oriented strand board (OSB), particle board, medium density fiber (MDF) board, plywood, laminated veneer lumber (LVL), etc., are used in exterior and interior applications (Laks, 2002).

Polymeric diphenylmethane diisocyanate (PMDI), phenol formaldehyde (PF), urea formaldehyde (UF), and melamine urea-formaldehyde (MUF) is the most common adhesive used in the wood composite production. Currently, formaldehyde-based adhesives like PF and UF in wood composites are under stricter regulations by the environmental protection agency (EPA and EPA-40 CFR Part 770 2016) due to formaldehyde emissions which is a known carcinogen (Programme, 2004). Nowadays, PMDI is used as the main binder in most of the wood composites displacing PF. Epoxy resins are thermosetting polymer rarely used in the wood composite industry and are generally used in wood bonding where the other adhesives do not perform well such wood repair,

room temperature bonding under low bonding pressure (Frihart 2005). However, epoxy resins like PMDI are expensive and are petroleum derived, therefore raises sustainability, eco-friendliness and environmental health concerns. Research to modify PMDI and epoxy resins aimed at a price reduction and utilization of less petrochemicals have received increased attention (Barde et al. 2019; Bandara and Wu 2018; Hand 2018; Liu et al. 2017; Mao and Shi 2012; El Mansouri, Yuan, and Huang 2011; Mao et al 2011; Mekonnen et al. 2014; Wang, Li, and Zhang 2008). Present technology aiming at 100% replacement of petroleum based adhesive is not attainable, but a compromise utilization of bio-based materials with petroleum based engineered products could meet both performance related properties and cost reduction benefits.

This study focused on two bio-based materials, bio-oil and soy flour, as partial replacement of PMDI and epoxy resin. Bio-oil is a thermochemical liquefied product from lignocellulosic biomass through decomposition by pyrolysis, organic solvent liquefaction or hydrothermal liquefaction. Bio-oil has high hydroxyl numbers and could be used as a cross-linker and biopolyol in epoxy resin formulation and PMDI modification. Lignocellulosic biomass is a common and abundant natural resource that is ecologically robust to meet the current needs of partial petroleum-based material replacement. USA alone annual production capacity of lignocellulosic biomass is estimated at 1.3 billion dry tons and has attracted interests as a feedstock for industrial polymer production. On the other hand, soybeans in the native state contain about 20% oil, 34%, carbohydrates, 40% protein and 4.9% ash (Hettiarachchy and Kalapathy, 1998). Soy flour is obtained from soybeans through cleaning, cracking, dehulling and flaking processes. Soybean oil is normally removed from the soybean powder through solvent-extraction process. Hexane is the most used solvent. After the removal of oil from soybean, the resultant powder is called defatted soybean meal or soy flour.

1.1 Research Plan

The main hypotheses of this dissertation were divided into two. The first hypothesis was that the physical and mechanical properties of OSB and particle board depend on the reaction behavior of the epoxide groups in the epoxy resin and the hydroxyl groups in the substituted bio-oil. The second hypothesis is that the reaction behavior and subsequent physical and mechanical properties of OSB, particle boards, and MDF depend on the optimal interaction of the isocyanate moieties in PMDI and amine and hydroxyl groups in the soy flour.

The objectives of this dissertation were carried out in three phases for each adhesive system studied (i.e., bio-based epoxy resin and soy-based PMDI resin). For the epoxy and bio-oil study, the first phase objective was to determine the effect of fast pyrolysis and hydrothermal liquefaction processes of the bio-oil quality as a suitable polymer for crosslinking epoxy resins, and PMDI. The second phase was to determine the effect of bio-oil replacement in epoxy resin on the adhesive properties and their subsequent effect on the mechanical and physical properties of OSB and particle board. For the soy flour based adhesives, the first phase objective was to elucidate the mechanism of interaction of soy flour with MDI resin and how soy flour influences the tack of the adhesive system. The second phase objective was to characterize the mechanical and physical performance of partial substitution of MDI with soy flour on OSB, particle board and MDF. The thermal behavior was characterized in each adhesive employing thermogravimetric analysis (TGA), differential scanning calorimetry (DSC) analysis, and Fourier transform-infrared (FT-IR) spectral analysis to examine how bio-oil, and soy products affected the overall adhesive systems studied respectively.

1.2 Motivation

Primarily, the motivation for this research was cost reduction. The price of defatted soy flour ranges from \$0.35-\$0.40/lb, which is a doubled price of the commodity soybean meal sold at \$0.2/lb due to further processing (NASDAQ, 2019). On the other hand, PMDI resin used in the production of OSB range in price from \$0.86-\$1.4/lb (Alibaba, 2020). The defatted soy flour price was about a third of the price of PMDI and a potential cost saving if substituted into PMDI. For instance, 15% SF substitution in PMDI would result in a savings of about 11% for the overall wood adhesive system.

Similarly, it is anticipated that the relatively low-price of bio-oil (\$0.20–0.35/lb) than epoxy (\$1.35 – \$1.50/lb) will result in overall cost-effective bio-based epoxy system (Raizada, 2020; Stewart 2004).

The second motivation was to reduce the consumption of non-renewable resources and associated health concerns used to manufacture wood composite through partial substitution of pMDI, and epoxy resins with bio-oil, and soy. The main reactive functional group, isocyanates, contained in pMDI is known to trigger adverse health effects such as asthma (Mehta et al. 1990). Bisphenol A, a reactive polyol, in epoxy synthesis, is also known to show toxicity (EU 2011, FDA 2013).

1.3 Dissertation Organization

The dissertation is divided into two parts. Part one begins with chapter 2 with a literature review on OSB, particle board, MDF, epoxy resins, thermomechanical liquefaction of biomass (fast pyrolysis (FP) and hydrothermal liquefaction (HTL) processes), soy flour and PMDI. Chapter 3, covers the elucidation of the effect of FP and HTL processes on the characteristics of bio-oil. In chapter 4, partial substitution of commercial epoxy resin with fast pyrolysis bio-oils was studied

and improved hydrophobic OSB was manufactured from the bio-based epoxy resin system. The cured epoxy substituted bio-oil was characterized for a better understanding of the resin behavior.

Part two of the dissertation focuses on the compatibility of soy flour and PMDI as wood composite binder. In Chapter 5 and 6, the influence of soy substitution in PMDI on the resin performance was assessed with FTIR and panel strength testing. An additional benefit of PMDI cold tack improvement in using soy in PMDI was evaluated via modification of ASTM D3121, 2017. Tack performance of particle board properties and platen release after hot pressing were also highlighted. In chapter 7, the fundamental understanding of the reaction kinetics via CO₂ evolution was analyzed during PMDI and Soy blending and its applications in OSB and MDF production were studied. For commercialization of the partial substituted PMDI with soy flour, the bond durability of the PMDI/soy resin system was assessed to pass the recommendations of the Performance Standard for wood base structural use (PS-2 -10; 2011 PS-2), a single and six cycled vacuum-water soak test. Chapter 8 concludes the thesis with a summary of key results and recommendations for future research.

1.4 References

1. Bandara, Nandika and Jianping Wu. 2018. "Randomly Oriented Strand Board Composites from Nanoengineered Protein-Based Wood Adhesive." *ACS Sustainable Chemistry and Engineering* 6(1):457–66.
2. Barde, Mehul, Yusuf Celikbag, Brian Via, and Sushil Adhikari and Maria L. Auad. 2019. "Semi-Interpenetrating Novolac-Epoxy Thermoset Polymer Networks Derived from Plant Biomass." *Journal of Renewable Materials* 6(7):724–36.
3. Barnes, H. M. 2012. "Durable Composites: An Overview." *Proc Am Wood Prot Assoc (AWPA)*, 107 1(July):267–79.
4. By, Modification and Reactive Blending. n.d. "Chapter 3 MODIFICATION BY REACTIVE BLENDING." 101–92.
5. El Mansouri, Nour Eddine, Qiaolong Yuan, and Farong Huang. 2011. "Synthesis and Characterization of Kraft Lignin-Based Epoxy Resins." *BioResources* 6(3):2492–2503.
6. EPA and EPA-40 CFR Part 770. 2016. "Formaldehyde Emission Standards for Composite Wood Products." *Federal Register* 81(238):89674–743.
7. Frihart, Charles R. 2005. "Adhesive Bonding and Performance Testing of Bonded Wood Products." *Journal of ASTM International* 2(7):455–66.
8. Hand, William. 2018. "Defatted Soy Flour Substitution in Phenol Formaldehyde and Methylene Diphenyl Diisocyanate Wood Adhesives and Their Curing Kinetic Behavior."
9. Hettiarachchy, N.S. and U. Kalapathy, Functional properties of soy proteins. *ACS Symposium Series*, 1998. 708(Functional Properties of Proteins and Lipids): p. 80-95.
10. Laks, P. E. 2002. Biodegradation susceptibility of untreated engineered wood products. In: *Enhancing the Durability of Lumber and Engineered Wood Products. FPS Symposium Proceedings No. 7249. Forest Products Society: Madison, WI.*, pp. 125-130.
11. Liu, Yi, Brian K. Via, Yuanfeng Pan, Qingzheng Cheng, Hongwu Guo, Maria L. Auad, and Steven Taylor. 2017. "Preparation and Characterization of Epoxy Resin Cross-Linked with High Wood Pyrolysis Bio-Oil Substitution by Acetone Pretreatment." *Polymers* 9(3).
12. Mao, An and Sheldon Q. Shi. 2012. "Dynamic Mechanical Properties of Polymeric Diphenylmethane Diisocyanate/Bio-Oil Adhesive System." *Forest Products Journal* 62(3):201–6.

13. Mao, An, Sheldon Q. Shi, and Philip Steele. 2011. "Flakeboard Bonded with Polymeric Diphenylmethane Diisocyanate/ Bio-Oil Adhesive Systems." *Forest Products Journal* 61(3):240–45.
14. Mekonnen, Tizazu H., Paolo G. Mussone, Phillip Choi, and David C. Bressler. 2014. "Adhesives from Waste Protein Biomass for Oriented Strand Board Composites: Development and Performance." *Macromolecular Materials and Engineering* 299(8):1003–12.
15. Perlack, R. D., L. L. Wright, A. F. Turhollow, R. L. Graham, B. J. Stokes, and D. C. Erbach. 2005.
16. Biomass as feedstock for a bioenergy and bioproducts industry: the technical feasibility of a billion-ton annual supply. DTIC Document.
17. Polymeric-isocyanate-MDI-PM200-price Product on Alibaba.com. [Online]. Available: https://www.alibaba.com/product-detail/Polymeric-isocyanate-MDI-PM200-price_60493212025.html?spm=a2700.galleryofferlist.0.0.21147765gZ2moX [Accessed: 20 June, 2020].
18. Programme, M., 2004. IARC classifies formaldehyde as carcinogenic. *Oncol. Times* 26 (3), 72.
19. P. S. Mehta, A. S. Mehta, S. J. Mehta, and A. B. Makhijani, "Bhopal tragedy's health effects: a review of methyl isocyanate toxicity," *J. Am. Med. Assoc.*, vol. 264, no. 21, pp. 2781–2787, 1990.
20. Stewart, Gerald W. 2004. "Bio-Oil Commercialization Plan." (July):56–81.
21. Soybean Meal Price: Latest Price & Chart for Soybean Meal - NASDAQ.com." [Online]. Available: <https://www.nasdaq.com/markets/soybean-meal.aspx>. [Accessed: July-8-2019].
22. Raizada T. (2020) US May epoxy soft amid competitive material slower demand. [Online]. Available: <https://www.icis.com/explore/resources/news/2020/05/19/10509240/us-may-epoxy-soft-amid-competitive-material-slower-demand> [Accessed: June 20, 2020].
23. Wang, W. H., X. P. Li, and X. Q. Zhang. 2008. "A Soy-Based Adhesive from Basic Modification." *Pigment and Resin Technology* 37(2):93–97.

Chapter 2

Literature Review

2.1 Oriented Strand Board (OSB)

Oriented strand board is known to evolve from waferboard in the late 1970s and it is ascribed to the conceptual development by Armin Elmendorf in 1965 as waferboard (Zerbe et al., 2015). OSB production has provided an efficient way to utilize about 80% of the wood volume removed from the forest into marketable products compared to plywood, which generates about 60% of residue materials (Haynes 2003). This is because in OSB production, small diameter logs, low quality and wood logging could be used. OSB is an engineered wood panel characterized by thin wood strands that are compacted under high pressures and temperatures.

OSB share similar construction design with plywood where wood strands at the core are oriented at a right angle to the orientation of the face and back layers. However, in place of wood strands, plywood uses veneer sheets. Generally, chips used in OSB dimensions are 75 mm to 150 mm long, 5 mm to 30 mm wide, and 0.4 mm to 0.8 mm thick (Chen et al. 2008). The wood strands usually have an aspect ratio (strand length divided by width) of at least 3. The global OSB market size was valued at USD 11.3 billion in 2017 with growth expected to increase by 14.3% from 2018-2025 (Grand View Research, 2019). The growth in the market size of OSB is partly attributed to the beneficial characteristics of OSB, such as low cost, high strength and durability. It is also partly due to increasing replacement of plywood with OSB. OSB demand is increasing in the areas of I-joints, floor trusses, structural core panels, and construction, furniture application and packaging (Vlosky and Rouge, 2017).

The U.S. OSB market was driven by construction, in terms of product usage, because of high demand from the residential construction sector. The number of residential units in the country increased by 4.17% in 2017 and it is expected to gain additional growth (Grand View Research, 2019).

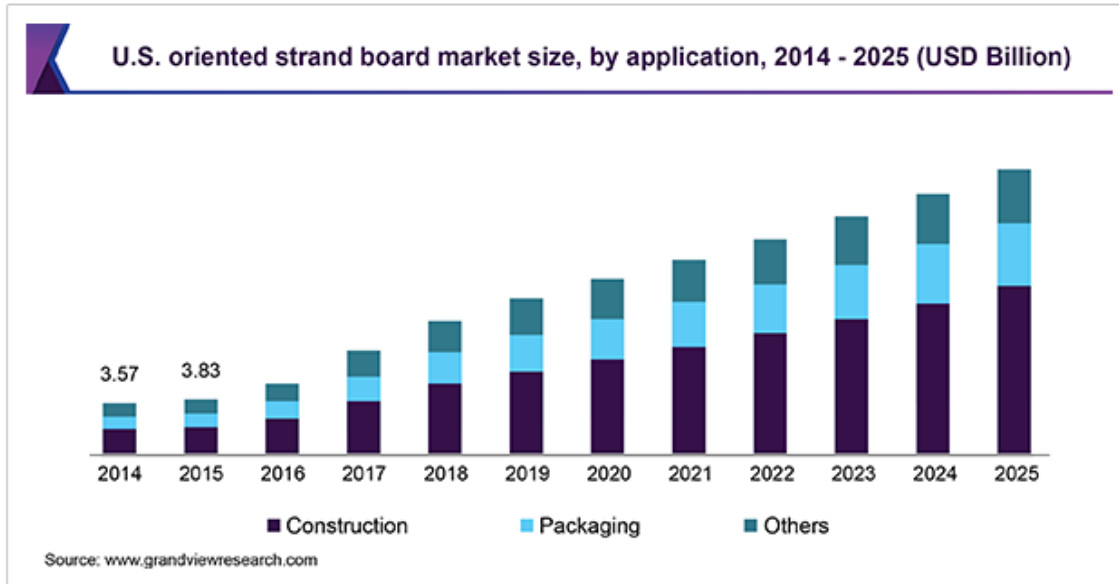


Figure 2.1 U.S OSB market size (USD Billion), by application, from 2014 – 2025 (Grand View Research, 2019).

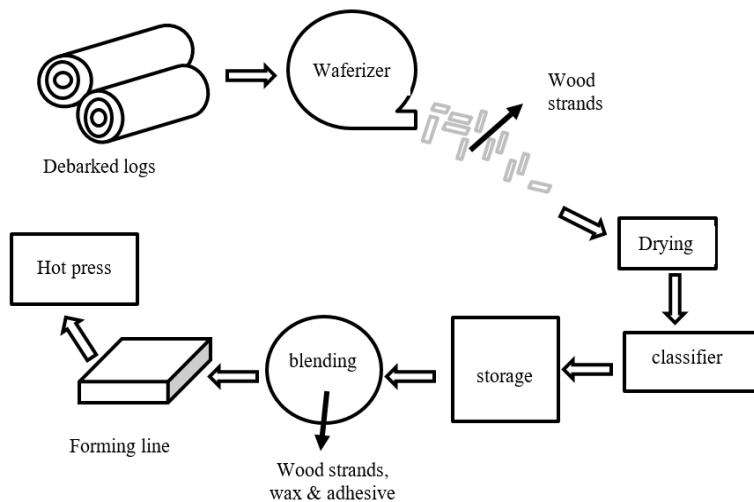
2.2 Manufacturing Process of Oriented strand Board

For simplification, OSB panel manufacturing process flow diagram is illustrated in Figure 2.2. OSB manufacturing begins with log debarking, which is essential to remove debris and stones which can dull the cutting knives. The debarked logs are then cut into strands. Dried strands are screened and smaller strands are usually used as core material. The orientation gives OSB panels anisotropic mechanical properties because the bending strength parallel to the long edge of the board is higher than that parallel to the short edge. Placing larger surface strands on top increases

the bending strength of the panels relative to their respective densities (Rowell 2012). Strands not in immediate use are stored. The dried strands are blended with adhesives, wax, and other additives. This is an important step because the overall panel properties are affected by resin dispersion, distribution, bond-line thickness, and resin penetration (Gagliano and Frazier 2001).

Resinated strands are sent to mat formers. Normally, different resin formulations are used for face and core layers. Face resins may be liquid or powdered PF, whereas core resins may be isocyanates. Interestingly, PF resin use is gradually replaced with PMDI resins. Oriented layers of strands within the mat are successively dropped onto a moving conveyor. The loose, layered mat is transferred from the conveyor into the hot press. The formed mat is pressed under heat and pressure to a certain thickness to achieve a target density. The pressing step is critical and factors such as time, temperature, and pressure are the most important parameters. The hot-pressing consolidates the mat by heating it at 177 to 204 °C (350 to 400 °F), which cures the resin in about 3–5 minutes depending on the resin used. The formed OSB panels are then trimmed and inspected for certification.

A



B

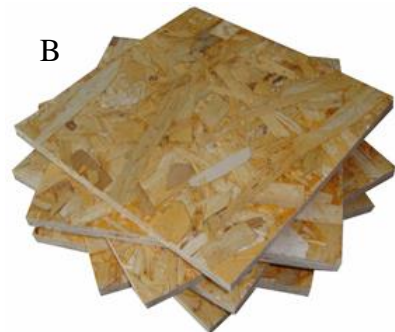


Figure 2.2 A) Oriented strand board panel manufacturing process; B) OSB panels

2.3 Particleboard

Particle board is an engineered wood product manufactured by mechanically reducing the woody materials into discrete small particles, adhesively compacted under high temperature and pressure. Particle board is structurally different from the other wood composites in terms of the particle size used in its production. Raw materials used in the production of particle boards include industrial small diameter wood species, wood residue such as sawdust, shavings, offcuts, slabs, logging residues, and thinning (Hermawan et al., 2009; Nemli et al., 2008). Agricultural residues like wheat straw, corn pith, waste grass, kenaf, etc. (Boquillon, 2004; Wang and Sun, 2002; Nemli et al., 2009) have been reported as potential alternative raw materials for particle board production.

Historically, particle boards originated in Germany and it dates back in the 1880's. However, a patent to automate the production of particleboards was presented in 1936 by Loetscher from USA. In 1937, a description of particle board with dry particles and powder resins (Bakelite) was presented by a Swiss national, Chappuis. Production of particle board using liquid resins was patented between 1938 and 1940 by a German company called Torfit. Torfit first built the first plant for the industrial manufacturing of particleboards in 1941 in Bremen (Germany) (Rowell, 2012). Today, particle board application include furniture, sliding doors, shelving table tops, kitchen cabinets, TV and stereo cabinet, packaging, etc. (Bowyer et al., 2007, Maloney, 1993). Urea formaldehyde resins are the most commonly used adhesive for making particleboard. PF, and melamine-urea-formaldehyde (MUF) are sometimes used (Li et al., 2004).

Particle board market was valued at US\$ 19.3 Billion in 2018, growing at a Compound Annual Growth Rate (CAGR) of 6.1% during 2011-2018. Particle board demand in household furniture

and other applications are expected to increase the particle board market share to reach a value of US\$ 25 Billion by 2024 (Research and Market, 2019)

2.4 Particle board Classification

Particle board properties classification requirement based on the American National Standard Institute A208.1 (ANSI/A208.1, 1999) is detailed in Tables 2.1 for different classes of particle board and Table 2.2 for various grades of Particle board flooring products. The standard takes into consideration some performance mechanical properties such as bending strength (MOR and MOE), internal bond strength and hardness. Grade assignment typifies the final densities of the finished product and is classified as follows: H- high density ($>800 \text{ kg/m}^3$), M- medium density ($640\text{-}800 \text{ kg/m}^3$), LD- low density ($< 640 \text{ kg/m}^3$), D- manufactured for home-decking and PBU- used as an underlayment. The digit following a letter states the grade of the panel within that classification.

Table 2.1 Property Requirements Specified by the American National Standards Institute A208.1 (ANSI/A208.1, 1999) for Various Classes of Particleboard Products.

Grade	MOR (MPa)	MOE (GPa)	Internal	
			Bonding (MPa)	Hardness (N)
H-1	16.5	2400	0.9	2225
H-2	20.5	2400	0.9	4450
H-3	23.5	2750	1	6675
M-1	11	1725	0.4	2225
M-S	12.5	1900	0.4	2225
M-2	14.5	2225	0.45	2225
M-3	16.5	2750	0.55	2225
LD-1	3	550	0.1	NS
LD-2	5	1025	0.15	NS

MOR = modulus of rupture, MOE = modulus of elasticity, NS = not specified. 1 MPa = 145 lb/in²; 1 N = 0.22 lb. Grade M-S refers medium density; “special” grade added to standard after grades M-1, M-2, and M-3. Grade M-S falls between M-1 and M-2 in physical properties.

Table 2.2 Property Requirements Specified by the American National Standards Institute A208.1 (ANSI/A208.1, 1999) for Various Grades of Particleboard Flooring Products.

Grade	MOR (MPa)	MOE (MPa)	Internal	
			Bonding (MPa)	Hardness (N)
PBU	11.5	1725	0.4	2225
D-2	16.5	2750	0.55	2225
D-3	19.5	3100	0.55	2225

2.5 Particle board Production Process

In particle board production, lignocellulosic materials used are reduced into consistently long and thin sized particles. The process will start with debarking if the starting materials is a log. The size reduction is usually achieved with a hammer mill, flakes or refiners. Wood particles are screened and classified into finer sized and oversized particles using either a gyrating screen or a vibrating screen. The screened particles conveyed into storage bins usually have a moisture content ranging from 10% to 200%. High moisture content (MC) in wood particles during production increases the panel pressure at the core resulting in delamination, also known as “blow”. The particles are dried to a lower moisture content around 4% to 8%, usually with rotary dryers (Stark et al., 2010).

The dried wood particles are blended with wax (0.3-1% of the wood solids), adhesives (usually with urea formaldehyde (UF) for interior application or PF for exterior application) and other additives. Adhesive and wax distribution is critical to the overall formed panel properties, thus atomizer under high pressure is employed to achieve fine resin droplet size. This resin and wax application method is also used in OSB production. Formed particle boards are then sent for finishing, which includes trimming, sanding and may also include cutting, laminating and packaging according to consumer specifications. Random samples are selected for quality control inspection and board properties testing (Youngquist, 1999). A schematic diagram of particle board production is shown in Figure 2.3.

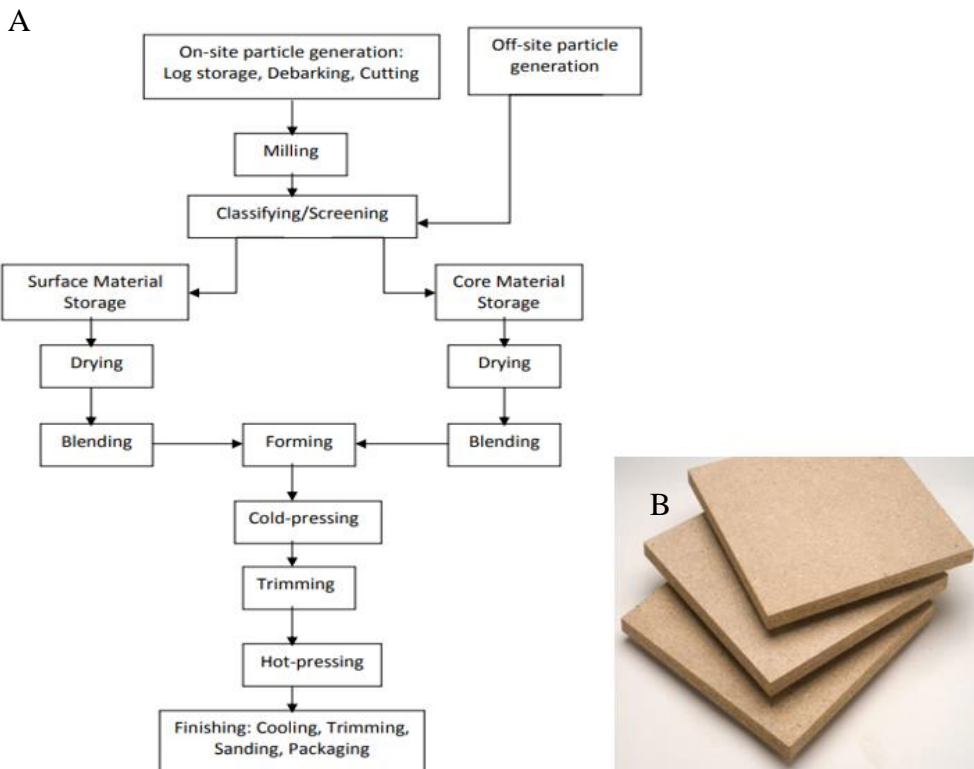


Figure 2.3: A) Particle board production process; B) Particle board panel

2.6 Medium Density Fiber Board (MDF)

Medium density board is an engineered wood product very distinct from OSB and particle board in that MDF exploits the inherent strength of wood by breaking the bonds between wood fibers. MDF is engineered such that wet wood fibers are mixed with wax, additives and adhesives before the fibers are dried and compacted under high temperature and pressure. The furnish for MDF is reduced to chips and then thermo-mechanically pulped. The use of fibers for MDF gives a fine smooth finishing consistency and good machining characteristics. MDF panel density are usually between made 500 and 800 kg/m³ (Wang, 1998). Unlike OSB and particle board where resin is applied through an atomizer under high pressure, MDF has a blowline blending system where resin, wax, and other additives are injected into wet fiber passing through a blowline. The wet wood fibers are used to prevent fiber clumping due to hydrogen bonding (Beutel, 1996) and electrostatic attraction. The –OH groups in the polymer chain of the wet fibers (predominantly cellulose) are attached to water molecules and are not free to bond with other wood fibers. However, hydrogen bonding is promoted as the cellulose chain dries and fiber clumping increases as a consequence.

Generally, MDF is widely used in furniture, decoration, transportation, and other industries due to its moderate density, good physical and mechanical properties, and low cost (Sun et al., 2012). Nowadays, MDF is used to substitute solid wood, plywood, and particleboard in many furniture applications. ANSI A208.2 classifies MDF by physical and mechanical properties and identifies dimensional tolerances and formaldehyde emission limits (CPA 2009). UF, MUF and PF resins are common adhesives used in MDF production. Because of formaldehyde emission concerns, industries have switched to using PMDI (Ruffing et al. 2010)

In 1965, the first MDF panel was produced in a particleboard plant in Deposit, New York. MDF characteristics of been smooth surface and adaptable to the application of solid wood saw a growth in its demand in USA. However, a decade later, significant production plant growth occurs in other places such as Japan, Germany, in addition to 9 plants in USA. The Canterbury Timber Products Ltd. plant at Rangiora started up in 1976, the 13th plant in the world and the first in the southern hemisphere (Chapman, 2004). The global MDF market size was valued at USD 61.3 billion in 2019 and is expected to grow at a compound annual growth rate (CAGR) of 6.6% from 2020 to 2027. The forecasted growth is particularly pivoted on expanding applications in furniture and construction over the estimated period (Grand View Research, 2020).

2.7 Medium Density Board Manufacturing

To obtain wood fibers for MDF production, wood is reduced to chips and then thermo-mechanically pulped. This process differs from the process used to obtain fibers for paper making. MDF Fiber pulping employs heating the wood in steam under pressure (about 8 bar before mechanical separation) to reach the softening temperature of lignin. This minimizes fiber damage and eases cellulose separation. Wax is added to the wet fibers and resinated in a pressured tube. The resinated fibers are dried in a flash tube at high temperature and dropped onto a conveyor line. The fibers lay flat within the plane of the mat of the resulting panel as a result of gravity. The mat is pressed under high temperature and pressure to the desired density (Wang, 1998).

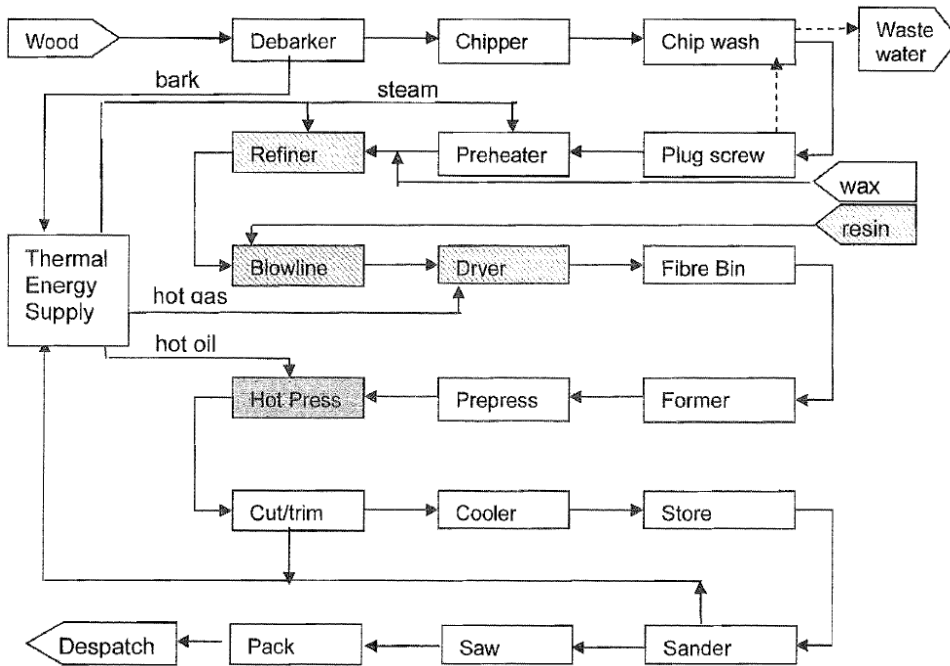


Figure 2.4: Medium Density Fiber Board production process (Chapman, 2004)

2.8 Epoxy Resin

Epoxy resin is a thermoset polymer synthesized by the condensation reaction of an epoxide (also called glycidyl or oxirane) functionality with a polyol in the presence of a catalyst. The first epoxy resin was commercially produced in 1940. However, it was initially synthesized and patented in 1891 and 1930 respectively (Ellis 2012). Diglycidyl ether of Bisphenol A (DGEBA), one of the commonly used epoxy resins, is derived from bisphenol A (a condensation product of phenol and acetone) and epichlorohydrin reaction (Figure 2.5). DGEBA contributes to about 75% of the current epoxy resin market today (Pham and Marks 2000). Nonetheless, bisphenol A has closely been associated with negative interaction with hormones and brain chemistry. This has led to a ban on using epoxy resin as coatings in drinking water pipelines (Auvergne et al. 2014, Okada et al. 2008, vom Saal and Myers 2008). Hence the need to limit the use of epoxy resin containing

bisphenol A with renewable materials motivated this study. Besides, bisphenol A is petroleum-derived.

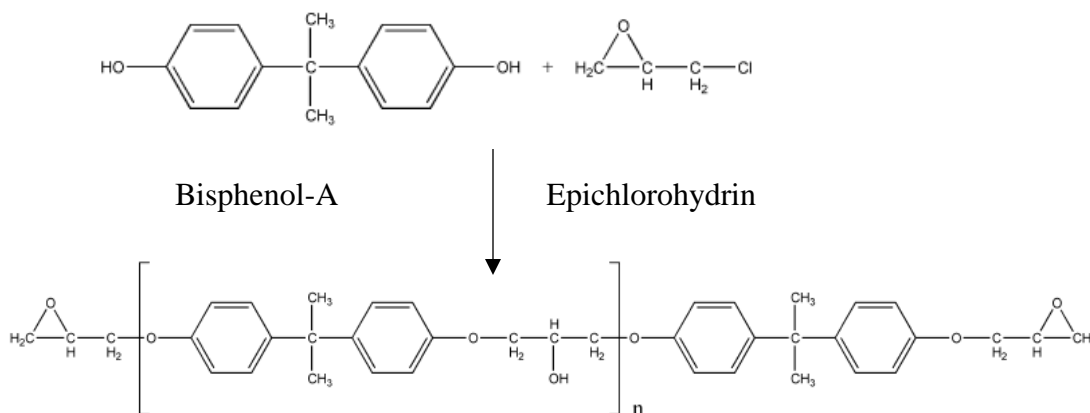


Figure 2.5 : Diglycidyl ether of bisphenol A (DGEBA)

However, the toxicity of BPA has raised questions and concerns regarding its use in epoxy resins. The negative effects of BPA on hormones and brain chemistry have been previously documented in the literature (vom Saal and Hughes 2005, Okada et al. 2008). The use of BPA in epoxy resin to be used in coatings for drinking water pipelines was recently banned (Auvergne et al. 2014). Moreover, the U.S. Food and Drug Administration (FDA) and European Union (EU) have also banned the use of BPA-based epoxy resins as coatings in infant formula packaging in 2013 and 2011, respectively (EU 2011, FDA 2013). Therefore, there is an increasing effort to explore bio-based aromatic polyol resources to be used in epoxy synthesis as an alternative to BPA. Moreover, the uncertainty in the price of petroleum as well as the social tendency toward materials from renewable and sustainable resources, have also motivated researchers to focus on bio-based materials.

2.8.1 Synthesis of Epoxy Resin

Synthesis of epoxy resin begins with the reaction of aromatic polyols (1) and sodium hydroxide (NaOH) (2), a catalyst, with the formation of phenate ion (3) as exemplified in Figure 2.6. Two reaction paths are suggested for the reaction of epichlorohydrin (4) and the phenate ion: (i) one-step nucleophilic substitution (SN2), and/or (ii) ring-opening reactions (Bradley et al. 1951). The phenate ion attacks the Cl–C bond in the case of SN2 reaction, and with the introduction of epoxide group in epichlorohydrin to the aromatic polyol, epoxy resin (5) is formed. The other possible reaction is the ring opening of ECH which produces an intermediate compound of (6). Epoxy resin (5) is formed as a result of dehydrochlorination of the intermediate compound (6) with NaOH as a catalyst. Conversely, incomplete dehydrochlorination could occur, resulting in the formation of 1-chloro-3-aryloxypropan-2-ols (7) as a side product.

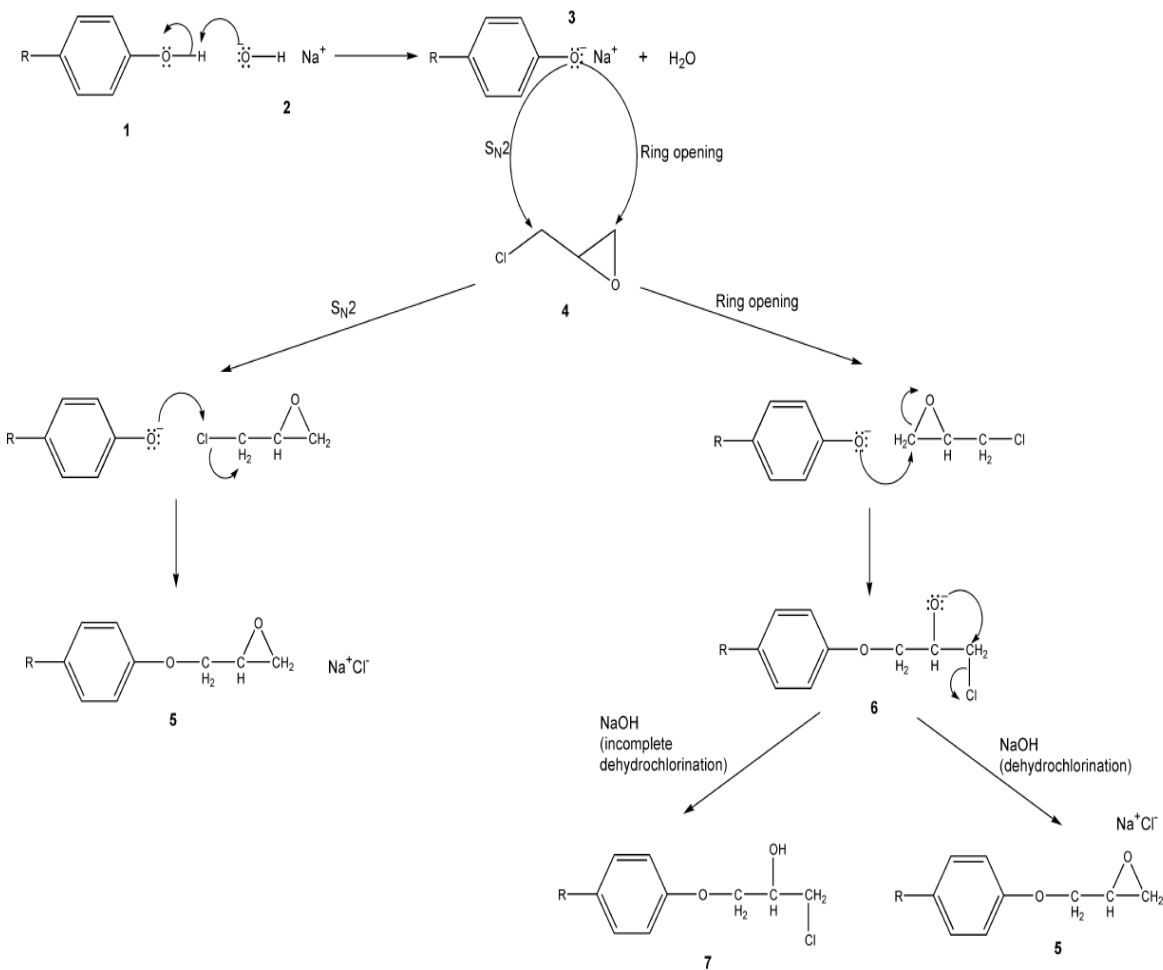


Figure 2.6: Reaction mechanisms of Epoxy resin

2.8.2 Epoxy Resin Application

The epoxide functional group can react with a wide variety of functional groups such as hydroxyl groups, amino groups, and carboxylic acid groups. Epoxy resins have good adhesion properties to many materials because the epoxide group is highly reactive and can undergo homopolymerization or can be crosslinked with different curing agents to yield network structures. Consequently, epoxy resin exhibit good mechanical and thermal properties, low cure shrinkage, and as well offers good chemical resistance. Pham and Marks, attributed the good mechanical properties and thermal resistance to the aromatic ring in polyol; good adhesion properties to the epoxide group of

epichlorohydrin and hydroxyl (OH) groups; and the chemical resistance to the ether linkages (Pham and Marks 2000). Thus, epoxy resins are widely used in different applications such as coatings, composites, construction and electrical/electronic field (Figure. 2.7).

As an indicator of their varied applications, the market size of epoxy resin in North America was about USD 1.07 billion in 2015, and it is predicted to be USD 1.4 billion by 2020 (Research and Market 2016). On the other hand, the global epoxy production was expected to be 3 million tons by 2017 with a market size of USD 21.5 billion (Auvergne et al. 2014). The drawbacks of epoxy resins are inherent brittleness, high cost, high cure requirements for high strength (Ratna, 2003). Epoxy resin remains as a minor adhesive in the wood composite industry, and the bond between epoxy bonded composite is known to weaken considerably with repeated moisture exposure (Frihart, 2005). In this study, bio-oil was proposed to improve the moisture tolerance of epoxy resin used in wood composites.

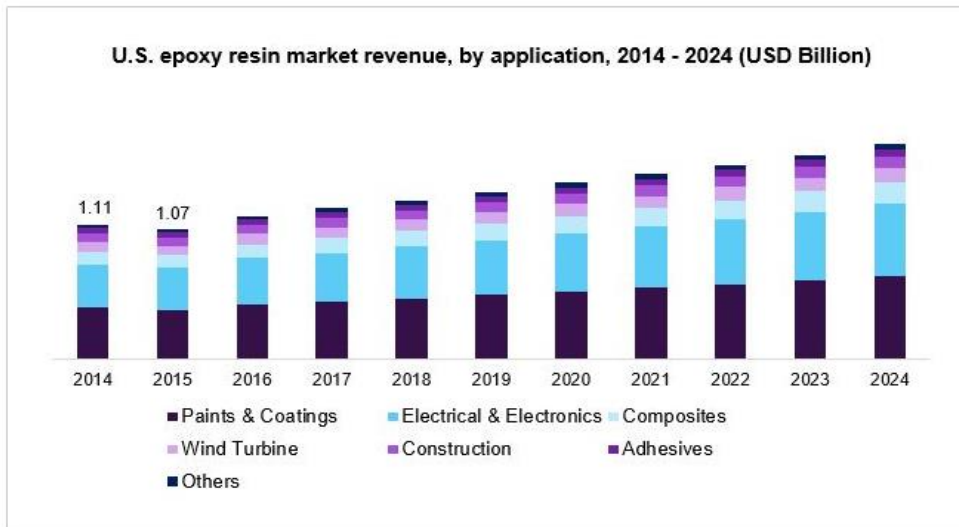


Figure 2.7: U.S. Epoxy resin market revenue by application, 2014 – 2024 ((USD) (Research and Market, 2016).

2.9 Bio-oil

Bio-oil describes liquefied biomass formed by lignocellulosic biomass decomposition through thermomechanical conversion processes. Three liquefaction processes are mostly used to produce bio-oil: (i) fast pyrolysis (FP)—the liquefaction in the absence of oxygen and solvent at elevated temperatures, (ii) organic solvent liquefaction (OSL)—the liquefaction of lignocellulosic biomass using organic solvents such as ethyleneglycol at moderate temperature, and (iii) hydrothermal liquefaction (HTL)—the liquefaction using water at high temperature and pressure. The liquid product from these processes is generally termed as bio-oil. A detailed literature about OLS process and OSL-bio-oil is discussed elsewhere (Lange 2018). Hence, only FP and HTL processes have been reviewed in this section. Bio-oil obtained from FP, and HTL processes are termed as FP-bio-oil, and HTL-bio-oil, respectively, in this chapter.

2.9.1 Hydrothermal Liquefaction (HTL)

Hydrothermal liquefaction (HTL) is a thermomechanical conversion technique to convert lignocellulosic biomass into liquid (bio-oil), gas and solid products using subcritical or supercritical water at elevated temperature (250 – 370 °C) and pressure (2 – 24 MPa). Bio-oil manufactured from the HTL process has the potential for commercialization in terms of price and life cycle assessment (Elliott et al. 2015). The effect of process parameters such as temperature, pressure, reaction time and feedstock type on the bio-oil yield in HTL process has been widely investigated and valuable literature reviews can be found elsewhere (Akhtar and Amin 2011, Toor et al. 2011). About 30 – 40 wt. % bio-oil yield (based on dry mass of biomass) is reported from HTL of lignocellulosic biomass (Akhtar and Amin 2011). It is worthy to note that several feedstocks such as microalgae have been studied recently via HTL processes.

Due to the low yield and high viscosity of HTL using water only as solvent, recent studies had focused on the use of hydrogen donor solvents like ethanol as a co-solvent in the HTL process. Yuan et al. (2007) noted that the highly reactive free radicals produced from the HTL of biomass were stabilized by the ethanol, which acts as a hydrogen-donor solvent. Bio-oil yield increased from 40 to 65 wt.% when ethanol was used along with water in a sub-critical condition (Cheng et al. 2010). In another study, alkaline lignin was liquefied in hot compressed water/ethanol medium, and found that the addition of ethanol increased the degradation of lignin, which resulted in a lower amount of solid residue (Yuan et al. 2007). This improvement was attributed to the low dielectric constant of ethanol, which facilitates dissolving of high molecular weight lignin at supercritical temperatures (Krammer and Vogel 2000). The synergistic effect of water/ethanol mixture in the liquefaction of rice husk for bio-oil production via the HTL process was also observed by (Liu et al. 2013). Also the addition of ethanol to water also is reported to affect the distribution of phenolics such as phenol, ethylphenol and guaiacols, ethylguaiacol and syringol in the bio-oil as well (Ouyang et al. 2015). Recently, Kosinkova et al. (2015) reported that aqueous ethanol improved the higher heating value (HHV) of bio-oil to be used in the field of biodiesel applications.

Lignocellulosic biomass is degraded to fragments and free radicals are generated during the HTL process. When there is no hydrogen donor solvent, these reactive free radicals recombine and forms high molecular weight products called solid residue or char. In case a sufficiently high amount of a hydrogen donor solvent such as ethanol is present in the HTL, free radicals can be stabilized and which decreases char formation, as shown in Figure. 2.8 (Vasilakos and Austgen 1985). Liu et al. (2013) summarized the synergetic effect of water/ethanol, the high bio-oil and low residue yield were accredited to (i) enhanced hydrogen donor capability of ethanol at subcritical and supercritical conditions and acting as a reaction substrate, (ii) high ability of ethanol

to dissolve oily products, (iii) ability of ethanol to stabilize the free radicals resulting in lower residue content, and (iv) the increased solubility of high molecular weight products in water/ethanol mixture at subcritical conditions. Another reason for the low char yield was the conversion of highly reactive carbonyl groups in the bio-oil to more stable acetal groups by ethanol in the ethanol/water HTL process. Carbonyl groups such as aldehydes and ketones are primarily responsible for the repolymerization of bio-oil due to their high reactivity and consequently result in the generation of solid residue as well as an increase in the viscosity of bio-oil (Czernik et al. 1994).

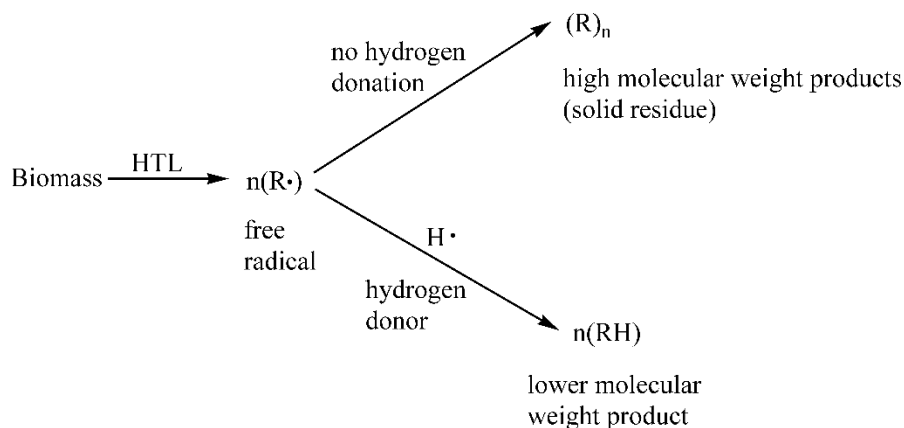


Figure 2.8: Schematic representation of residue formation in the presence and absence of hydrogen donor solvent.

2.9.2 Pyrolysis

Lignocellulosic biomass, known to rival petroleum derived fuels and chemicals, is made up of three biopolymers: hemicellulose (20-40%), cellulose (40-60%) and lignin (10-25%) weight (Ponder, 1994). During biomass pyrolysis, which is thermal decomposition in the absence of oxygen, these organic components are thermally decomposed. Biomass pyrolysis undergoes 4

main steps; moisture evolution, hemicellulose, cellulose, and then lignin decomposition (Yang, 2007).

Depending on the heating rate, pyrolysis temperature varies for hemicellulose, cellulose, and lignin is 180–240, 230–310, and 300–400 °C, respectively (Liu 2017). This process is irreversible and generally produces various chemical species in the form of pyrolysis vapors, aerosols, and solid residue. The condensation of pyrolysis vapors and aerosols yields a dark brown colored liquid with a strong smoky odor known as bio-oil. On the other hand, the non-condensable fraction of pyrolysis vapors mainly contains carbon monoxide, carbon dioxide, methane and hydrogen. The remnant of the pyrolytic biomass is called char. Reaction temperature, residence time and heating rates are considered the most important parameters that affect the quality of pyrolysis products and yield. These parameters define the three types of pyrolysis: slow, fast and flash, as shown in Table 2.1. This research focused on fast pyrolysis at 450 °C at a residence time of 2 s. Only a brief description on fast pyrolysis is given. More extensive reviews on fast pyrolysis are given in the literature (Bridgwater 2012; Venderbosch and Prins, 2010; Mohan et al., 2006; Kersten et al. 2005) to which order readers may refer to for additional detailed information.

Table 2.3 Types of pyrolysis (Wang et al., 2017)

Pyrolysis mode	Condition		
	Temperature (°C)	Residence time	Heating rate (°C/s)
Slow or conventional	400 - 500	5 - 30 mins	10
Fast	400 - 550	0.5 - 2 s	100 - 500
Flash	700 - 1000	< 0.5 s	> 500

2.9.2.1 Fast Pyrolysis

A fast pyrolysis process involves drying the biomass to typically < 10% moisture content to reduce the overall water content in the bio-oil, grinding the biomass to small particles to ensure rapid heating, efficient separation of solids (char), rapid quenching and collection of the liquid product. During fast pyrolysis, biomass decomposes rapidly to generate mostly vapors and aerosols and some charcoal and gas at moderate temperatures (400-550 °C), at short resident time <2s. Upon rapid quenching of vapors, bio-oil is formed (Bridgwater 1999). Characteristic attributes of fast pyrolysis process for bio-oil production are:

- Very high heating rates and very high heat transfer rates at the biomass particle reaction interface usually require a finely ground biomass feed of typically less than 3 mm as biomass generally has a low thermal conductivity,
- Carefully controlled pyrolysis reaction temperature of around 500 °C to maximize the liquid yield for most biomass
- Short hot vapor residence times of typically less than 2 s to minimize secondary reactions,
- Rapid removal of product char to minimize cracking of vapors,
- Rapid cooling of the pyrolysis vapors to give the bio-oil product (Bridgwater, 2010).

Processes that minimize the formation of char by reducing biomass exposure to low-temperature exposure are critical and the optimization of heating rates is essential (Tsubaki et al., 2020). One way this can be attained is by utilizing small particles. Another possibility is to transfer heat very quickly only to the particle surface that contacts the heat source.

2.9.2.2 Fast Pyrolysis Mechanisms

Lignocellulosic biomass cell wall materials (cellulose, hemicellulose and lignin) undergo different depolymerization mechanisms under fast pyrolysis conditions because of the differences in chemical structure. Heating of the biomass break down the cell wall polymers and volatiles are evolved. Two separate mechanisms occur during fast pyrolysis (Collard & Blin, 2014). The first mechanism, also called primary reactions, involves depolymerization, fragmentation and char formation. A secondary reaction may occur if the volatiles undergoes additional change such as secondary cracking, recombination and condensation, which reduce the quality of bio-oil by forming undesired compounds (Basu, 2018).

Cellulose degradation reaction occurs in four stages: dehydration producing “active cellulose” which is intermediate. Decarboxylation and carbonylation take place, producing mainly char and non-condensable gases (CO₂, CO and H₂O) (Basu, 2018). At the same time, depolymerization occur producing pyrolysis vapors and condensable gases, which yields levoglucosan and furans. Secondary cracking of depolymerization products contributes principally to the formation of char, tar and non-condensable gases reducing pyrolytic liquid yield (Collard & Blin, 2014). However, hemicelluloses depolymerize relatively earlier as the (~ 200°C) dehydration temperature is lower than cellulose (~ 300°C). This causes hemicellulose decomposition to yield more gases but less char and tar (Soltes and Elder, 1981). The decomposition of lignin produces the most char (55%) followed by tar (15%) and aqueous components. Lignin contains aromatic rings which lead to the formation of phenolic compounds in bio-oil. High lignin content is closely associated with increased viscosity as a result of higher molecular weight compounds (Collard and Blin, 2014).

2.10 ³¹P-NMR

Nuclear Magnetic Resonance (NMR) is a versatile analytical technique used in different fields study for structural characterization of chemical compounds. Common NMR used in the field of bio-oil characterization is ¹³C-NMR and ¹H-NMR. These are mainly used to analyze the carbon and hydrogen atoms in different functional groups in the bio-oil and the decomposition pathway of biomass in thermomechanical conversion processes (Ben and Ragauskas 2011; Mullen et al. 2009).

³¹P-NMR is used to quantitatively determine the amount and distribution of OH groups in bio-oil. OH groups belonging to aliphatic, phenolic, carboxylic units are phosphitylated with a phosphorous-containing derivatizing reagent followed by quantitative ³¹P-NMR. The mixture of pyridine and deuterated chloroform (1.6/1.0, v/v) is used as the solvent system in ³¹P-NMR analysis. In the phosphitylation reaction (Fig. 2.9), 2-Chloro-4,4,5,5-tetramethyl-1,3,2-dioxaphospholane (TMDP) reacts with the accessible OH groups in the bio-oil, and yields to derivatized compound and hydrochloric acid (HCl). HCl could decompose the derivatized compound. Hence pyridine is used in the solvent system as the base to neutralize the HCl. The reasons for using deuterated chloroform (CDCl₃) in the solvent system are (i) to dissolve derivatized sample, (ii) to inhibit precipitation of pyridine-HCl salt, and (iii) to get a deuterium signal for NMR experiment (Pu et al. 2011).

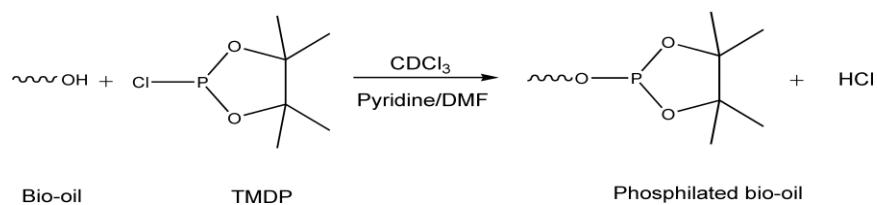


Figure 2.9: Phosphitylation of free OH group with TMDP in the solvent system of CDCl₃/Pyridine/DMF.

N-hydroxy compounds are used as an internal standard in ^{31}P -NMR analysis in the field of bio-oil. Other N-hydroxy compounds and cyclohexanols as an internal standard for the determination of OH groups in lignin structure were studied. It was observed that some signals of cyclohexanol-phosphite product overlap with aliphatic and phenolic lignin structures, while N-hydroxy compounds were better in terms of signal separation (Zawadzki and Ragauskas 2001). They also compared 4 different N-hydroxy compounds: N-hydroxyphthalimide, 1-hydroxy-7-azabenzotriazole, N-hydroxy-5-norbornene-2,3-dicarboximide, and N-hydroxy-1,8-naphthalimide (Fig. 2.10) and reported that N-hydroxy-5-norbornene-2,3-dicarboximide (Fig. 2.11c) was the most suitable internal standard for ^{31}P -NMR analysis of lignin.

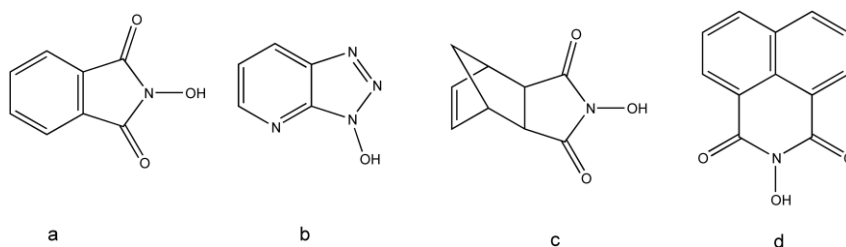
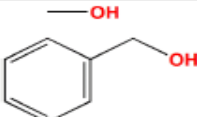
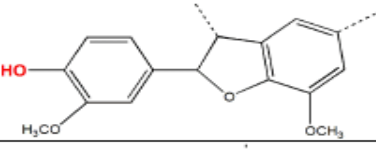
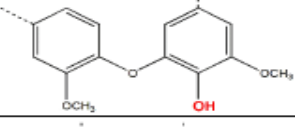
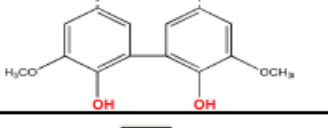
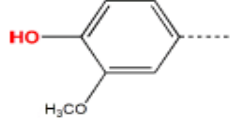
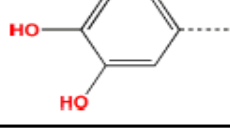
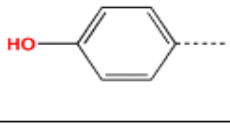
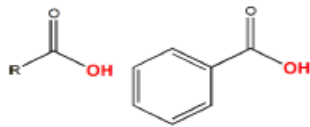


Figure 2.10: N-hydroxy compounds used as an internal standard in ^{31}P -NMR analysis: (a) N-hydroxyphthalimide, (b) 1-hydroxy-7-azabenzotriazole, (c) N-hydroxy-5-norbornene-2,3-dicarboximide, and (d) N-hydroxy-1,8-naphthalimide. Table 2.2 shows ^{31}P -NMR chemical

Table 2.4 Chemical shifts and integration regions of bio-oil phosphilated by TMDP (Pu et al. 2011).

Type of OH group	Example of Chemical Structure	Integration Region (ppm)
Aliphatic OH		150.0 - 145.5
Phenolic OH	β -5 	144.7 - 142.8
	C5 substituted Condensed phenolic OH 4-O-5 	142.8 - 141.7
	5-5 	141.7 - 140.2
	Guaiacyl phenolic OH 	140.2 - 139.0
	Catechol type OH 	139.0 - 138.2
<i>p</i> -hydroxy-phenyl OH 	138.2 - 137.3	
Acidic OH		136.6 - 133.6

2.11 Polymeric diphenyl-methane diisocyanate (pMDI)

Polymeric diphenyl-methane diisocyanate (PMDI), preferably called MDI in the forest product industry, is among the most commonly used resin in North America (Dettmer, 2013). Since its introduction, PMDI has been competing with formaldehyde based resins such as phenol-

formaldehyde (PF), urea–formaldehyde (UF), melamine–urea–formaldehyde in the wood composite industry. PMDI has received significant utilization in OSB production, supplanting PF.

The growth in PMDI utilization is due to its characteristic advantage over PF and other wood based adhesives. Compared to other wood-based resins, PMDI has high reactivity and reacts rapidly with the available hydroxyls in wood (Steiner 1991). Unlike other formaldehyde-based resins, PMDI provides formaldehyde free gluing. The utilization of pPMDI in wood bonding shows dimensional stability due to strong adhesive bond and moisture resistance. These properties are achieved with the use of less resin on a weight-percent basis than other liquid resins (Dunky, 2003). PMDI has high water tolerance and often is used at the core of OSB to improve bonding and also reduce blows in wood composite panels (Zheng et al., 2004). The isocyanates are extremely reactive. However, this very attractive feature of PMDI is also one of its greatest pitfalls; it would bond to metal pieces, so a realizing agent is always required (Sonnenschein and Wendt 2005). In this research study, an additional benefit of soy incorporation into PMDI to reduce platen adhesion is discussed later in the ensuing chapters. PMDI binds at lower temperatures and shorter pressing cycles. These characteristics give rise to additional savings in the manufacturing process (Dunky, 2003).

PMDI has excellent wetting behavior of wood surface and good wood penetration (Larimer, 1999). PMDI can penetrate 5–10 times further into wood than PF resins, penetrating even into the wood cell wall polymer structure via capillary action. This promotes good mechanical anchorage (Kamke and Lee 2007; Marcinko 1995). The good wetting and penetration behavior of PMDI can sometimes cause starved glue lines. Soy amendment of PMDI has been proposed to enrich the glue line of PMDI bonded panel in the cold talk studies further discussed in this dissertation. Also, PMDI is expensive; it will bond to the press platen, the isocyanate is toxic, so greater working care

is required. PMDI has low vapor pressure and needs special precaution during its use was also proposed that soy modification of PMDI will aid in cost savings.

PMDI has good mobility and it is influenced by PMDI containing no water; it cannot lose its mobility during adsorption on the wood surface; its low surface tension (ca. 50 mN/m) compared to water (76 mN/m) its low viscosity. Viscosities of pPMDI are approximately 0.18–0.25 Pa s (170–255 cP). PMDI has a density of 1.23 g/cm³ at 25 °C, having high-temperature tolerance and low flammability risk because it has a flashpoint of over 200 °C. However, PMDI starts to decompose at temperatures above 230 °C (Dunky, 2003).

2.11.1 Polymeric diphenyl-methane diisocyanate (pPMDI) Synthesis

PMDI is synthesized by the condensation reaction of aniline and formaldehyde, using hydrochloric acid as a catalyst to form a mixture of diamine precursors, as well as their corresponding polyamines:

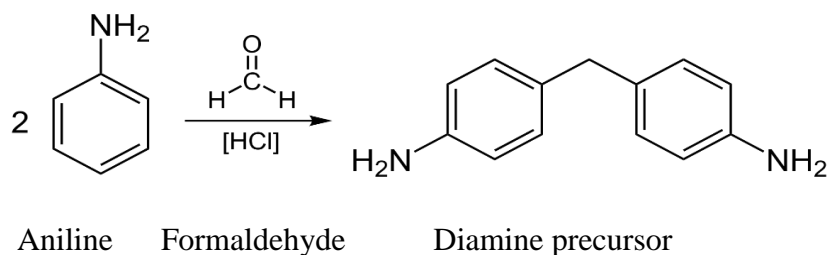


Figure 2.11: Reaction of aniline with formaldehyde

One mole of formaldehyde and two moles of aniline form the three possible isomers (4,4'-, 2,4'-, and 2,2'-) of methylenedianiline diamine (Figure 2.12). The diamine isomers then react to form methylene bridged polyphenylene polyamines. Then, these diamines are treated with phosgene to form a mixture of isocyanates, the isomer ratio being determined by the isomeric composition of

the diamine. Distillation of the mixture gives a mixture of oligomeric polyisocyanates, known as polymeric MDI, and a mixture of MDI isomers, which has a low 2,4' isomer content. Further purification entails fractionation of the MDI isomer mixture.

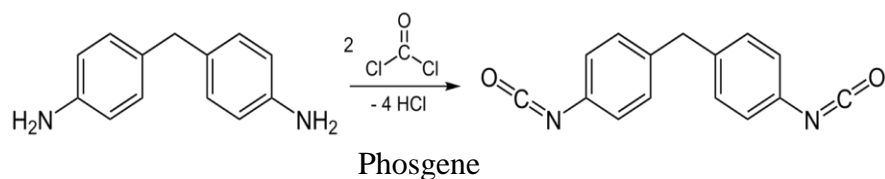


Figure 2.12: Phosgenation of the methylenedianiline diamine

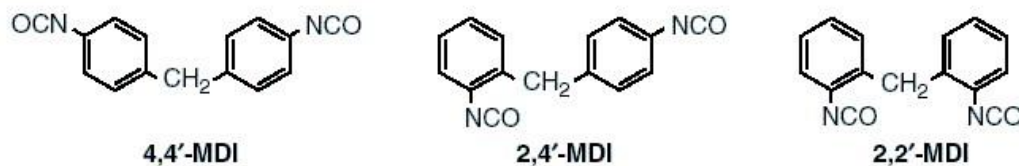


Figure 2.13: 3 possible MDI isomers.

These monomers make up to about 50% of polymeric MDI with the primary isomer formed being the 4,4'-MDI isomer, which constitutes about 95% of the monomers formed. The other half of the PMDI (Figure 2.14) mixture consists of the oligomeric polyisocyanate (Frazier 2003).

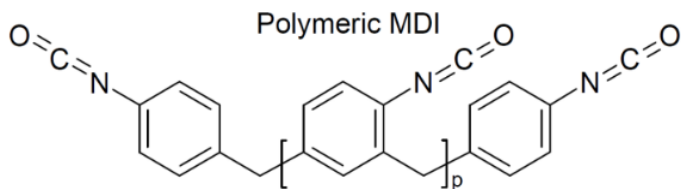


Figure 2.14: Polyisocyanate structure found in polymeric MDI

PMDI reactivity occurs because the isocyanate functionality can react with primary and secondary amines, primary alcohols, water, secondary alcohols, and phenols. The comparative reactivity of

these compounds with isocyanate depends upon the nucleophilicity and steric structure. Theoretically, isocyanate groups from pMDI can react with wood hydroxyl groups and water hydroxyl groups to form irreversible urethane linkage (Pizzi, 1994).

The bio-oil and soy studied in this research have water and mixed functional groups like carboxylic acids and a plethora of hydroxyl moieties, which is expected to react with the isocyanate group of pMDI and the wood polymers. Possible reactions with the isocyanate groups of PMDI include:

2.11.1.1 Water reaction with PMDI

The water present in bio-oil and soy can freely react with isocyanates (Figure 2.15). The reaction between isocyanate and water yields carbamic acid, which rapidly decomposes into an amine with carbon dioxide gas liberation.

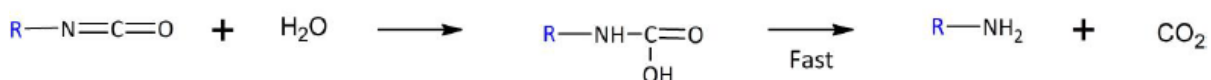


Figure 2.15: The reaction of isocyanate and water producing a primary amine and carbon dioxide.

The isocyanate group can readily react with amines from the water-isocyanate reaction or a substance that contains them (soy) to form substituted urea (Figure 2.16.)

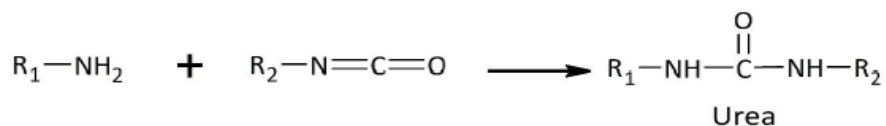


Figure 2.16: Reaction between an isocyanate group and urea producing biuret linkage

Other isocyanate groups of the pMDI can further react with the substituted urea to form biuret bridges (Figure 2.17). The formed biuret linkage can strengthen crosslinking and aid in the hardening of the cured adhesive (Frazier 2003).

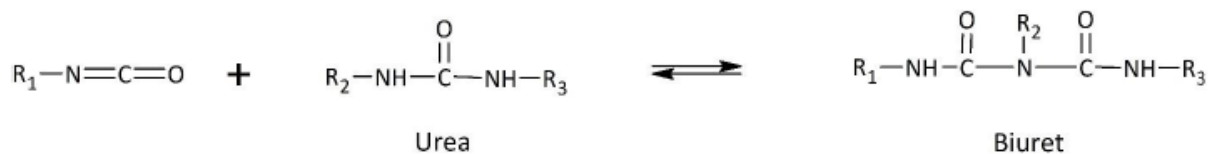


Figure 2.17: The reaction of urea with an isocyanate group to form biuret linkage.

2.11.1.2 Hydroxyl reaction with pMDI

Isocyanate reaction with hydroxyls of wood to form urethane linkages is thought of as the primary reaction pathway.

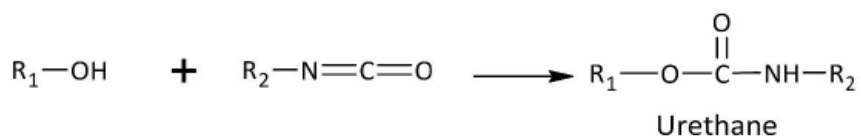


Figure 2.18: Reaction between a hydroxyl group from bio-oil and isocyanate group to produce urethane linkage

The secondary amine in the urethane in turn, can continue to react with other isocyanate groups from other pMDI molecules to form allophanate bridges (Figure 2.19). This further the adhesive crosslinking and hardening (Pizzi 1994).

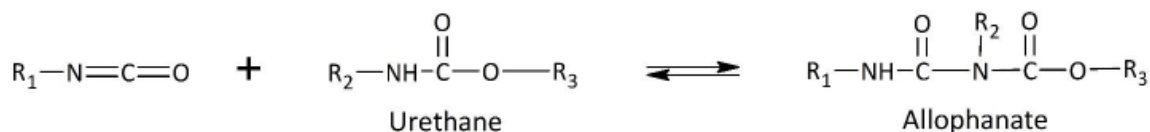


Figure 2.19: The reaction of an isocyanate and urethane to form an allophanate bridge

There is a possibility of hydrogen bonding occurring in a crosslinked structure of urethane and urea. The N-H group acts as a proton donor while the carbonyl acts as a proton acceptor. Figures 6 and 7 show hydrogen bonding between urethane groups and urea groups, respectively. The adhesive bonding strength is further improved with hydrogen bonding (Wang 1998).

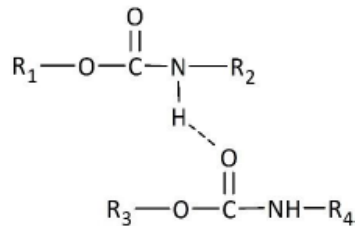


Figure 2.20: Hydrogen bonding between urethane groups

The hydrogen bonding occurring in urea could be monodentate (one hydrogen bond) or bidentate (two hydrogen bonds)

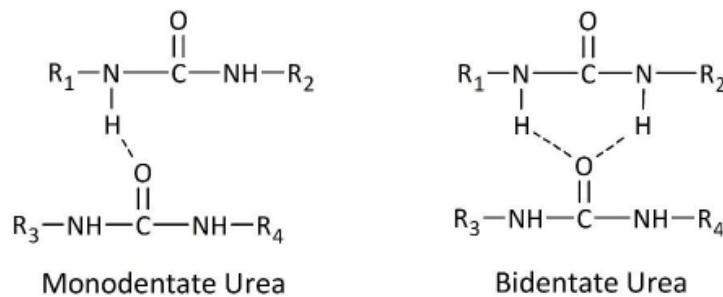


Figure 2.21: Hydrogen bonding between urea groups

2.11.1.3 Carboxylic acid

The carboxylic acids can with the isocyanate of PMDI to form anhydride which degrades to Amide and carbon dioxide. The amide could then react with another isocyanate group to form biuret

(Figure 2.22).

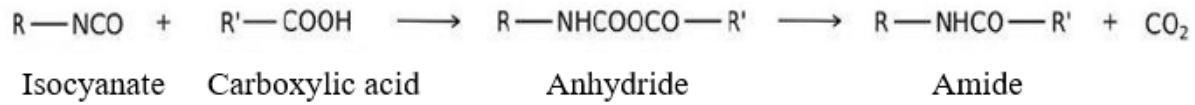


Figure 2.22: Reaction of carboxylic acid with isocyanate

2.11.1.4 Isocyanate reaction with Phenol

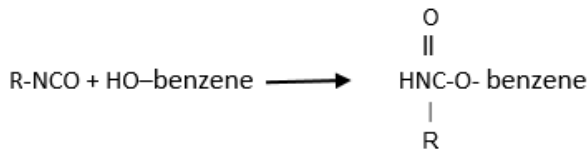


Figure 2.23: Reaction of phenol with isocyanate

Apart from OSB, PMDI application in other wood composites such as plywood and particle board is limited due to its low tack, and over-penetration into wood. Frazier has reported urethane amendment of PMDI to improve with gap-filling problems associated with PMDI (Frazier 2003). Urethane linkage with PMDI could be achieved with bio-based polymers (e.g., soy flour and bio-oil). This can open other markets for pMDI in the composite wood industry.

2.12 Soy Products

Soybeans is made up of about 20% oil, 34% carbohydrates, 40% protein and 4.9% ash (Liu and Li, 2004). The oil is mainly extracted with hexane and the defatted soy flakes or hulls ground into a soy flour (Kuo et al. 20014). Aleem et al. have characterized the composition of defatted soy flour as having 63% protein, 0.8% crude fat, 21% carbohydrates, 6.43% ash and 8% moisture (Aleem et al., 2012). The protein content of this type of defatted soy flour is about half of the total composition. This protein has been reported as a likely primary source of soybean flour adhesive

strength (Malhotra and Coupland, 2004). The carbohydrates consist of complex polysaccharides, including cellulose, hemicelluloses, and pectin and should not be overlooked as a possible adhesive source as well as the carbohydrate-protein Maillard reaction (Dastidar and Netravali 2013). Further protein extraction from the soy flour can be performed to achieve higher protein contents of about 70% protein for soy protein concentrates (SPC) and about 90% protein for soy protein isolates (SPI) (Malhotra and Coupland, 2004).

Approximately, 18 amino acids can be found in soy protein and include acidic amino acids (aspartic acid and glutamic acid), non-polar amino acids (alanine, valine and leucine), basic amino acids (lysine and arginine) and uncharged polar amino acids (glycine). Aspartic acid and glutamic acid account for almost 30% of all amino acids in soy protein (Kumar 2002). Soy protein is primarily a globular protein, of which about 70% consisted of globulin proteins. These globulins are primarily glycinin or conglycinin. Glycinin comprised of six acidic and six basic protein subunits. The subunits alternate in two structural rings partially joined by disulfide bridges. Conglycinin, on the other hand, contains more neutral amino acids and less thiol groups to form disulfide bridges. Instead, the protein subunits were held together by hydrophilic interactions through the polar functional groups referred to above. These separated proteins can make a useful adhesive, but the isolation process can denature and eliminate some of the components needed to crosslink (Frihart et al., 2010).

Soybased-based adhesives were extensively used in the production of wood composites from the 1930s to the 1960s (Yamakawa, 1998). Soy-based adhesives have many advantages, such as low cost and easy handling (Li and Peshkova, 2004). However, wood composite panels bonded with the soy-based adhesives had relatively low strength and low water-resistance, which caused the adhesives to be replaced by formaldehyde-based adhesives. A blend of soy and formaldehyde have

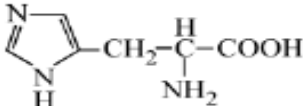
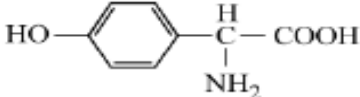
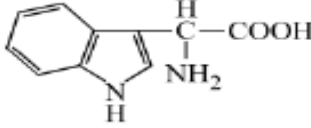
shown a possible reactive side-chain amino acid groups in the proteins, glycinin and conglycinin have been shown to react with formaldehyde (Table 2.3) (Kelly et al, 1977; Tome and Naulet 1981). These reactions improve the crosslinking density, but a drawback arises in the form of additional formaldehyde. The reaction was also easily reversed in moist environments.

The side chains of soy protein can be aliphatic or polar (hydroxyl, thiol, carboxylic, and many nitrogen-containing compounds), although, the backbone structure of the soy protein has a 2-aminoacetic acid. This varies with most adhesives in which there was only one to a few monomers. The primary structure of the protein involved the linear polymer chain of amino acids (Figure 2.24 – bottom left). Crystallites form in the secondary structure due to intra-chain and inter-chain interactions. These interactions form beta-sheets and alpha-helices. The tertiary structure is formed with the folding in of the protein structure due to the intra-chain interactions in an aqueous environment where non-polar side chains minimize their interactions by folding the structure in on their own (Figure 2.24 – top). These interactions are due to hydrophobic, hydrogen bond, salt, and disulfide formation. Inter-chain interactions also play a role in disulfide groups from thiols, acid-base interactions, salt bridges with multivalent cations, and hydrogen bonds.

When the globules formed in the tertiary structures interact with each other, a quaternary structure is formed (Figure 2.24 – top left). These interactions are due to hydrogen bond, hydrophobic, salt, and disulfide formation (Frihart et al., 2010). The quaternary structure is the innate state of soy protein. The quaternary structure obscures a large amount of the active groups that contribute to adhesive bonding through disulfide bridges with thiols, polar bonds such as hydrogen bonds and acids, electrostatic attraction between oppositely charged groups, hydrophobic interactions bases as salt bridges.

Denaturation can expose these groups by unfolding the protein structure to a certain degree. Denaturation breaks the quaternary structure, which was followed by the opening of the tertiary structure, providing more reactive sites contributing to adhesive strength. There is a challenge in not destroying too much of the tertiary structure as this improves the strength of the adhesive (Figure 2.24– top right). There must be a balance between an open structure for reactive sites and a partially intact structure for stability. This can be very challenging when working with soy flour, which only consists of about half proteins (Frihart et al., 2010).

Table 2.5: Amino acids in soy protein with high reactivity (Bjorksten, 1951)

Amino acid	Structure	wt%
Lysine	$\text{H}_2\text{NH}_2\text{CH}_2\text{CH}_2\text{CH}_2\text{C}-\underset{\text{NH}_2}{\overset{\text{H}}{\text{C}}}-\text{COOH}$	6.8
Histidine		3.4
Arginine	$\text{H}_2\text{N}-\overset{\text{NH}}{\parallel}{\text{C}}-\text{NHCH}_2\text{CH}_2\text{CH}_2-\underset{\text{NH}_2}{\overset{\text{H}}{\text{C}}}-\text{COOH}$	7.7
Tyrosine		4.2
Tryptophan		1.3
Serine	$\text{HOH}_2\text{C}-\underset{\text{NH}_2}{\overset{\text{H}}{\text{C}}}-\text{COOH}$	5.4
Cysteine	$\text{HSH}_2\text{C}-\underset{\text{NH}_2}{\overset{\text{H}}{\text{C}}}-\text{COOH}$	2.5
Total		31.3

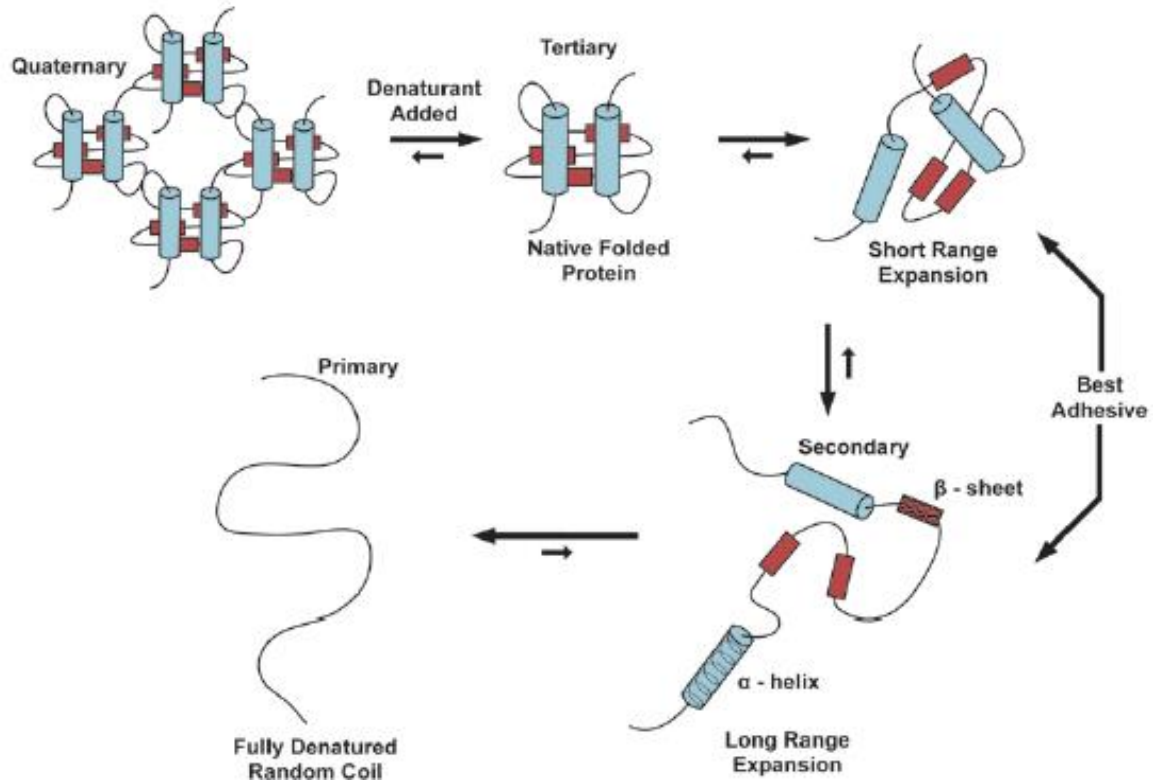


Figure 2.24: Denaturation of the protein structure (Frihart et. al., 2010).

Soy flour also contains soluble and insoluble carbohydrates. Insoluble carbohydrates play a minor role in strengthening the adhesive. The soluble sugars are made up of about 18-30% of the defatted soy flour (Wendler and Frazier, 1996). They are made up of glucose, fructose, sucrose, raffinose, and stachyose. The soluble sugars play a negative role in the use as an adhesive due to an increase in dispersion viscosity, consumption of some of the crosslinker, and increase in water absorption which softens the adhesive under high moisture conditions (Frihart et. al., 2010).

There is renewed interest in soy-based adhesives in recent years because soybean is abundant, inexpensive, and readily available. The crosslinked soy protein can be used as a resin on its own or as a partial substitution with other petroleum-based resins (Pizzi, 2004).

2.13 Adhesion Theory

Adhesion is the adhering of similar or dissimilar types of materials to each other. Polymer molecules are large and fairly bristle with attractive charge sites along their length. The primary forces involved in adhesion and those exclusively involved in cohesion are the results of unlike charge attractions between molecules. The internal forces between molecules that are responsible for adhesion are chemical bonding, dispersive bonding (mostly present in all adhesive systems), and diffusive bonding. These intermolecular forces can make cumulative bonding and bring certain emergent mechanical effects. Adhesion involves both mechanical and chemical factors that control the adhesive's ability to hold together two wood surfaces.

Marra has presented an overview of three potential failure mechanisms with wood adhesives: i) wood/adhesive interface, ii) the adhesive itself, or iii) the wood itself. The different zones linked with the wood and adhesive interaction, as well as the defect associated with the wood/resin interface are depicted in (Figure 2.25) (Marra 1992). Region 1 signifies the pure adhesive. It is considered a cohesive failure in this zone, and the adhesive failure at this zone is considered unsatisfactory. The adhesive boundary is represented by Regions 2 and 3. It is the beginning of the interphase region and it is not homogeneous, and it is considered the beginning of the interphase region. This was the point where the local properties began to change from that of the bulk adhesive to the point where the local properties reflect that of the bulk adherend. Regions 4 and 5 represent the interface of the boundary layer and substrate. This represented the primary adhesive mechanism. Regions 6 and 7 showed areas modified by the adhesive in the wood cell structure where the adhesive penetration mechanism established. In regions 8 and 9, the pure wood dominates and failure in this region is considered satisfactory.

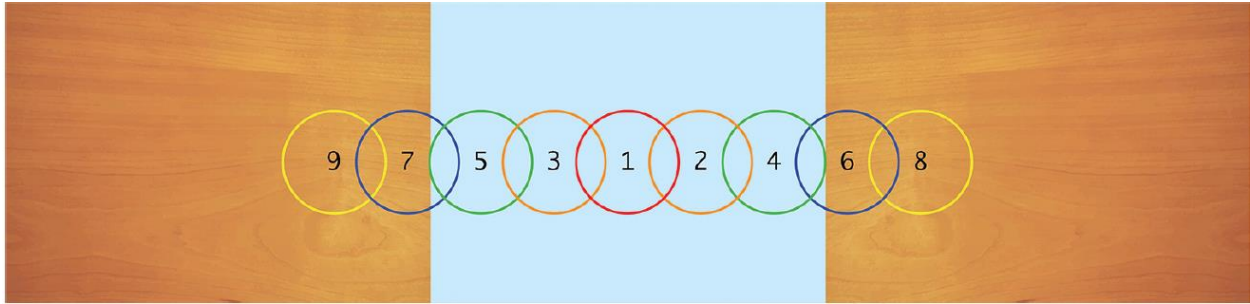


Figure 2.25: Chain link analogy for an adhesive bond in wood proposed by (Marra 1992)

Several theories of adhesion are discussed in literature, namely: mechanical entanglement/interlocking theory, diffusion theory, electronic theory, adsorption/specific adhesion theory, and the covalent bonding theory are discussed. These theories can differ in their contribution to adhesion forces at the adhesive/substrate interface as well as different according to the class of adhesive studied. The mechanical entanglement/interlocking theory of adhesion is mainly influenced via penetration. Therefore a certain amount of adhesive penetration in the first few shallow layers of wood substrate was desirable. Bonded joint strength required two parameters: intrinsic adhesion and energy (viscoelastically and plastically dissipated around the tip of the propagating crack). Mechanical interlocking did not appear to be the main contributor to wood adhesion because thermosetting resins were brittle and cohesive by themselves (Pizzi 1994).

Bond strength dependence on time of contact and resin molecular weight could be explained by the effect of wetting of the substrate surface and that diffusion does not play a significant role in bond formation (Anand 1973; Anand and Karam 1969). The authors assumed that the increase in bond strength was due to an increase in interfacial contact. They believed the mechanism of adhesion depended on the formation of secondary, van der Waals forces across the interface of the adhesive and substrate (adsorption/specific adhesion theory). Polymers that were highly crosslinked (like thermosetting wood adhesives) and polymers that were highly crystalline (like

wood cellulose) were highly unlikely to exhibit interdiffusion as a mechanism of adhesion [44]. The exception would be fiberboard, where elevated levels of moisture, pressure, and long-pressing time lower the glass transition temperature of lignin. Lignin would then be mobilized, and interdiffusion between lignin polymers would contribute to bonding fiberboard together. Secondary forces still appeared to be the primary contributors to adhesion (Pizzi 1994).

The diffusion theory was first advanced by Voyutskii in the early 1960s. The theory proposed a mutual diffusion of polymer molecules across their interface – a polymeric resin and a polymeric substrate (wood) (Voyutskii 1965, 1963). There were two requirements of diffusion: similar solubility parameter values and being amorphous. A high degree of crystallinity tends to resist dissolving in a solvent, and there must be sufficient mobility (Pizzi, 2003). Wood is not a homogeneous polymer; it is made up of three polymers. This means that there are three different solubility parameters with the resin. Cellulose is crystalline and amorphous, while hemicellulose and lignin were amorphous. Diffusion could be thought of as a molecular level of mechanical interlocking, but a small molecular weight was required to flow in the wood cell walls (Frihart, 2004).

The electronic theory of adhesion was pioneered by Deryaguin and others (Deryaguin et al. 1957). The theory states that an electron transfer upon contact if the substrate and adhesive had different electronic band structures promote a double layer of electrical charges at the interface – contributing significantly to adhesion (Deryaguin and Smilga 1969). Roberts's experiments displayed a contribution from the electrical double layer at a rubber-glass interface of about 10^{-5} mJ/m² – negligible to van der Waals forces at 60 mJ/m². (Roberts, 1977). Electrostatic forces were more likely to occur in debonding rather than bond forming (Frihart, 2004).

The adsorption/specific adhesion theory suggests that an adhesive adhered to a substrate due to the intermolecular and interatomic forces between atoms and molecules of the two materials Pizzi (2003). Adhesion of wood is complicated by the role of hydrogen bonds, electrostatic interactions, and van der Waals interactions. Electrostatic interactions tended to be repulsive and quite insignificant compared to van der Waals and hydrogen bonds between PF and cellulose from the wood substrate (Table 2.4). The dielectric constant of water is considered due to residual moisture of wood. Pizzi concluded secondary chemical bonds are the dominant mechanism for bonding wood.

Table 2.6: Relative contributions (kcal/mol) of van der Waals, hydrogen bonds, and electrostatic secondary forces to the adhesion of species from a PF resin to wood cellulose (Pizzi 2003).

	Van der Waals	Hydrogen bonds	Electrostatic	Total energy of cellulose- phenol interaction
<i>o</i> -Monomethylol phenol	-12.60	-0.23	0.64	-12.190
<i>p</i> -Monomethylol phenol	-10.77	-0.46	0.66	-10.567
<i>o,o</i> -Dimethylol phenol	-10.45	-0.77	0.67	-10.550
<i>o,p</i> -Dimethylol phenol	-12.47	-10.00	0.65	+3.119
PF dimers				
<i>o,o</i> -Dimer	-5.34	-7.75	0.77	-12.329
<i>o,p</i> -Dimer	-7.00	-5.81	0.73	-12.080
<i>p,p</i> -Dimer	-6.51	-4.37	0.68	-10.203

^aNegative values indicate attractive secondary forces; positive values indicate repulsive secondary forces.

Under normal conditions, the formation of covalent bonds between adhesive and wood substrates has never been observed (We 1989). It is either not present or undetectable because there is a low proportion of covalent bonds compared with other bonds. Therefore, the author concludes that covalent bonding between resin and wood is either absent or negligible.

Polymeric diphenyl methane diisocyanate (pMDI) had been assumed to covalently bond with the hydroxyls of the wood substrate, but We (1989) concludes that there is no covalent bonding between pMDI and the wood substrate due to the more likely reaction of pMDI with water. The reaction of isocyanates from pMDI with water to form polyurea proceeds at $7.4 \times 10^{-6} \text{ L mol}^{-1} \text{ s}^{-1}$, while hydroxyls from wood carbohydrates to form polyurethane proceeds at $2 \times 10^{-7} \text{ L mol}^{-1} \text{ s}^{-1}$, and aliphatic hydroxyl groups such as is found in lignin to form polyurethane proceeded at $6 \times 10^{-6} \text{ L mol}^{-1} \text{ s}^{-1}$. This demonstrates that isocyanates are more likely to react with water to form polyurea rather than with hydroxyls from wood to form polyurethane. Polyurea from the reaction of pMDI and water are shown to adhere to the wood substrate by secondary forces alone (Frisch et al. 1983). The adsorption/specific adhesion theory claims that an adhesive adheres to a substrate due to the intermolecular and interatomic forces between atoms and molecules of the two materials (Pizzi 1994). Pizzi (1994) concludes that intermolecular and interatomic forces such as hydrogen bonds, electrostatic interactions, and van der Waals interactions are the dominant mechanism for bonding wood.

2.14 Press Theory

Hot pressing is essential in wood composite manufacturing. The overall board properties is in part, greatly influenced by the press parameters such as temperature, time and pressure. The main transport mechanism of hot pressing is heat and mass transfer. The heated press platens evaporate the bound water of wood strands at the surface during the initial stage of pressing. This built-up vapor pressure that drives the evaporated water to the cold center of the mat. This vapor would then condense in the cold mat center. The core temperature would gradually increase, and the water in the core would eventually vaporize. The increased vapor pressure would then drive the vapor to the surface or outside the boundary of the mat and exit the mat (Zombori et al. 2001).

The steam flow assists heat transport but would diminish as the water content of the mat gets depleted. The rate of moisture and heat transfer depends on the structure geometry of the mat and how it is changed during the compression. A void volume occurs as a result of the compression process and wood particle geometry that always changes and creates a pathway for fluid flow. Thermal conductivity, permeability, and diffusivity of the mat changes during the pressing process.

It should be noted that when the moisture content of the mat is very high and the press time is short to allow the generated heat to escape from the core of the mat, pressure builds up at the panel core. Upon opening the press with the stress released, the wood particles begin to relax and delamination or blow is often seen at the core of the pressed panels.

2.15 References

1. Akhtar, J., & Amin, N. A. S. (2011). A review on process conditions for optimum bio-oil yield in hydrothermal liquefaction of biomass. *Renewable and Sustainable Energy Reviews*, 15(3), 1615–1624. <https://doi.org/10.1016/j.rser.2010.11.054>
2. Aleem Zaker MD, Genitha TR, Hashmi SI (2012) Effects of Defatted Soy Flour Incorporation on Physical, Sensorial and Nutritional Properties of Biscuits. *J Food Process Technol* 3:149. doi:10.4172/2157-7110.1000149
3. Auvergne, R., S. Caillol, G. David, B. Boutevin, and J. P. Pascault. 2014. Biobased Thermosetting Epoxy: Present and Future. *Chemical Reviews* 114:1082-1115.
4. Basu, P. *Biomass Gasification, Pyrolysis and Torrefaction: Practical Design and Theory*; Academic Press: Cambridge, MA, USA, 2018.
5. Beutel, P., 1996. The Manufacturing Process Medium Density Fibreboard. [Online] Available at: <http://fennerschool-associated.anu.edu.au/fpt/mdf/manufacture.html> [Accessed 1 June 2019]. Breyer,
6. Ben, H., and Ragauskas, A. J. (2011). NMR Characterization of Pyrolysis Oils from Kraft Lignin. *Energy & Fuels*, 25(5), 2322–2332. <https://doi.org/10.1021/ef2001162>
7. Bjorksten, J. “Cross linkages in protein chemistry,” *Adv. Protein Chem.*, vol. 6, pp. 343–381, 1951.
8. Boquillon, N., Elbez, G., Schonfeld, U., 2004. Properties of wheat straw particleboards bonded with different types of resin. *Journal of Wood Science* 50, 230-235.
9. Bowyer, J.L., Shmulsky, R., Haygreen, J.G., 2007. *Forest products and wood science: an introduction*. Wiley-Blackwell.
10. Bradley, W., J. Forrest, and O. Stephenson. 1951. 359. The catalysed transfer of hydrogen chloride from chlorohydrins to epoxides. A new method of preparing glycidol and some of its derivatives. *Journal of the Chemical Society (Resumed)*:1589-1598.
11. Bridgwater, A. V. (2010). Fast pyrolysis of biomass for energy and fuels. In *RSC Energy and Environment Series (Vol. 2010, Issue 1)*. <https://doi.org/10.1039/9781849732260-00146>

12. Bridgwater, A. V. (2012). Review of fast pyrolysis of biomass and product upgrading. *Biomass and Bioenergy*, 38, 68–94. <https://doi.org/10.1016/j.biombioe.2011.01.048>
13. Bridgwater, A. V., & Peacocke, G. V. C. (2000). Fast pyrolysis processes for biomass. *Renewable and Sustainable Energy Reviews*. [https://doi.org/10.1016/S1364-0321\(99\)00007-6](https://doi.org/10.1016/S1364-0321(99)00007-6)
14. Bridgwater, A. V. (1999). “An introduction to fast pyrolysis of biomass for fuels and chemicals,” in *Fast Pyrolysis of Biomass: A Handbook*. CPL Press, Newbury, UK. pp1-13. Chan, F., Riedl,
15. Chapman, K. M. (2004). *A Study of Two Aspects of Medium Density Fibreboard Manufacturing (Issue March)*. University of Canterbury.
16. Chen, Z., Ning Y., Pau C., 2008. “Predicting Performance of Oriented Strandboard under Concentrated Static Loading Conditions Using Finite Element Modeling.” *Wood and Fiber Science* 40(4):505–18.
17. Collard F-X, Blin J. A review on pyrolysis of biomass constituents: mechanisms and composition of the products obtained from the conversion of cellulose, hemi- celluloses and lignin. *Renewable Sustainable Energy Rev* 2014;38 (Supplement C):594–608.
18. CPA. (2009b). *Medium density fiberboard (MDF)*. ANSI A 208.2–2009. Leesburg, VA: Composite Panel Association.
19. Czernik, S., & Bridgwater (2013), A. V. (2004). Overview of Applications of Biomass Fast Pyrolysis Oil. *Energy & Fuels*, 18(2), 590–598. <https://doi.org/10.1021/ef034067u>
20. Dastidar, T. G. and A. N. Netravali, “A soy flour based thermoset resin without the use of any external crosslinker,” *Green Chem.*, vol. 15, no. 11, pp. 3243–3251, 2013.
21. Dettmer, J. (2013). *Properties Comparison of North American Manufactured Particleboard and Medium Density a Thesis Submitted in Partial Fulfilment of the Requirements for the Degree of. November.*
22. Dunky M. (2003). *Adhesives in the Wood Industry*. Dynea Austria GmbH, Krems, Austria. DOI: 10.1201/9780203912225.ch47
23. Ellis, B. (2012). *Chemistry and Technology of Epoxy Resins*. Springer Netherlands.

24. Elliott, D. C., P. Biller, A. B. Ross, A. J. Schmidt, and S. B. Jones. (2015). Hydrothermal liquefaction of biomass: Developments from batch to continuous process. *Bioresource Technology* 178:147-156.
25. Frihart, C. R. (2005). Adhesive bonding and performance testing of bonded wood products. *Journal of ASTM International*, 2(7), 455–466. <https://doi.org/10.1520/JAI12952>
26. Frihart, C. R. M. J. Birkeland, A. J. Allen, and J. M. Wescott, “Soy Adhesives that Can Form Durable Bonds for Plywood , Laminated Wood Flooring , and Particleboard,” *Proc. Int. Conv. Comm. Eur. – Timber Comm.* Oct. 11-14, 2010, Geneva, Switz., no. August, pp. 1–13, 2010.
27. Frihart, C. R. “Adhesive interaction with wood,” *Fundam. Compos. Process. Proc. a Work.*, pp. 29–54, 2004.
28. Gagliano, J. and Frazier, C. (2001). Improvements in the fracture cleavage testing of adhesively-bonded wood. *Wood and Fiber Science*. 33(3):377–385.
29. Grand View Research. (2019). Oriented Strand Board Market Size, Share & Trends Analysis Report By Application, (Construction, Packaging), By Region, (Central & South America, North America, MEA, APAC, Europe), And Segment Forecasts, 2019 - 2025. 3–9.
30. Grand View Research (2020). Medium Density Fiberboard Market Size, Share & Trends Analysis Report By Product (Standard MDF, Moisture Resistant MDF), By Application (Furniture, Construction), By Region, And Segment Forecast, 2020 – 2027 Available: <https://www.grandviewresearch.com/industry-analysis/medium-density-fiberboard-market> [Accessed: June 24, 2020].
31. Haynes, R.W. Technical Coordinator.2003. An analysis of the timber situation in the United States: 1952–2050: A technical document supporting the 2000 USDA Forest Service RPA Assessment. General Technical Report PNW–GTR– 560. U.S. Department of Agriculture, Forest Service, Pacific Northwest Research Station, Portland, Oregon.
32. Hermawan, A., Ohuchi, T., Fujimoto, N., Murase, Y., 2009. Manufacture of composite board using wood prunings and waste porcelain stone. *Journal of Wood Science* 55, 74–79.
33. Kamke, F. and Lee J. (2007). Adhesive penetration in wood: a review. *Wood and Fiber Science*.27 39(2):205–220.

34. Kersten S.R.A., Wang X., Prins W., van Swaaij W.P.M. Biomass pyrolysis in a fluidized bed reactor. Part 1: literature review and model simulations. *Ind. Eng. Chem. Res.*, 44, 8773- 8785, 2005.
35. Kelly, D. P. M. K. Dewar, R. B. Johns, S. Wei-Let, and J. F. Yates, "Cross-linking of amino acids by formaldehyde. Preparation and ¹³C NMR spectra of model compounds," in *Protein Crosslinking*, Springer, 1977, pp. 641–647.
36. Kosinkova, J., J. A. Ramirez, J. Nguyen, Z. Ristovski, R. Brown, C. S. K. Lin, and T. J. Rainey. 2015. Hydrothermal liquefaction of bagasse using ethanol and black liquor as solvents. *Biofuels, Bioproducts and Biorefining*. DOI: 10.1002/bbb.1578.
37. Krammer, P. and H. Vogel. 2000. Hydrolysis of esters in subcritical and supercritical water. *The Journal of Supercritical Fluids* 16:189-206.
38. Kumar, R., et al., Adhesives and plastics based on soy protein products. *Industrial Crops and Products*, 2002. 16(3): p. 155-172.
39. Kuo, P. Y., Sain, M., & Yan, N. (2014). Synthesis and characterization of an extractive-based bio-epoxy resin from beetle infested *Pinus contorta* bark. *Green Chemistry*, 16(7), 3483–3493. <https://doi.org/10.1039/c4gc00459k>
40. Lange, Jean Paul. 2018. "Lignocellulose Liquefaction to Biocrude: A Tutorial Review." *ChemSusChem* 11(6):997–1014.
41. Li, K., S. Peshkova, and X. Geng, Investigation of soy protein-Kymene adhesive systems for wood composites. *Journal of the American Oil Chemists' Society*, 2004. 81(5): p. 487-491.
42. Liu, Y. and K. Li, Modification of soy protein for wood adhesives using mussel protein as a model: The influence of a mercapto group. *Macromolecular Rapid Communications*, 2004. 25(21): p. 1835-1838.
43. Liu, Yan, Yuan, X. Z., Huang, H. J., Wang, X. L., Wang, H., & Zeng, G. M. (2013). Thermochemical liquefaction of rice husk for bio-oil production in mixed solvent (ethanol-water). *Fuel Processing Technology*. <https://doi.org/10.1016/j.fuproc.2013.03.005>
44. Liu, Yi, Via, B. K., Pan, Y., Cheng, Q., Guo, H., Auad, M. L., & Taylor, S. (2017). Preparation and characterization of epoxy resin cross-linked with high wood pyrolysis bio-oil substitution by acetone pretreatment. *Polymers*, 9(3). <https://doi.org/10.3390/polym9030106>

45. Malhotra A. and J. N. Coupland, "The effect of surfactants on the solubility, zeta potential, and viscosity of soy protein isolates," *Food Hydrocoll.*, vol. 18, no. 1, pp. 101–108, 2004.
46. Maloney, T.M., 1993. *Modern particleboard and dry-process fiberboard manufacturing*. Miller Freeman Incorporated.
47. Marcinko J. J., W. H. Newman, C. Phanopoulos, and M. A. Sander, *Proc. 29th Washington State University Int. Particleboard/Composite Materials Symposium, Pullman, WA, 1995*, pp. 175–183.
48. Marra, A. A. *Technology of wood bonding*. Van Nostrand Reinhold, 1992.
49. Mohan, D., Pittman, C. U., & Steele, P. H. (2006). Pyrolysis of Wood/Biomass for Bio-oil: A Critical Review. *Energy & Fuels*, 20(3), 848–889. <https://doi.org/10.1021/ef0502397>
50. Mullen, C. A., & Boateng, A. A. (2008). Chemical Composition of Bio-oils Produced by Fast Pyrolysis of Two Energy Crops †. *Energy & Fuels*, 22(3), 2104–2109. <https://doi.org/10.1021/ef700776w>
51. Nemli, G., Demirel, S., Gümüşkaya, E., Aslan, M., Acar, C., 2009. Feasibility of incorporating waste grass clippings (*Lolium perenne* L.) in particleboard composites. *Waste Management* 29, 1129–1131.
52. Nemli, G., Yildiz, S., Derya Gezer, E., 2008. The potential for using the needle litter of Scotch pine (*Pinus sylvestris* L.) as a raw material for particleboard manufacturing. *Bioresource technology* 99, 6054–6058.
53. Okada, H., T. Tokunaga, X. Liu, S. Takayanagi, A. Matsushima, and Y. Shimohigashi. 2008. Direct Evidence Revealing Structural Elements Essential for the High Binding Ability of Bisphenol A to Human Estrogen-Related Receptor- γ . *Environmental Health Perspectives* 116:32-38.
54. Ouyang, X., X. Huang, Y. Zhu, and X. Qiu. 2015. Ethanol-Enhanced Liquefaction of Lignin with Formic Acid as an in Situ Hydrogen Donor. *Energy & Fuels* 29:5835-5840.
55. Ponder, Glenn R. and Geoffrey N. Richards. 1994. "A Review of Some Recent Studies on Mechanisms of Pyrolysis of Polysaccharides." *Biomass and Bioenergy* 7(1–6):1–24.
56. Feasibility of a Billion-Ton Annual Supply. *Agriculture*, 59. http://www1.eere.energy.gov/biomass/pdfs/final_billionton_vision_report2.pdf
57. Pham, H. Q. and M. J. Marks. 2000. Epoxy Resins. *Ullmann's Encyclopedia of Industrial Chemistry*. Wiley-VCH Verlag GmbH & Co. KGaA.
58. Pizzi, A. *Advanced wood adhesives technology*. CRC Press, 1994.

59. Pizzi, A., Mittal, K., & Dunky, M. (2003). Adhesives in the Wood Industry. In Handbook of Adhesive Technology, Revised and Expanded (Issue August 2003). <https://doi.org/10.1201/9780203912225.ch47>
60. Pu, Y., Cao, S., & Ragauskas, A. J. (2011). Application of quantitative ³¹P NMR in biomass lignin and biofuel precursors characterization. *Energy and Environmental Science*, 4(9), 3154–3166. <https://doi.org/10.1039/c1ee01201k>
61. Ratna, D., Modification of epoxy resins for improvement of adhesion: a critical review. *Journal of Adhesion Science and Technology*, 2003. 17(12): p. 1655-1668.
62. Rowell, R. M. (2012). Handbook of wood chemistry and wood composites, second edition. In Handbook of Wood Chemistry and Wood Composites, Second Edition. <https://doi.org/10.1201/b12487>
63. Ruffing, T. C., Smith, P. M., & Brown, N. R. 2010. Resin Suppliers Perspective on Greening the NA Interior Wood Composites Market. *Forest Products J.*, 60(2), 119-125.
64. Stark M. N., Cai Z., Carll C. (2010). Wood handbook—Wood as an engineering material. General Technical Report FPL-GTR-190. Madison, WI: U.S. Department of Agriculture, Forest Service, Forest Products Laboratory. 508 p.
65. Soltes E and Elder T. Pyrolysis (1981). In: IS Goldstein (ed.), *Organic Chemicals from Biomass*. CRC Press.
66. Sun, L., Wang, F., Xie, Y., Feng, J., & Wang, Q. (2012). The combustion performance of medium density fiberboard treated with fire retardant microspheres. *BioResources*, 7(1), 593–601. <https://doi.org/10.15376/biores.7.1.0593-0601>
67. Tome D. and N. Naulet, “Carbon 13 Nuclear Magnetic Resonance Studies on Formaldehyde Reactions with Polyfunctional Amino Acids,” *Chem. Biol. Drug Des.*, vol. 17, no. 4, pp. 501–507, 1981.
68. Toor, S. S., Rosendahl, L., & Rudolf, A. (2011). Hydrothermal liquefaction of biomass: A review of subcritical water technologies. *Energy*, 36(5), 2328–2342. <https://doi.org/10.1016/j.energy.2011.03.013>
69. Tsubaki, S., Nakasako, Y., Ohara, N., Nishioka, M., Fujii, S., & Wada, Y. (2020). Ultra-fast pyrolysis of lignocellulose using highly tuned microwaves: Synergistic effect of a cylindrical cavity resonator and a frequency-auto-tracking solid-state microwave generator. *Green Chemistry*, 22(2), 342–351. <https://doi.org/10.1039/c9gc02745a>

70. Uddin, M. N., Techato, K., Taweekun, J., Rahman, M. M., Rasul, M. G., Mahlia, T. M. I., & Ashrafur, S. M. (2018). An overview of recent developments in biomass pyrolysis technologies. *Energies*, 11(11). <https://doi.org/10.3390/en11113115>
71. Vasilakos, N. P. and D. M. Austgen. 1985. Hydrogen-donor solvents in biomass liquefaction. *Industrial & Engineering Chemistry Process Design and Development* 24:304-311.
72. Venderbosch, RH and W. Prins. 2010. "Fast Pyrolysis Technology Development." *Biofuels, Bioproducts and Biorefining* 6(3):181–208.
73. Vlosky, R. P., & Rouge, B. (2017). Industry trends, OSB Forecast. January.
74. vom Saal, F. S. and J. Myers. 2008. BIsphenol A and risk of metabolic disorders. *JAMA* 300:1353-1355.
75. Wang, S., Dai, G., Yang, H., & Luo, Z. (2017). Lignocellulosic biomass pyrolysis mechanism: A state-of-the-art review. *Progress in Energy and Combustion Science*, 62, 33–86. <http://doi.org/10.1016/j.pecs.2017.05.004>.
76. Wang, B., X. M., Lu, X., Amen-Chen, C., & Roy, C. (2002). Performance of pyrolysis oil-based wood adhesives in OSB. *Forest Products Journal*, 52(4), 31–38.
77. Wang, D., Sun, X.S., 2002. Low density particleboard from wheat straw and corn pith. *Industrial Crops and Products* 15, 43-50.
78. Wang, F. "Polydimethylsiloxane Modification of Segmented Thermoplastic Polyurethanes and Polyureas," 1998.
79. We, J. (1989). The chemical bonding of wood. *Wood Adhesive Chemistry and Technology*, Vol 2. Marcel Dekker, New York, NY.
80. Yamakawa, K., development of Urea-melamine-formaldehyde Resin Adhesive for Bonding Tropical Hardwood, in *Adhesive Technology and Bonded Tropical Wood Products*. 1998: Taipei, Taiwan.
81. Youngquist, J.A. (1999), *Wood-based Composites and Panel Products*, *Wood Handbook*: pp. 31.
82. Yuan, X. Z., Li, H., Zeng, G. M., Tong, J. Y., & Xie, W. (2007). Sub- and supercritical liquefaction of rice straw in the presence of ethanol-water and 2-propanol-water mixture. *Energy*, 32(11), 2081–2088. <https://doi.org/10.1016/j.energy.2007.04.011>
83. Zerbe, J. I., Cai, Z., & Harpole, G. B. (2015). An Evolutionary History of Oriented Strandboard (OSB). USDA Forest Service, Forest Products Laboratory, General Technical

Report, FPL-GTR-236, 2015; 10 P., 236(February), 1–10. <https://doi.org/10.2737/FPL-GTR-236>

84. Zheng, J., Fox, S. C., & Frazier, C. E. (2004). Rheological, wood penetration, and fracture performance studies of PF/pMDI hybrid resins. *Forest Products Journal*, 54(10), 74–81.
85. Zombori, B. G. F. A. Kamke, and L. T. Watson, “Simulation of the Mat Formation Process,” *Wood Fiber Sci.*, vol. 33, pp. 564–579, 2001.

Chapter 3

Elucidation of the effect of Fast Pyrolysis and Hydrothermal Liquefaction on the Physico-chemical properties of Bio-oil from Loblolly Pine Biomass

3.1 Abstract

Bio-oils obtained from loblolly pine biomass from two thermochemical conversion processes, fast pyrolysis and hydrothermal liquefaction (HTL), were investigated. Water/ethanol mixture (1/1, wt/wt) was used as a liquefying solvent in the HTL process at 300 °C, and the pyrolysis bio-oil was produced at 450 °C. The effect of FP and HTL on the physical and chemical properties of the bio-oils were characterized. The water/ethanol co-solvent used improved the bio-oil yield and reduced char yield relative to the FP process. Also, the results indicated that the physico-chemical properties of HTL bio-oil and pyrolysis bio-oil were similar. However, there were variations in the composition of the bio-oils from the same biomass. The studies found low ash content of 0.01 and pH of 2.3 ± 0.5 for both FP and HTL bio-oils. From the GC-MS analysis, esterified chemical compounds dominated the HTL bio-oil, while a substantial amount of phenols and phenolic derivatives were found in the FP bio-oil. The bio-oil analysis further revealed that the FP and HTL bio-oils are rich in phenolic OH and aliphatic OH functionalities, which could serve as a potential bio-polyol.

3.2 Introduction

Recent environmental impacts and concerns from fossil-derived energy and chemicals have heightened the interest in environmental-friendly alternatives. Paramount among the renewable natural alternatives is lignocellulosic biomass, which has been shown as a potential substitute (Palizdar and Sadrameli 2020; Mathanker et al. 2020; Chiodo et al. 2016; Mohan et al. 2006;

Scholze and Meier 2001). This is because lignocellulosic biomass is abundant, relatively cheap, inherently CO₂ neutral, renewable, and ecologically robust to withstand sustainable use. According to the US Department of Energy (DOE) report, 368 million dry tons of lignocellulosic biomass could sustainably be fetched from US forestlands annually (Perlack et al. 2005). To maximize the potential of lignocellulosic biomass as a fuel and chemical feedstock, different techniques have been researched, namely: thermochemical conversion (e.g. direct combustion, pyrolysis gasification and, liquefaction) and bioprocesses (e.g. fermentation and enzymatic reaction) (Ni et al. 2006; Bridgwater and Peacocke 2000). Besides being able to degrade most of the biomass polymers into complex mix monomers, the thermochemical process is generally considered efficient in terms of processing time, which takes few seconds to minutes as against bioprocess, which could take days or even weeks (Bridgwater, 2010).

Of the thermochemical conversion processes, fast pyrolysis (FP) and hydrothermal liquefaction (HTL) have received considerable attention as a viable route to bio-based chemicals and liquid fuels. FP process relies on the thermal decomposition of the polymers in biomass in the absence of oxygen. Relatively high temperatures (450 °C–500 °C), usually at atmospheric pressure with short residence time (~1-2s) are employed. FP technique is considered as a simple process relatively easy to scale up, requiring low capital and investment cost (Jo et al., 2018). However, drying of feedstock before pyrolysis is essential and dis-incentive at the same time. On the other hand, HTL is conducted at relatively high pressure (5-20 MPa) with temperature ranging from ~ 250 to 400 °C at ~ 12 to 60 minutes of residence time. Unlike FP, HTL utilizes water as a solvent in its operation, thus, obviating the need for drying, thereby accommodating wet biomass. Detailed reviews regarding FP and HTL processes could be found in the literature (Gollakota et al. 2018;

Uddin et al. 2018; Kruse and Dahmen 2015; Tekin, et al. 2014; Akhtar and Amin 2011; Jahirul et al. 2012; Toor et al. 2011; Peterson et al. 2008; Mohan et al. 2006)

FP and HTL processes produce gases, solids (char) and liquids (bio-oil). The distribution and composition of bio-oil, char and gaseous fractions formed depend mostly on the feedstock and processing parameters such as pre-treatment, temperature, heating rate, carrier gas, pressure, post-treatments etc. (Hu et al. 2019; Karagöz et al. 2006; Yaman 2004). The applications and utilization of char and gaseous products of FP and HTL can be found elsewhere (Borsodi et al. 2016; Laird et al. 2009). The scope of this study covers bio-oil only.

Bio-oil refers to the liquid product of pyrolysis and thermochemical liquefaction of biomass. Bio-oil is considered an invaluable thermochemical product to rival petroleum crude oil. Potential applications of bio-oil include fuel in engines and turbines (Yang et al., 2014). Phenols in bio-oil have been successfully incorporated into adhesives like phenol formaldehyde (Chaouch et al., 2014). Detailed application of bio-oil is discussed in literature (Czernik & Bridgwater, 2004). The physical properties of bio-oil, such as viscosity and pH play a major role in bio-oil end-use. For instance, low pH of bio-oil could catalyze novalac type adhesives. Oxygenated compounds present in bio-oil is known to affect its physical properties. Undesirable challenges such as low heating value, polymerization tendencies during storage, increased viscosity and fossil fuels mixing incompatibility are linked to oxygenates in bio-oil (Imam and Capareda 2012; Mullen and Boateng 2008).

While FP and HTL processes yield bio-oil as the end product, the physical and chemical properties of the bio-oil may vary depending on the processing. In order to compare the effect of FP and HTL on the composition of bio-oil, the same feedstock should be used in the process. Studies on the

characterization of bio-oil produced by HTL and FP using the same biomass is limited. The available literature has focused on algae (Chiaramonti et al. 2017; Hognon et al. 2015; Vardon et al. 2012; Jena and Das 2011) and there are only one of such studies on lignocellulosic biomass (beech, which is a hardwood), to our knowledge (Haarlemmer et al., 2016). Interestingly, different chemical composition and physical properties from the same biomass were reported from these studies. To the best of our knowledge, there is no studies evaluating FP, and HTL using water/ethanol as co-solvent. Haarlemmer et al. used NaOH as a catalyst in the HTL of beech biomass studies. In addition, this is the first work employing ^{31}P NMR in quantifying and elucidating the distribution of hydroxyl (OH) moieties in bio-oil obtained from pyrolysis and HTL from the same biomass. Characterization of the OH functionalities could be used to track bio-oil aging and also aids in the efficient utilization of bio-oil as a biopolyol (Celikbag et al., 2015). Therefore, the aim of this paper is to assess loblolly pine bio-oils from FP and HTL using water/ethanol as co-solvent and to characterize the effect of FP and HTL on the physical and chemical properties of bio-oil.

3.3 Materials and Methods

3.3.1 Materials

Loblolly pine biomass was used as feedstock for both the FP and the HTL processes. The feedstock was sourced from a local chipping plant in Starkville, Mississippi. Standard wet chemistry biomass protocol analysis from the National Renewable Energy Laboratory (NREL LAP, TP510-42618) was used to determine the composition (cellulose hemicelluloses, lignin and extractives) of the biomass. Loblolly pine chips were air-dried to 8-10% moisture content. In a hammer mill (New Holland grinder model 358, PA), the wood chips were ground, and the sawdust was sieved with a sieve shaker, and the pine particles retained between 0.3 and 0.5mm were used for both FP and HTL bio-oil production. Chemicals used in this study were purchased from VWR as reagent grade.

However, the 2-chloro-4,4,5,5-tetramethyl-1,3,2-dioxaphospholane (TMDP) and phosphorylating agent for ^{31}P -NMR analysis were purchased from Sigma Aldrich. The chemicals were used as received from vendors.

3.3.2 Hydrothermal liquefaction Process

Loblolly pine liquefaction by HTL process was made in a 1 L Parr reactor furnished with a stirrer (Model 4577 HP/HT pressure reactor, Parr Instrument Company, Moline, IL, USA) and controller. In a typical run, the reactor was charged with 50 g of loblolly pine saw dust (and 500 g of solvent (1/10: Biomass/solvent)). The solvent used comprised of water/ethanol mixture (1/1, wt/wt). The weight of the sample with the reactor was recorded (M1). After sealing the reactor, nitrogen gas was introduced into the reactor to displace the remaining air. The reactor was pressurized with nitrogen gas to 2 MPa and heated up to 300 °C with constant stirring. From the controller, the temperatures with its corresponding pressure profiles were recorded, and a typical run is shown in Figure 3.2. The reaction temperature was kept for 30 min, when the set temperature was reached. The reactor was submerged in a water/ice bath to terminate the liquefaction reaction process after the 30min. A schematic diagram of the Parr reactor is shown in Figure 3.1

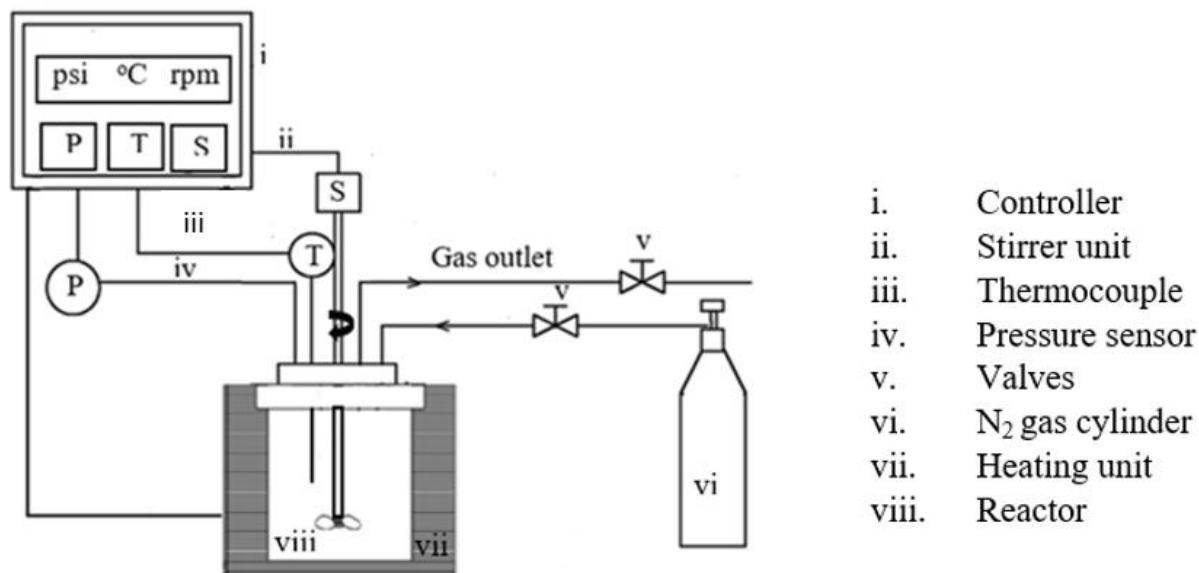


Figure 3.1: Schematic diagram of reactor for hydrothermal liquefaction.

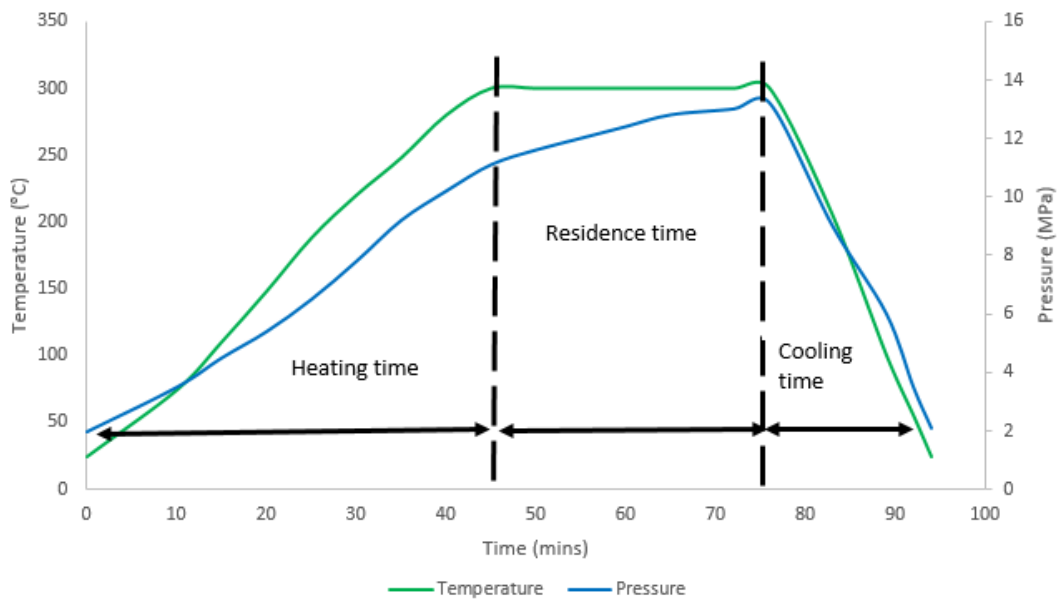


Figure 3.2: Temperature – pressure profile of HTL process at 300 °C

3.3.3 Separation of HTL Products and Yield Calculation

The cooling of the reactor discontinued when it reached room temperature. Before the reactor was opened, gas products built in the reactor were first released. The liquefied wood in the reactor (LW) was then weighed (M_2), and the gas yield computed as in equation 1. The LW was transferred into a beaker and dichloromethane (DCM) was used to rinse the residual components from the reactor. 500 mL of DCM was added to the LW and the diluted LW vacuum filtered with Whatman#5 filter paper. An additional 100 mL of DCM was used to wash the solid part remaining on the filter paper. The washed solids (residue) were then oven-dried at 100 °C, and the residue content evaluated from equation 2. A separatory funnel was used to separate the filtrate into the aqueous phase (light oil) and organic phase (dark oil) as DCM. The organic phase was collected into a flask and then transferred into a rotary evaporator. Water/ethanol remnant and DCM were removed from the organic phase by rotary evaporation at 65 °C under vacuum. Further analysis of the gas yield, residue, and the “light-colored” aqueous phase was not carried out in this experiment as it is not the main focus of this present study. The remaining dark viscous liquid was christened “bio-oil” and from this, all further analysis was based. Bio-oil yield and light oil yield were calculated using equations 3 and 4, respectively. The mass balance yields for gas bio-oil, light oil, and residue were defined as weight percentages relative to the dry biomass used.

$$\text{Gas yield (wt\%)} = \frac{M_1 - M_2}{\text{Weight of biomass}} \times 100 \quad \text{equation (1)}$$

$$\text{Bio-oil yield (wt\%)} = \frac{\text{Bio-oil weight after rotary evaporation}}{\text{Weight of biomass}} \times 100 \quad \text{equation (2)}$$

$$\text{Residue yield (wt\%)} = \frac{\text{dried solid products}}{\text{Weight of biomass}} \times 100 \quad \text{equation (3)}$$

$$\text{Light oil yield (wt\%)} = 100 - (\text{Bio-oil} + \text{Residue} + \text{Gas}) \text{ Yield} \quad \text{equation (4)}$$

3.3.4 Fast Pyrolysis Process

Fast Pyrolysis bio-oil was made from the same loblolly pine wood dust but further dried using a similar manner mentioned in a previous study (Li et al., 2013) without any spraying of chemicals or water to cool the vapors. Fast pyrolysis reactions of untreated loblolly pine were conducted in a 7 kg h^{-1} auger-fed pyrolysis reactor at Mississippi State University (MSU). Nitrogen gas was used to exclude oxygen from the system at the feed hopper. Pyrolysis reactions occurred in a reactor pipe 76.2 mm in diameter and 1143 mm long. The auger speed was 10 rpm at the applied pyrolysis temperature of $450 \text{ }^{\circ}\text{C}$ with a gas residence time of approximately 2 s. The heat for the pyrolysis reactions was provided by multiple heaters along the reactor pipe, including a preheating zone ($300 \text{ }^{\circ}\text{C}$), a pyrolysis zone ($450 \text{ }^{\circ}\text{C}$) and a post-reaction zone ($300 \text{ }^{\circ}\text{C}$). A schematic of the reactor can be seen in Figure 3.3.

3.3.5 Distillation

The bio-oil produced from each condenser was mixed and referred to as whole bio-oil (collected at a range of 25oC - $350 \text{ }^{\circ}\text{C}$). There was a separate collection from another run where bio-oil was collected from condenser 3 at a temperature range of 30 - $120 \text{ }^{\circ}\text{C}$ (referred to as “aqueous bio-oil”). The same lighter components were distilled from both the whole and aqueous bio-oil types at a range of 35 oC – $99 \text{ }^{\circ}\text{C}$. Distillation of the bio-oil was performed using the same equipment discussed in Steele et al. (Steele et al., 2014) and Street et al. (Street et al., 2016). The packed column distillation apparatus used in this study was a BR 9600 packed column distillation system. The distillation system was obtained from BR Instruments (Easton, MD). The bio-oil to be distilled was placed in a 3L round bottom flask, which contained a magnetic stirrer. The flask was placed in a heating mantle and secured to the column.

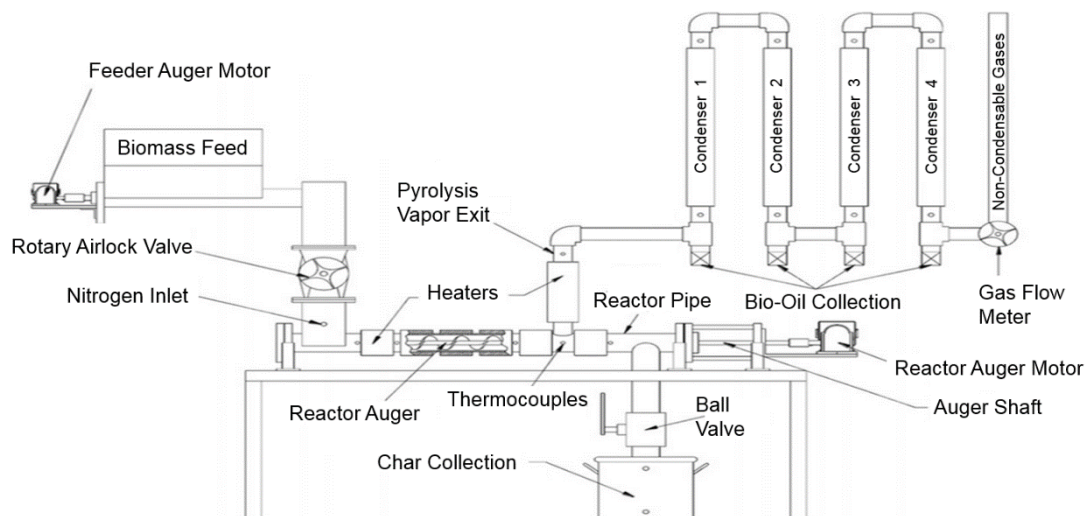


Figure 3.3: Schematic of the auger pyrolysis reactor at MSU used to produce bio-oil.

Two thermocouples were placed and secured in the system. One thermocouple was located in a glass thermowell in the round bottom flask to measure the temperature of the fluid in the flask, and the second thermocouple was placed on top of the packed bed distillation column to measure the temperature of the vapors leaving the column to be further cooled by the condenser.

Four calibrated receivers were placed and secured in the system after the condenser to collect the desired fractions. The distillation was automatically controlled with the BR M690 PC-interface. A heating rate (30% of the full power of the heater) was defined in the software to bring the fluid to the initial boiling point. The reflux ratio of 5:1 was controlled with an automatic solenoid valve and was controlled by the software. The temperature of each cut (temperature to change receivers), and final fluid temperature (temperature in the flask) were also controlled and recorded by the software. The distillation column was left to stabilize for approximately 1 hour after the bio-oil started boiling (until the pot and vapor temperature remained stable). The distillation process was

ceased when the boiling pot reached 120°C to keep the longer chained hydrocarbons from cracking and to lessen the possibility of instantaneous polymerization of the components.

3.3.6 Physical properties analysis of the HTL and FP Bio-oils

Physical properties comprising viscosity, elemental analysis, heating value, density, water content, ash content, and pH analysis of the biomass and both HTL and FP bio-oils were characterized. The dynamic viscosity of the bio-oils was determined using Bohlin rheometer (model CV100) at 25, 40 and 60 °C. Truncated cone and plate geometry with shears rates from 0.5 to 150 s⁻¹ and plate gap of 1000 μm was utilized in the viscosity analysis of the bio-oils.

The pH of the HTL, and FP bio-oils were measured using a digital pH meter (Oakton, model PC 510). Proximate analysis was performed following ASTM standards for ash (E1755), moisture (E871), volatile matter (E872) and fixed carbon was the balance. Volumetric Karl Fischer titrator (Mettler Toledo, model V20) using a hydranal-composite 5 solution (Sigma-Aldrich) was used to measure the water content of the bio-oils. The density of the bio-oils was determined using a 2 mL, calibrated density bottle (Cole-Parmer Model EW-34580-40) filled with a known mass of bio-oil. Using CHNS/O analyzer (PerkinElmer, model CHNS/O 2400), the ultimate analysis to determine the elemental composition of the bio-oils was performed. The oxygen content was calculated by difference. The ash content was performed following ASTM E1755. Oxygen calorimeter (IKA, model C2000) was used to determine the higher heating value (HHV) of the bio-oils.

3.3.7 GC-MS analysis of HTL and FP Bio-oils

Chemical constituents of the HTL and FP Bio-oils were conducted using an Agilent 7890 GC/5975 MS equipped with a DB-1701 column (30 m; 0.25 mm inner diameter; and 0.25 mm film

thickness). Approximately, 150 mg FP bio-oil was mixed with 3 mL of methanol, and it was diluted to 10 mL with dichloromethane. The HTL bio-oil followed similar procedure except that the dichloromethane was mixed first. The diluted samples were injected into the column, respectively. The initial column temperature (40 °C) was maintained for 2 min and then increased to 250 °C at 5 °C/min. The final temperature was held for 8 min. Ultrahigh-purity helium (99.999%) from Airgas, Inc. (Charlotte, NC) was used as the carrier gas set at a flow rate of 1.25 mL/min. HTL, and FP Bio-oils compounds were identified by comparing the mass spectra to the National Institute of Standards and Technology (NIST) mass spectral library.

3.3.8 Thermogravimetric Analysis (TGA)

Thermal gravimetric analysis (TGA) of the FP and HTL bio-oils were performed using a TA Instruments TGA Q500 thermal gravimetric analyzer. The bio-oil samples were heated under a N₂ atmosphere at 20 mL/min from ambient to 800 °C at heating rate of 10 °C/min.

3.3.9 Hydroxyl (OH) group analysis of HTL and FP bio-oils: ³¹P-NMR

Hydroxyl group analysis of the bio-oils (HTL and FP) were conducted using ³¹P-NMR. The phosphorylation method employed followed by Celikbag et al. (Celikbag et al., 2015). Briefly, a stock solution consisting of 40 mg internal standard (N-hydroxy-5-norbornene-2,3-dicarboximide [NHND]) and 40 mg relaxation reagent (chromium (III) acetylacetonate) dissolved in a solvent system of chloroform and pyridine (1.6/1, v/v) was prepared. At room temperature, about 20 ± 2.0 mg of bio-oil was completely dissolved in 500 µL of the stock solution. About 150 µL of the derivatization agent (TMDP) was mixed with the dissolved solution and vortexed for 4 min. Aliphatic, carboxylic, and phenolic OH groups were phosphorylated with 2-chloro-4,4,5,5-tetramethyl-1,3,2-dioxaphospholane (TMDP), which reacts with the free OH groups in the bio-oils resulting in derivatized compounds and hydrochloric acid (HCl). Pyridine was added in excess

relative to the TMDP in the solvent system as a base to neutralize the HCl, which can decompose the derivatized compounds. This was then followed by a quantitative ^{31}P -NMR analysis. ^{31}P -NMR spectra were obtained with a Bruker Avance II 250 MHz spectrometer using inverse gated decoupling pulse sequence, 90° pulse angle, 25s pulse delay and 128 scans following the methods of Ben and Ragauskas (Ben & Ragauskas, 2011). Two replicates of each sample bio-oils were made.

3.3.10 FTIR Analysis of the bio-oils of HTL, and FP Bio-oils

Attenuated Total Reflection Fourier Transform Infrared (ATR-FTIR) spectra of HTL, and FP Bio-oils, were respectively acquired between 4000 and 650 cm^{-1} with 4.00 cm^{-1} resolution and 32 scans using an ATR-FTIR spectrometer (Model Spectrum400, Perkin Elmer Co., Waltham, MA) to determine the functional groups.

3.4 Results and Discussion

3.4.1 Biomass Characterization

The inherent composition, elemental and proximate analyses of loblolly pine biomass used for the FP and HTL techniques are presented in Table 3.1. Cellulose and hemicellulose formed about three-fourth (73%) of the biomass composition followed by lignin (26%) and extractives (2%) in that order. The composition analysis, ultimate analysis and proximate analysis of the feedstock were consistent with other reported pine biomass species (Sannigrahi, et al. 2008; Mahadevan et al. 2015; Chiodo et al. 2016). Higher volatile matter coupled with low ash content is desirable features for the feedstock in thermal conversion. Ash is known to contain inorganic elements that may favor the formation of char reducing bio-oil yield; therefore, the lower ash content reported may promote high bio-oil yield. Also, the alkali metals in ash may serve as a catalyst to change the pyrolysis depolymerization mechanism and slag formation on the walls of operational

equipment (Mahadevan et al. 2015; Fahmi et al. 2007). Further analysis of ash content was not carried out in this study.

3.4.2 Fast Pyrolysis and Hydrothermal Liquefaction Product Yield and Characteristics.

Morphologically, FP and HTL bio-oils are viscous and dark brownish in color. However, FP bio-oil has a characteristic strong smoky scent, while HTL bio-oil (with water/ethanol as co-solvent) has a pungent sweet-smoky vanilla-like odor. FP product yields were estimated as the weight percentage of the individual product phase (bio-oil, light oil, and char) relative to the weight of the dried feedstock.

Table 3.1: Biomass Composition, Proximate, Ultimate, and Heating value analyses (dry basis as wt. %) room temperature.

Biomass Composition	Result	Ultimate analysis	Result	Proximate analysis	Result
Cellulose	44.3	C	45.12 ± 0.1	Ash content	0.55 ± 0.01
Hemicelluloses	28.2	H	6.34 ± 0.1	Volatile matter	79.14 ± 0.9
Lignin	25.6	O	48.14 ± 0.2	Moisture content	6.88 ± 0.01
Extractives	1.9	N	0.27 ± 0.02	Fixed carbon	13.43 ± 0.9
		S	0.13 ± 0.01	Heating value (MJ/Kg)	19.61 ± 0.02

Oxygen content is by difference. Wt. % = weight percent

Gas yield was by a difference (100 - (bio-oil, light oil, and char)). The product yields were influenced by the thermochemical conversion process (i.e., FP and HTL) given the same feedstock (Table 3.2). Comparatively, HTL process had about twice as much bio-oil yield (67%) as FP process bio-oil (34%). Apart from the process conditions, the increased bio-oil yield observed in the HTL could be attributed to the addition of ethanol in the HTL process. Previous work has

demonstrated a greater synergy between water/ethanol in increasing bio-oil yield compared to water only in HTL process. The bio-oil yield using water/ethanol as co-solvent was about three times higher than using water only (Celikbag et al., 2016). The bio-oil yield results from Celikbag et al. was consistent with the HTL bio-oil yield obtained in this study.

Additionally, the reduced amount of char formation is closely associated with improved bio-oil yield with the addition of ethanol to water (Liu et al., 2013). Hydrogen donor solvent like ethanol could reduce the formation of char by stabilizing reactive free radicals generated from the fragmentation of feedstock during the HTL process from repolymerization (Zhang and Zhang 2014; Yuan et al. 2007). It is also known that ethanol/water at subcritical water conditions enhances high molecular weight compounds solubility and oily product dissolvability (Liu et al. 2013). Thus, it could be inferred that the lack of hydrogen donor solvent in the FP process could have promoted char formation and reduced bio-oil yield. Nonetheless, it should be noted that other processing variables such as residence time, and heating rate may have been a contributing factor. FP and HTL of beech wood, revealed a similar pattern of improved bio-oil yield and reduced char yield in HTL process with NaOH as the catalyst. The FP bio-oil yield was lower than the HTL (Haarlemmer et al., 2016). Another study comparing pyrolysis and HTL of *Chlamydomonas reinhardtii*, a green microalgae, suggested that generally, HTL bio-oil yield was somewhat higher than pyrolysis bio-oil yield (Hognon et al., 2015). Analysis of slow pyrolysis and HTL of defatted algal biomass study also confirmed lower pyrolysis bio-oil and high solid (char) yields than the HTL (Vardon et al., 2012). While this study focused on bio-oil and was consistent with previous studies, it is noteworthy to mention that the char is essential in applications such as pollutant removal, storage capacity, carbon sequestration and soil remediation (Oliveira et al., 2017; Grierson et al. 2011).

Table 3.2 : Product yields for fast pyrolysis and hydrothermal liquefaction

Yield	Fast pyrolysis (wt %)	HTL (wt %)
Bio-oil	34 ± 3	67 ± 2
Light oil (aqueous phase)	20 ± 1	14 ± 2
Gas	19 ± 2	16 ± 3
Char	27 ± 1	3 ± 1

3.4.3 Bulk properties of fast pyrolysis and hydrothermal liquefaction bio-oil.

The ultimate analysis showing the elemental components of the bio-oils depicted a slightly lower oxygen content (31% for HTL, and 39% for FP) compared to the feedstock (48%) Tables 1 and 3. However, the FP bio-oil was much oxygenated than the HTL bio-oil. The high carbon content (61%) coupled with the lower oxygen content may have contributed to the slightly high heating value of HTL bio-oil compared to the FP bio-oil with 54% carbon. Bio-oil from lignocellulosic biomass is reported to contain a substantial amount of oxygenated compounds (Pinheiro et al. 2019), which was also confirmed in the ultimate analysis (Table 3.3). The high oxygen content may have resulted from functional groups such as alcohols, carboxylic acids and phenols during the thermochemical conversion process. High oxygenated compounds present challenges such as low heating value, polymerization tendencies during storage, increased viscosity and fossil fuels mixing incompatibility (Imam and Capareda 2012; Mullen and Boateng 2008). Nonetheless, these oxygenated compounds may be essential in bio-based polymer synthesis. For example, OH groups in bio-oil are considered the primary active functional groups giving bio-oil polyol attributes (Sasaki et al. 2013).

The N, S, H contents remained nearly unaltered relative to the feedstock. The density of fast pyrolysis bio-oil (1287 Kg/m³) was higher than the HTL bio-oil (1013 Kg/m³). The somewhat lower HTL bio-oil density could be attributed to the synergetic effect of the water/ethanol blend, which may have occluded the repolymerization of lower molecular weight compounds (J. Zhang & Zhang, 2014). The respective pH values of FP and HTL bio-oil were 2.27 and 2.83. This indicates that both bio-oils are acidic and is a disadvantage as a fuel but may serve as a catalyst in adhesive synthesis (Barde et al., 2019; Wei et al., 2014a).

Table 3.3: Ultimate analysis and physical properties of fast pyrolysis bio-oil and hydrothermal liquefaction bio-oil (dry wt % basis).

Ultimate analysis	FP Bio-oil	HTL Bio-oil	Properties	FP Bio-oil	HTL Bio-oil
C	54.45 ± 0.2	61.04 ± 0.3	Moisture content (%)	18.45 ± 0.1	16.55 ± 0.1
H	6.54 ± 0.1	7.19 ± 0.1	Heating Value (MJ/Kg)	23.26 ± 0.12	28.89 ± 0.20
O	38.81 ± 0.2	30.75 ± 0.3	pH	2.29 ± 0.02	2.83 ± 0.01
N	0.21 ± 0.0	0.15 ± 0.01	Ash (%)	0.01 ± 0.0	0.01 ± 0.0
S	0.13 ± 0.0	0.11 ± 0.01	Density (Kg/m ³)	1287 ± 17	1013 ± 13

Oxygen content estimated by difference.

3.4.4 Viscosity Analysis

Viscosity analysis carried out at 25 °C, 40 °C and 60 °C for FP and HTL bio-oil with varying shear rates from 0.1 to 150 s⁻¹ is presented in Figure 3.4. Generally, the viscosity of the bio-oils decreased with increased temperature. For example, the viscosity of FP bio-oil decreased from 0.226 Pa s at 25 °C to 0.164 Pa s at 60 °C. A Newtonian fluid behavior was observed at a higher shear rate

(shear rate $> 25 \text{ s}^{-1}$). Previous studies demonstrated that bio-oil viscosity is shear rate and temperature-dependent (Thangalazhy-Gopakumar et al., 2010; Ingram et al., 2008).

Comparatively, for all the temperatures studied, the viscosity of the FP bio-oil was higher than the HTL bio-oil. However, Haarlemmer et al. found that the viscosity of HTL bio-oil of beech wood was much higher than the fast pyrolysis bio-oil of the same feedstock. The seemingly conflicting findings could be explained by the HTL solvent or catalyst used. While Haarlemmer et al. used water and sodium hydroxide in the liquefaction process, it may not have been efficient in preventing repolymerization of the reactive low molecular weight compounds from forming high molecular weight compounds. It could, therefore, be inferred that the additional benefit of ethanol addition during the HTL process, may have promoted the solubility of high molecular weight compounds and prevented the re-polymerization of the bio-oil components, thus, the low viscosity.

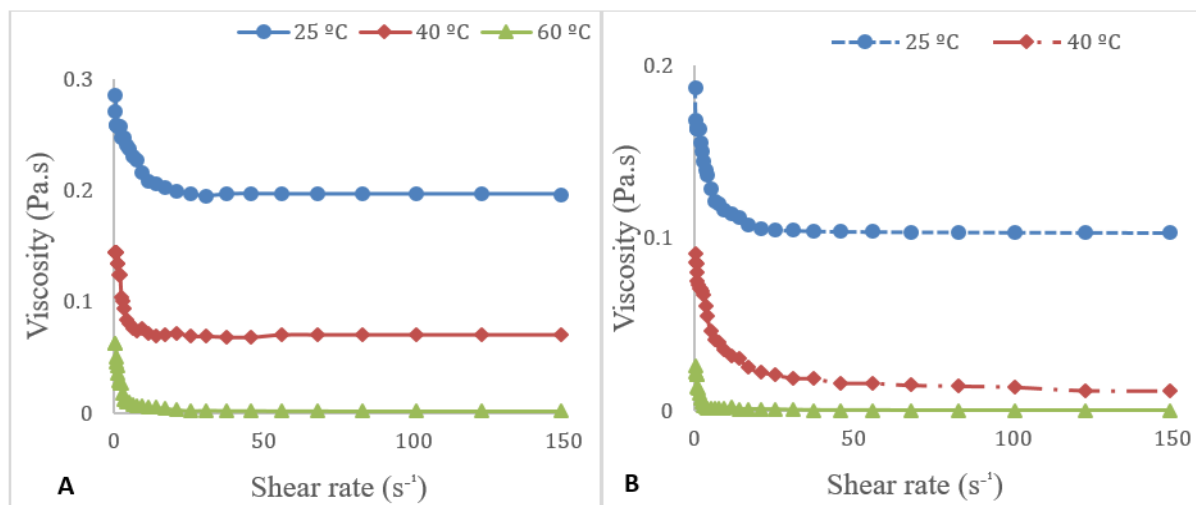


Figure 3.4: Variation of viscosity of bio-oil with temperature and shear rate produced by FP (A) and HTL (B)

3.4.5 Chemical characteristic of FP and HTL of bio-oils.

The GC-MS analysis of the FP and HTL bio-oils are shown in the supplementary data in detail (Appendix A and B) and summarized in Figure 3.5. The compounds identified were complex and were grouped into phenolics, acids, esters, ketones, aldehydes, anhydrosugars, furans and others. Phenolic compounds (phenols and phenolic derivatives) originating from lignin degradation were dominant in the bio-oils. Of the total % peak area analyzed, phenolic compounds constituted ~41% and ~32% of the FP and HTL bio-oils, respectively. Phenolic compounds such as phenol, p-cresol, guaiacol, vanillin, and isoeugenol were similar and common in both FP and HTL bio-oils. Previous studies on bio-oils from pine found similar compounds (Mahadevan et al. 2015; Thangalazhy-Gopakumar et al. 2010). Acetic acid was the main carboxylic acid in the bio-oils. Carboxylic acids are known to catalyze the repolymerization of bio-oil, leading to high viscosity and increased molecular weight (Jo, et al 2018; Boucher et al. 2000). While the acid peak area % of FP bio-oil was relatively high (~7%), the co-solvent (water-ethanol) of the HTL bio-oil may have reduced the formation of carboxylic acid species (~2%). It seems that the addition of ethanol favored the formation of esters by condensation reaction with the carboxylic acids (equation 5) in the HTL bio-oil. Thus, a higher ester % peak area (~25%) of HTL bio-oil compared to FP bio-oil (~ 4%).

Apart from the acids, the presence of aldehyde, ketones, anhydrosugars and furans indicated that the bio-oils contain a substantial amount of oxygenated compounds. The occurrence of these oxygenated compounds has mainly been linked with holocellulose degradation (Hu et al., 2019; Choi et al., 2014; Alén et al., 1996). The unidentified anhydrosugars peak in the HTL bio-oil could possibly be attributed to the efficient phase separation of the light-oil (aqueous phase) from the bio-oil in contrast to the FP bio-oil. Compounds grouped under the “other” category mainly consisted of hydrocarbons (like trans-1,4-hexadiene; ethylidenecyclobutane), nitrogenous (like 1,3

Propanediamine, N-methyl-) and sulfur (2-Acetyl-3-methylthiophene; 2-Hydroxyethyl vinyl sulfide) containing compounds.

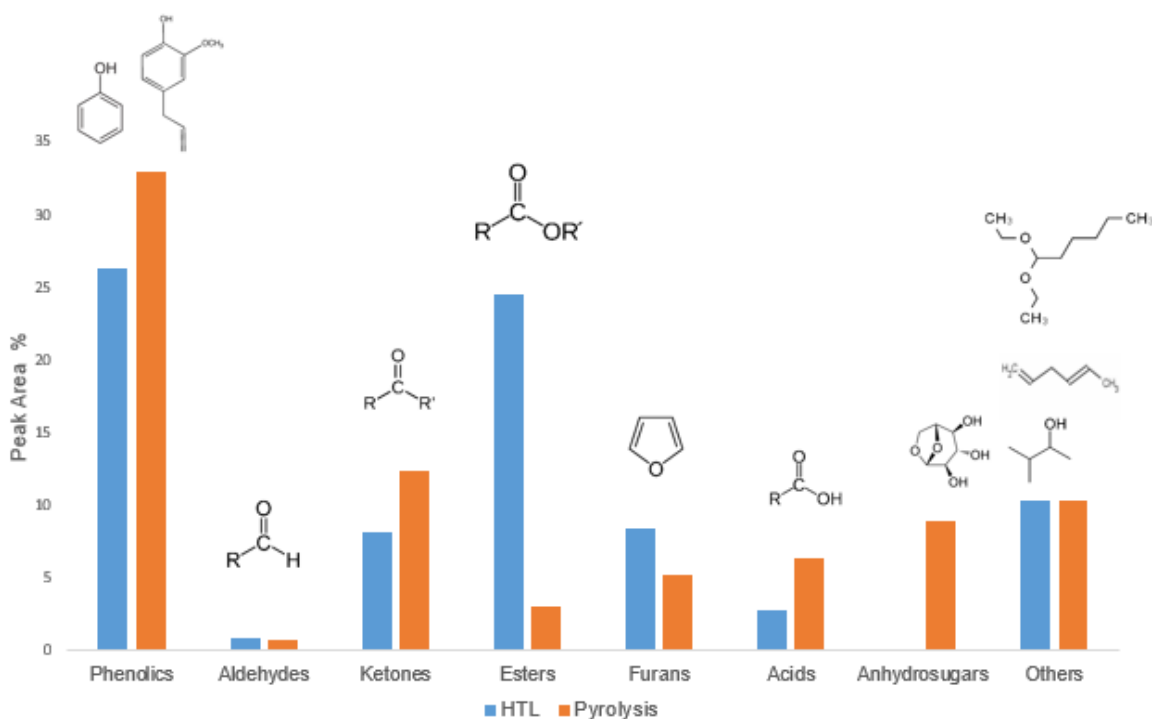
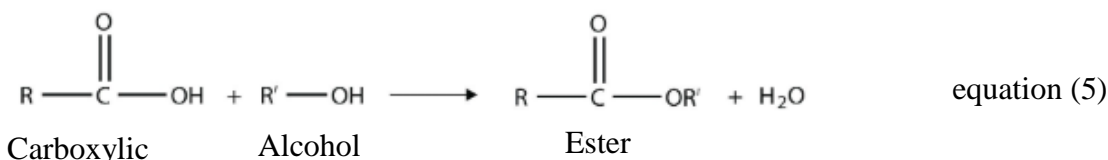


Figure 3.5: Chemical composition of FP and HTL bio-oil by GC-MS.

3.4.6 Thermogravimetric Analysis

The thermal stability of the FP bio-oil and HTL bio-oil was measured as weight percentage loss of the bio-oils with increased temperature. Several studies have underscored the intrinsic drawbacks of GC-MS in elucidating the total chemical constituents of bio-oil (Hu et al. 2019;

Zhang et al. 2017; He et al. 2012). This is because the GC column vaporizes highly volatile compounds with boiling points below the column temperature, usually less than 300°C (Nazari et al. 2015). At temperatures below 300°C, less than 20–50 wt% of bio-crude oils could be volatilized (Sun et al. 2010; Karagöz et al. 2006). The weight loss percentage curves (TG) with the corresponding derivative weight loss curves (DTG) for FP and HTL bio-oils are shown in Figure 3.6. The degradation profiles of the bio-oils presented three different major stages. The initial stage for the bio-oils was defined to occur between room temperature and 87°C for pyrolysis bio-oil, and 85 °C for HTL bio-oil. This stage was assigned to the dehydration of water and volatilization of low organic weight compounds like alcohols, carboxylic acids and aldehydes at low temperature (W. Zhang et al., 2017). The initial stage accounted for about 5% weight loss of HTL bio-oil and 3% weight loss of FP-bio-oil.

The maximum weight loss occurred in the second stage. At this stage, the weight loss was about 63% at a temperature range between 87°C and 350 °C for FP bio-oil and 65% weight loss at a temperature range of 85 °C – 470 °C for HTL bio-oil. This stage was attributed to cracking of phenolic compounds, vanillin and other oligomer compounds formed due to polymerization of the bio-oils. Weight loss at the third stage was 11% for HTL bio-oil at a temperature range of 470 – 800°C and 22% weight loss for FP bio-oil at a temperature range of 350 – 800°C.

The third stage weight loss was imputed to chemical bonds cleavage of the heavy components of the bio-oil (predominantly lignin derivatives) as the decomposition temperature increased. The high percent weight loss for FP bio-oil at the third stage suggested that FP process of producing bio-oil comparatively yields more macromolecule aromatic compounds like phenol, 2-methoxy-4-(1-propenyl) (Yi Liu et al., 2017). The observed difference in degradation regimes for the DTG curves could be ascribed to the different processing variables used during bio-oil production for

the two processes. The maximum degradation temperature for the FP and HTL were 580 °C and 451 °C, respectively. This suggests that HTL process with water/ethanol yields a considerable amount of low volatile compounds.

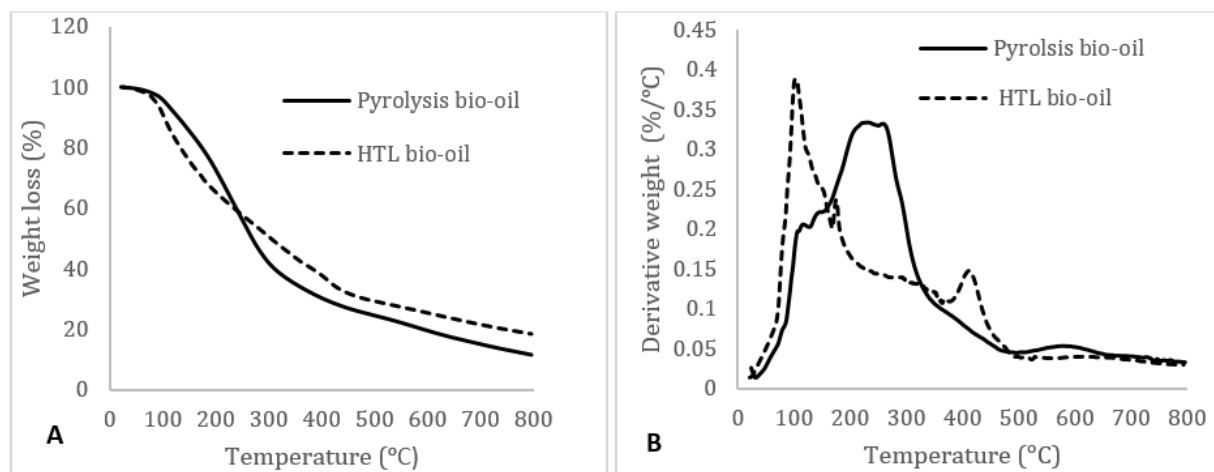


Figure 3.6: Thermogravimetric analysis (TGA) - A and derivative weight loss (DTG) - B curves of fast pyrolysis and hydrothermal liquefaction bio-oils.

3.4.7 FTIR Analysis

Functional group characterization of the FP and HTL bio-oil is shown in the FTIR spectra in Figure 3.7. It is fascinating to observe similar spectra characteristics from both FP and HTL bio-oils. The broad peak between 3100 and 3650 cm^{-1} indicated the presence of OH moieties resulting from aliphatic, acidic, phenolic, water and aromatic OH groups in the bio-oils. The C–H stretching vibrations between 2800 and 3000 cm^{-1} and the C–H bending vibrations between 1380 and 1450 cm^{-1} suggested the presence of alkanes. The characteristic C=O peak at $\sim 1712 \text{ cm}^{-1}$ indicated carbonyl groups, suggesting the presence of ketones, aldehydes, and carboxylic acids in the bio-oils.

The narrow absorbance peak at 1513 cm^{-1} C=C showed aromatic ring stretching vibration of alkenes due to lignin degradation products (Singh et al. 2015). The absorbance peak between $1300\text{-}1207\text{ cm}^{-1}$ revealed C-O stretching, and symmetrical C-O stretching at absorbance peak $\sim 1046\text{ cm}^{-1}$ suggested the possible presence of acids, phenols or alcohols in the bio-oil (Liu et al. 2017; Nazari et al. 2015). The presence of aromatic esters is evidenced by C=O stretching in addition to the occurrence of aromatic ring vibration between $900\text{ and }650\text{ cm}^{-1}$ (Qian et al., 2007). The HTL and pyrolysis spectra absorbance between $878\text{ - }650\text{ cm}^{-1}$ showed a likely presence of aromatic moieties (C-H in plane). Nonetheless, weak peak intensities were comparatively observed in the pyrolysis spectra in this region. These functional groups identified were also confirmed by the GC-MS analysis in Figure 3.6.

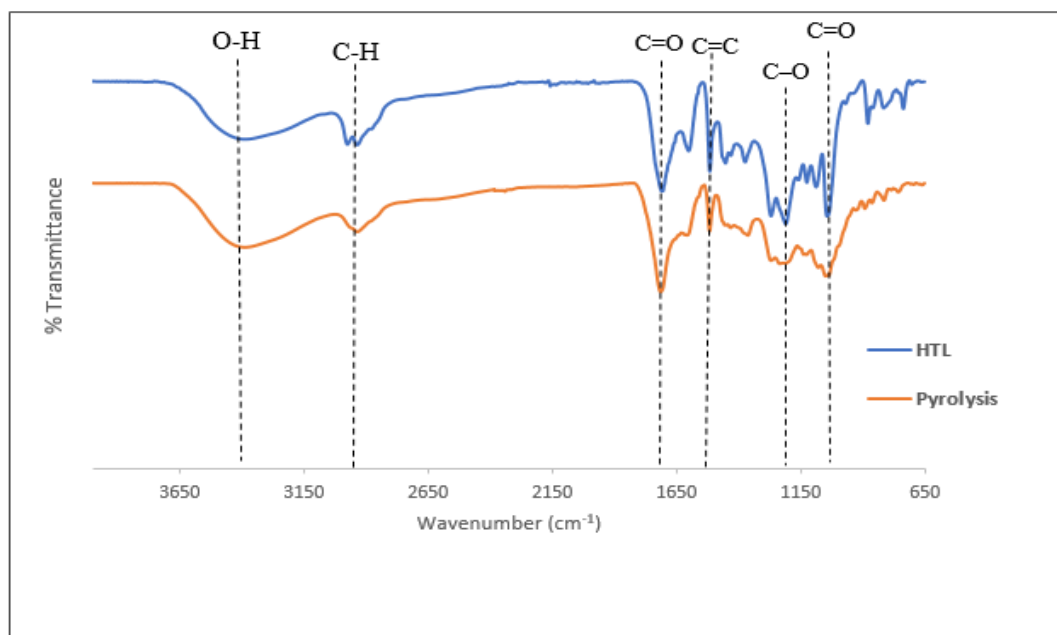


Figure 3.7: FTIR spectra of bio-oil samples from loblolly pine biomass obtained from hydrothermal liquefaction (HTL) and pyrolysis processes (FP).

3.4.8 Hydroxyl (OH) group analysis of HTL and FP bio-oils: ^{31}P -NMR

Bio-oil has been used as a biopolyol in the synthesis of phenol formaldehyde resin (Cui et al., 2017), epoxy resin (Celikbag et al., 2017), polyurethane (Wu et al., 2009) and polyester (Matjaz̃ Kunaver et al., 2010). Pu, et al. have detailed the use of ^{31}P -NMR in characterizing the hydroxyl numbers of biomass lignin and biofuel precursor. They noted that ^{31}P NMR method carries an exceptional advantage over ^1H -NMR and ^{13}C -NMR in elucidating the hydroxyl content. For example: (i) ^{31}P -NMR requires relatively small amounts of sample in its preparation. (ii) quantitative analysis of the different major hydroxyl groups is achieved within a shorter time compared to ^{13}C -NMR. (iii) Unlike ^1H -NMR, which suffers from spectral overlap, the ^{31}P nucleus has a large range of chemical shifts providing better signal resolution and separation (Pu, et al. 2011).

Quantitative ^{31}P -NMR analysis of the hydroxyl number (OHN) and integration regions for both FP and HTL bio-oils are presented in Figure 3.8 and the OH distribution presented in Table 3.4. No significant difference in the total hydroxyl number (OHN) of the bio-oils was found. The OHN of HTL and FP bio-oils were calculated to be 9.25 mmol/g and 10.30 mmol/g, respectively. Aliphatic, phenolic, and acidic hydroxyl groups were identified and quantified respectively for HTL and FP bio-oils (in parenthesis) as 54% (55%) %, 35% (31%), and 11% (14%) of the total OHN. Previous studies have closely associated aliphatic OH types to the degradation of cellulose and hemicellulose, a major component of the wood (Changi et al. 2015; Peterson et al. 2008). Thus, the highest aliphatic OHN recorded. The p-hydroxyphenyl, monomeric phenols, catechol and guaiacyl type of OH groups in bio-oils were attributed to the cleavage of ether bonds of lignin

during FP and HTL conversion of the pine biomass (Xu et al. 2014; Brand et al. 2013; Barbier et al. 2012).

Acidic OH in the HTL and FP bio-oils were 1.04 mmol/g and 1.47mmol/g, respectively. Acidic OH moieties may have resulted mainly from the degradation products of hemicelluloses (Qu et al. 2011).

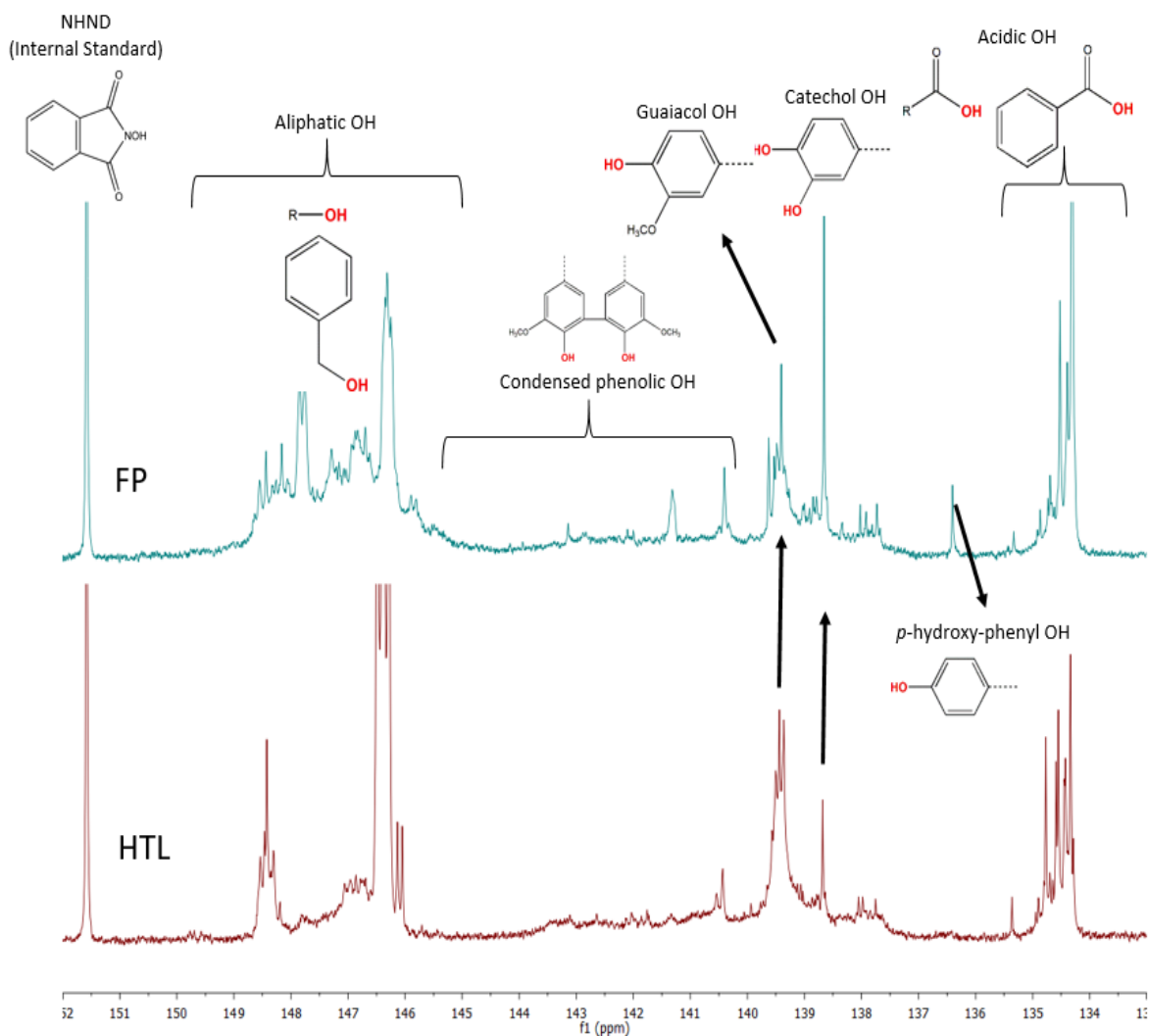


Figure 3.8: ³¹P-NMR spectra for the FP and HTL bio-oils phosphitylated with TMDP.

Table 3.4: Hydroxyl (OH) group distribution of HTL and FP bio-oils by 31P-NMR.

OH Type	HTL (mmol/g)	Pyrolysis (mmol/g)	Integration (ppm)	Region
Aliphatic	5.01 ± 0.09	5.61 ± 0.03	150.0 -145.5	
Phenolic	3.21 ± 0.1	3.22 ± 0.1	144.7 – 137.3	
<i>B-5</i>	0.16 ± 0.0	0.26 ± 0.01	144.7 – 142.8	
<i>4-O-5</i>	0.27 ± 0.01	0.30 ± 0.02	142.8 – 141.7	
<i>5-5</i>	0.60 ± 0.02	0.69 ± 0.08	141.7 – 140.2	
<i>Guaiacyl</i>	1.43 ± 0.09	1.04 ± 0.01	140.2 – 139.0	
<i>Catechol</i>	0.47 ± 0.01	0.65 ± 0.0	139.0 – 138.2	
<i>p-OH</i>	0.27 ± 0.02	0.26 ± 0.0	138.2 – 137.3	
Acidic	1.04 ± 0.09	1.47 ± 0.11	136.6 – 133.6	
Total	9.25 ± 0.09	0.02		

3.5 Conclusions

The effect of FP and HTL processes on the bio-oil properties from loblolly pine biomass was investigated. The synergetic effect of water/ethanol co-solvent in the HTL process showed improved bio-oil characteristics compared to the FP process. FP derived bio-oil was higher in viscosity relative to the HTL bio-oil. Similar chemical functional groups were observed via FTIR. However, the GC-MS analysis revealed that the bio-oils have different chemical compositions. Esterified chemical compounds characterized the HTL bio-oil. FP bio-oil had a substantial amount of phenols and phenolic derivatives. , The high concentration of aliphatic and phenolic OH

moieties were demonstrated via quantitative ^{31}P -NMR from the FP and HTL bio-oils. The OHN of FP bio-oil makes it an attractive option over HTL bio-oil for bio-polyol based on the ^{31}P NMR. Life cycle assessment, cost of production and product characteristics are needed to fully compare the FP and HTL processes for particular end-use.

3.6 Acknowledgements

This work was supported by the Agriculture and Food Research Initiative – “Hydrophobic Bio-Oil-Epoxy Binders for Wood Composites” (Project Award Number 2017-67021-26134). The Auburn University Intramural Grants Program (Auburn, AL, United States) is recognized for startup funding for part of this project. Furthermore, Regions Bank provided partial support, and the Forest Products Development Center (Auburn University, Auburn, AL, United States) is acknowledged for supplementary funding of materials and supplies. The Center for Bioenergy and Bio products (Auburn University, Auburn, AL, United States) is acknowledged for the use of their facilities. The Center for Polymers and Advanced Composites (Auburn University, Auburn, AL, United States) is also recognized for the use of their facilities. The college of Forest Resources, (Mississippi State University, Mississippi State, United States) is also acknowledged for the use of their facilities.

3.7 References

1. Akhtar, Javaid and Nor Aishah Saidina Amin. 2011. "A Review on Process Conditions for Optimum Bio-Oil Yield in Hydrothermal Liquefaction of Biomass." *Renewable and Sustainable Energy Reviews* 15(3):1615–24.
2. Alén, Raimo, Eeva Kuoppala, and Pia Oesch. 1996. "Formation of the Main Degradation Compound Groups from Wood and Its Components during Pyrolysis." *Journal of Analytical and Applied Pyrolysis*.
3. Barbier, Jérémie, Nadège Charon, Nathalie Dupassieux, Anne Loppinet-Serani, Laure Mahé, Jérémie Ponthus, Marion Courtiade, Annie Ducrozet, Anne Agathe Quoineaud, and François Cansell. 2012. "Hydrothermal Conversion of Lignin Compounds. A Detailed Study of Fragmentation and Condensation Reaction Pathways." *Biomass and Bioenergy* 46:479–91.
4. Barde, Mehul, Yusuf Celikbag, Brian Via, and Sushil Adhikari and Maria L. Auad. 2019. "Semi-Interpenetrating Novolac-Epoxy Thermoset Polymer Networks Derived from Plant Biomass." *Journal of Renewable Materials* 6(7):724–36.
5. Ben, Haoxi and Arthur J. Ragauskas. 2011. "NMR Characterization of Pyrolysis Oils from Kraft Lignin." *Energy & Fuels* 25(5):2322–32.
6. Borsodi, N., A. Szentés, N. Miskolczi, Chunfei Wu, and Xiaotong Liu. 2016. "Carbon Nanotubes Synthesized from Gaseous Products of Waste Polymer Pyrolysis and Their Application." *Journal of Analytical and Applied Pyrolysis* 120:304–13.
7. Boucher, M. E., A. Chaala, and C. Roy. 2000. "Bio-Oils Obtained by Vacuum Pyrolysis of Softwood Bark as a Liquid Fuel for Gas Turbines. Part I: Properties of Bio-Oil and Its Blends with Methanol and a Pyrolytic Aqueous Phase." *Biomass and Bioenergy*.
8. Brand, Steffen, Ratna Frida Susanti, Seok Ki Kim, Hong shik Lee, Jaehoon Kim, and Byung In Sang. 2013. "Supercritical Ethanol as an Enhanced Medium for Lignocellulosic Biomass Liquefaction: Influence of Physical Process Parameters." *Energy* 59:173–82.
9. Bridgwater, A. V. 2010. *Fast Pyrolysis of Biomass for Energy and Fuels*. Vol. 2010.
10. Bridgwater, A. V. and G. V. C. Peacocke. 2000. "Fast Pyrolysis Processes for Biomass." *Renewable and Sustainable Energy Reviews*.
11. Celikbag, Yusuf, Shatori Meadows, Mehul Barde, Sushil Adhikari, Gisela Buschle-Diller, Maria L. Auad, and Brian K. Via. 2017. "Synthesis and Characterization of Bio-Oil-Based Self-Curing Epoxy Resin." *Industrial and Engineering Chemistry Research* 56(33):9389–9400.

12. Celikbag, Yusuf, Thomas J. Robinson, Brian K. Via, Sushil Adhikari, and Maria L. Auad. 2015. "Pyrolysis Oil Substituted Epoxy Resin: Improved Ratio Optimization and Crosslinking Efficiency." *Journal of Applied Polymer Science* 132(28):n/a-n/a.
13. Celikbag, Yusuf, Brian K. Via, Sushil Adhikari, Gisela Buschle-Diller, and Maria L. Auad. 2016. "The Effect of Ethanol on Hydroxyl and Carbonyl Groups in Biopolyol Produced by Hydrothermal Liquefaction of Loblolly Pine: ³¹P-NMR and ¹⁹F-NMR Analysis." *Bioresource Technology* 214:37–44.
14. Changi, Shujauddin M., Julia L. Faeth, Na Mo, and Phillip E. Savage. 2015. "Hydrothermal Reactions of Biomolecules Relevant for Microalgae Liquefaction." *Industrial and Engineering Chemistry Research* 54(47):11733–58.
15. Chaouch, Mounir, Papa Niokhor Diouf, Aziz Laghdir, and Suzhou Yin. 2014. "Bio-Oil from Whole-Tree Feedstock in Resol-Type Phenolic Resins." *Journal of Applied Polymer Science* 131(6):n/a-n/a.
16. Chiamonti, David, Matteo Prussi, Marco Buffi, Andrea Maria Rizzo, and Luigi Pari. 2017. "Review and Experimental Study on Pyrolysis and Hydrothermal Liquefaction of Microalgae for Biofuel Production." *Applied Energy* 185:963–72.
17. Chiodo, V., G. Zafarana, S. Maisano, S. Freni, and F. Urbani. 2016. "Pyrolysis of Different Biomass: Direct Comparison among *Posidonia Oceanica*, Lacustrine Alga and White-Pine." *Fuel* 164:220–27.
18. Choi, Yong S., Patrick A. Johnston, Robert C. Brown, Brent H. Shanks, and Kyong Hwan Lee. 2014. "Detailed Characterization of Red Oak-Derived Pyrolysis Oil: Integrated Use of GC, HPLC, IC, GPC and Karl-Fischer." *Journal of Analytical and Applied Pyrolysis* 110(1):147–54.
19. Cui, Yong, Xiaopeng Hou, Wenliang Wang, and Jianmin Chang. 2017. "Synthesis and Characterization of Bio-Oil Phenol Formaldehyde Resin Used to Fabricate Phenolic Based Materials." *Materials* 10(6):1–9.
20. Czernik, S. and A. V. Bridgwater. 2004. "Overview of Applications of Biomass Fast Pyrolysis Oil." *Energy & Fuels* 18(2):590–98.
21. Demirbaş, A. 2000. "Mechanisms of Liquefaction and Pyrolysis Reactions of Biomass." *Energy Conversion and Management*.
22. Fahmi, R., A. V. Bridgwater, L. I. Darvell, J. M. Jones, N. Yates, S. Thain, and I. S. Donnison. 2007. "The Effect of Alkali Metals on Combustion and Pyrolysis of *Lolium* and *Festuca* Grasses, Switchgrass and Willow." *Fuel* 86(10–11):1560–69.

23. Gollakota, A. R. K., Nanda Kishore, and Sai Gu. 2018. "A Review on Hydrothermal Liquefaction of Biomass." *Renewable and Sustainable Energy Reviews*.
24. Grierson, Scott;, Vladimir; Strezov, and Pushan Shah. 2011. "Properties of Oil and Char Derived from Slow Pyrolysis of Tetraselmis Chui." *Bioresource Technology* 102(17):8232–40.
25. Haarlemmer, Geert, Chamseddine Guizani, Suzanne Anouti, Maxime Déniel, Anne Roubaud, and Sylvie Valin. 2016. "Analysis and Comparison of Bio-Oils Obtained by Hydrothermal Liquefaction and Fast Pyrolysis of Beech Wood." *Fuel* 174:180–88.
26. Hognon, Céline, Florian Delrue, Jonathan Texier, Maguelone Grateau, Sébastien Thiery, Hélène Miller, and Anne Roubaud. 2015. "Comparison of Pyrolysis and Hydrothermal Liquefaction of Chlamydomonas Reinhardtii. Growth Studies on the Recovered Hydrothermal Aqueous Phase." *Biomass and Bioenergy* 73:23–31.
27. Hu, Xun, Hongyu Guo, Mortaza Gholizadeh, Behnam Sattari, and Qing Liu. 2019. "Pyrolysis of Different Wood Species: Impacts of C/H Ratio in Feedstock on Distribution of Pyrolysis Products." *Biomass and Bioenergy* 120(October 2018):28–39.
28. Imam, Tahmina and Sergio Capareda. 2012. "Characterization of Bio-Oil, Syn-Gas and Bio-Char from Switchgrass Pyrolysis at Various Temperatures." *Journal of Analytical and Applied Pyrolysis* 93:170–77.
29. Ingram, Leonard, Dinesh Mohan, Mark Bricka, Philip Steele, David Strobel, David Crocker, Brian Mitchell, Javeed Mohammad, Kelly Cantrell, and Charles U. Pittman. 2008. "Pyrolysis of Wood and Bark in an Auger Reactor: Physical Properties and Chemical Analysis of the Produced Bio-Oils." *Energy & Fuels* 22(1):614–25.
30. Jahirul, Mohammad I., Mohammad G. Rasul, Ashfaque Ahmed Chowdhury, and Nanjappa Ashwath. 2012. "Biofuels Production through Biomass Pyrolysis- A Technological Review." *Energies* 5(12):4952–5001.
31. Jena, Umakanta and K. C. Das. 2011. "Comparative Evaluation of Thermochemical Liquefaction and Pyrolysis for Bio-Oil Production from Microalgae." *Energy and Fuels* 25(11):5472–82.
32. Jo, Heuntae, Deepak Verma, and Jaehoon Kim. 2018. "Excellent Aging Stability of Upgraded Fast Pyrolysis Bio-Oil in Supercritical Ethanol." *Fuel* 232(June):610–19.
33. Karagöz, Selhan, Thallada Bhaskar, Akinori Muto, and Yusaku Sakata. 2006. "Hydrothermal Upgrading of Biomass: Effect of K₂CO₃ Concentration and Biomass/Water Ratio on Products Distribution." *Bioresource Technology* 97(1):90–98.

34. Laird, David A., Robert C. Brown, James E. Amonette, and Johannes Lehmann. 2009. "Review of the Pyrolysis Platform for Coproducing Bio-Oil and Biochar." *Biofuels, Bioproducts and Biorefining* 6(3):246–56.
35. Li, Qi, Philip H. Steele, Fei Yu, Brian Mitchell, and El Barbary M. Hassan. 2013. "Pyrolytic Spray Increases Levoglucosan Production during Fast Pyrolysis." *Journal of Analytical and Applied Pyrolysis* 100:33–40.
36. Liu, Yan, Xing Zhong Yuan, Hua Jun Huang, Xue Li Wang, Hou Wang, and Guang Ming Zeng. 2013. "Thermochemical Liquefaction of Rice Husk for Bio-Oil Production in Mixed Solvent (Ethanol-Water)." *Fuel Processing Technology*.
37. Liu, Yi, Brian K. Via, Yuanfeng Pan, Qingzheng Cheng, Hongwu Guo, Maria L. Auad, and Steven Taylor. 2017. "Preparation and Characterization of Epoxy Resin Cross-Linked with High Wood Pyrolysis Bio-Oil Substitution by Acetone Pretreatment." *Polymers* 9(3).
38. Mahadevan, Ravishankar, Rajdeep Shakya, Sneha Neupane, and Sushil Adhikari. 2015. "Physical and Chemical Properties and Accelerated Aging Test of Bio-Oil Produced from in Situ Catalytic Pyrolysis in a Bench-Scale Fluidized-Bed Reactor." *Energy & Fuels* 29(2):841–48.
39. Mathanker, Ankit, Deepak Pudasainee, Amit Kumar, and Rajender Gupta. 2020. "Hydrothermal Liquefaction of Lignocellulosic Biomass Feedstock to Produce Biofuels: Parametric Study and Products Characterization." *Fuel* 271(March):117534.
40. Matjaz̃ Kunaver, Edita Jasiukaityte, Natasa Cuk, and James T. Guthrie. 2010. "Liquefaction of Wood, Synthesis and Characterization of Liquefied Wood Polyester Derivatives Matjaz̃." *Journal of Applied Polymer Science* Vol. 115(5):2658–67.
41. Meier, D. and O. Faix. 1999. "State of the Art of Applied Fast Pyrolysis of Lignocellulosic Materials - A Review." *Bioresource Technology* 68(1):71–77.
42. Mohan, Dinesh, Charles U. Pittman, and Philip H. Steele. 2006. "Pyrolysis of Wood/Biomass for Bio-Oil: A Critical Review." *Energy & Fuels* 20(3):848–89.
43. Mullen, Charles A. and Akwasi A. Boateng. 2008. "Chemical Composition of Bio-Oils Produced by Fast Pyrolysis of Two Energy Crops †." *Energy & Fuels* 22(3):2104–9.
44. Nazari, Laleh, Zhongshun Yuan, Sadra Souzanchi, Madhumita B. Ray, and Chunbao Xu. 2015. "Hydrothermal Liquefaction of Woody Biomass in Hot-Compressed Water: Catalyst Screening and Comprehensive Characterization of Bio-Crude Oils." *Fuel* 162:74–83.
45. Ni, Meng, Dennis Y. C. Leung, Michael K. H. Leung, and K. Sumathy. 2006. "An Overview of Hydrogen Production from Biomass." *Fuel Processing Technology*.

46. Oliveira, Fernanda R., Anil K. Patel, Deb P. Jaisi, Sushil Adhikari, Hui Lu, and Samir Kumar Khanal. 2017. "Environmental Application of Biochar: Current Status and Perspectives." *Bioresource Technology*.
47. Palizdar, A. and S. M. Sadrameli. 2020. "Catalytic Upgrading of Beech Wood Pyrolysis Oil over Iron- and Zinc-Promoted Hierarchical MFI Zeolites." *Fuel*.
48. Perlack, Robert D. ..., Lynn L. .. Wright;, Robin L. .. Graham, Anthony F. Turhollow;, Bryce J. .. Stokes;, and Donald C. Erbach. 2005. "Biomass as Feedstock for a Bioenergy and Bioproducts Industry: The Technical Feasibility of a Billion-Ton Annual Supply." *Agriculture* 59.
49. Peterson, Andrew A., Frédéric Vogel, Russell P. Lachance, Morgan Fröling, Michael J. Antal, and Jefferson W. Tester. 2008. "Thermochemical Biofuel Production in Hydrothermal Media: A Review of Sub- and Supercritical Water Technologies." *Energy and Environmental Science* 1(1):32–65.
50. Pinheiro Pires, Anamaria Paiva, Jesus Arauzo, Isabel Fonts, Marcelo E. Domine, Alberto Fernández Arroyo, Marta Estrella Garcia-Perez, Jorge Montoya, Farid Chejne, Peter Pfromm, and Manuel Garcia-Perez. 2019. "Challenges and Opportunities for Bio-Oil Refining: A Review." *Energy and Fuels* 33(6):4683–4720.
51. Pu, Yunqiao, Shilin Cao, and Arthur J. Ragauskas. 2011. "Application of Quantitative ³¹P NMR in Biomass Lignin and Biofuel Precursors Characterization." *Energy and Environmental Science* 4(9):3154–66.
52. Qian, Yejian, Chengji Zuo, Jian Tan, and Jianhui He. 2007. "Structural Analysis of Bio-Oils from Sub-and Supercritical Water Liquefaction of Woody Biomass." *Energy* 32(3):196–202.
53. Qu, Tingting, Wanjun Guo, Laihong Shen, Jun Xiao, and Kun Zhao. 2011. "Experimental Study of Biomass Pyrolysis Based on Three Major Components: Hemicellulose, Cellulose, and Lignin." *Industrial and Engineering Chemistry Research* 50(18):10424–33.
54. Sasaki, Chizuru, Mio Wanaka, Hitoshi Takagi, Satoshi Tamura, Chikako Asada, and Yoshitoshi Nakamura. 2013. "Evaluation of Epoxy Resins Synthesized from Steam-Exploded Bamboo Lignin." *Industrial Crops and Products* 43(1):757–61.
55. Scholze, B. and D. Meier. 2001. Characterization of the Water-Insoluble Fraction from Pyrolysis Oil (Pyrolytic Lignin). Part I. PY-GC/MS, FTIR, and Functional Groups. Vol. 60.
56. Singh, Rawel, Aditya Prakash, Bhavya Balagurumurthy, Raghuvir Singh, Sandeep Saran, and Thallada Bhaskar. 2015. "Hydrothermal Liquefaction of Agricultural and Forest Biomass Residue: Comparative Study." *Journal of Material Cycles and Waste Management* 17(3):442–52.

57. Steele, P. H. ..., S. K. .. Gajjela, T. .. Mlsna, C. U. Jr; Pittman, and F. Yu. 2014. "United States Patent Application : UPGRADING OF BIO-OIL USING SYNTHESIS GAS." 1(19).
58. Street, J., F. Yu, Q. Yan, J. Wooten, E. Columbus, and E. Hassan. 2016. "Pilot-Plant Production of Gas-to-Liquid Synthetic Fuel Using Gasified Biomass over a Novel Biochar-Supported Catalyst." *Transactions of the ASABE* 59(6):1485–96.
59. Sun, Peiqin, Mingxing Heng, Shaohui Sun, and Junwu Chen. 2010. "Direct Liquefaction of Paulownia in Hot Compressed Water: Influence of Catalysts." *Energy* 35(12):5421–29.
60. Tekin, Kubilay, Selhan Karagöz, and Sema Bektaş. 2014. "A Review of Hydrothermal Biomass Processing." *Renewable and Sustainable Energy Reviews* 40:673–87.
61. Thangalazhy-Gopakumar, Suchithra, Sushil Adhikari, Harideepan Ravindran, Ram B. Gupta, Oladiran Fasina, Maobing Tu, and Sandun D. Fernando. 2010. "Physiochemical Properties of Bio-Oil Produced at Various Temperatures from Pine Wood Using an Auger Reactor." *Bioresource Technology* 101(21):8389–95.
62. Toor, Saqib Sohail, Lasse Rosendahl, and Andreas Rudolf. 2011. "Hydrothermal Liquefaction of Biomass: A Review of Subcritical Water Technologies." *Energy* 36(5):2328–42.
63. Uddin, M. N., Kuaanan Techato, Juntakan Taweekun, Md Mofijur Rahman, M. G. Rasul, T. M. I. Mahlia, and S. M. Ashrafur. 2018. "An Overview of Recent Developments in Biomass Pyrolysis Technologies." *Energies* 11(11).
64. Vardon, Derek R., Brajendra K. Sharma, Grant V. Blazina, Kishore Rajagopalan, and Timothy J. Strathmann. 2012. "Thermochemical Conversion of Raw and Defatted Algal Biomass via Hydrothermal Liquefaction and Slow Pyrolysis." *Bioresource Technology* 109:178–87.
65. Wei, Nan, Brian K. Via, Yifen Wang, Tim McDonald, and Maria L. Auad. 2014. "Liquefaction and Substitution of Switchgrass (*Panicum Virgatum*) Based Bio-Oil into Epoxy Resins." *Industrial Crops and Products* 57:116–23.
66. Wu, Jianping, Yuanhua Wang, Yiqin Wan, Hanwu Lei, Fei Yu, Yuhuan Liu, Paul Chen, Lirong Yang, and Roger Ruan. 2009. "Processing and Properties of Rigid Polyurethane Foams Based on Bio-Oils from Microwave-Assisted Pyrolysis of Corn Stover." *International Journal of Agricultural and Biological Engineering* 2(1):40–50.
67. Xu, Chunping, Rick Arneil D. Arancon, Jalel Labidi, and Rafael Luque. 2014. "Lignin Depolymerisation Strategies: Towards Valuable Chemicals and Fuels." *Chemical Society Reviews* 43(22):7485–7500.
68. Yaman, Serdar. 2004. "Pyrolysis of Biomass to Produce Fuels and Chemical Feedstocks." *Energy Conversion and Management* 45(5):651–71.

69. Yang, S. I., T. C. Hsu, C. Y. Wu, K. H. Chen, Y. L. Hsu, and Y. H. Li. 2014. "Application of Biomass Fast Pyrolysis Part II: The Effects That Bio-Pyrolysis Oil Has on the Performance of Diesel Engines." *Energy* 66:172–80.
70. Yuan, X. Z., H. Li, G. M. Zeng, J. Y. Tong, and W. Xie. 2007. "Sub- and Supercritical Liquefaction of Rice Straw in the Presence of Ethanol-Water and 2-Propanol-Water Mixture." *Energy* 32(11):2081–88.
71. Zhang, Jixiang and Yuanhui Zhang. 2014. "Hydrothermal Liquefaction of Microalgae in an Ethanol-Water Co-Solvent to Produce Biocrude Oil." *Energy and Fuels* 28(8):5178–83.
72. Zhang, Wennan, Till Henschel, Ulf Söderlind, Khanh Quang Tran, and Xu Han. 2017. "Thermogravimetric and Online Gas Analysis on Various Biomass Fuels." *Energy Procedia* 105(June):162–67.

Chapter 4

Development and Characterization Oriented Strand Board (OSB) with Epoxy and Partially Substituted Epoxy Resins with Fast Pyrolysis Bio-oil as Adhesive

4.1 Abstract

Epoxy resins have strong dry strength with good thermal resistance. However, it is brittle, expensive and the linkage between epoxy and wood can become considerably weakened after exposure to moisture. There is no literature documentation of using epoxy as a binder for OSB production. OSB production utilizing epoxy resin blended with fast pyrolysis bio-oil was studied. The aim of the study was to improve the hydrophobicity of the wood-epoxy matrix without compromising the mechanical properties. The effect of bio-oil substitution and resin content on the physical and mechanical properties of OSB was examined. The properties include an internal bond (IB), modulus of rupture, modulus of elasticity, thickness swelling (TS), and water absorption (WA). Hot stacking effects on the mechanical and physical properties was also assessed. The results showed that higher bio-oil content in the epoxy resin reduced the mechanical and physical properties of the OSB. Epoxy resin with bio-oil content of 30% showed comparable bonding properties to that of polymeric diphenylmethane diisocyanate (PMDI). Bio-oil substitution of 20% improved the hydrophobicity of the OSB. Hot stacking also improved the dimensional stability and mechanical properties of the boards. The maximum degradation temperature was high for the epoxy substituted bio-oil at 20% bio-oil content (471 °C). The soxhlet chemical resistance was low at 50% bio-oil content (38% mass loss), but the relative improvement of the epoxy chemical resistance was recorded at 20% bio-oil substitution level (6% mass loss). It was concluded that

epoxy resin could be used in the production of OSB. The addition of bio-oil could help to reduce the cost of the epoxy resin and as well improve the hydrophobicity of epoxy resin bonded to wood.

4.2 Introduction

Lignocellulosic biomass is known to be a suitable replacement for fossil-derived chemicals through thermochemical conversion processes. Biomass sourced chemicals are “green” and could reduce environmental pollution. One of the thermochemical processes which have received myriad attention is pyrolysis. Biomass pyrolysis to obtain high liquid fraction termed as bio-oil occurs under anoxic conditions at high temperatures (~ 500 °C). At a short residence time of about less than 2s, the process is called fast pyrolysis (Bridgwater, 2012). Detailed characterization of fast pyrolysis process and products are well documented (Uddin et al., 2018; Bardalai and Mahanta, 2015; Pan et al., 2013; Vispute, 2011; Demirbaş, 2000). Reactive organic compounds in biomass fast pyrolysis bio-oil such as phenolic monomers and oligomers, furans, carboxylic acids, ketones, etc. (Pan et al., 2013; Zhang et al., 2007) make it an attractive chemical feedstock for polymer synthesis and modification. Inwood composite (e.g., oriented strand board) manufacturing industry, wood residues from off-cut could be converted into fast pyrolysis bio-oil to provide energy for heating and chemicals for adhesive synthesis.

Oriented strand board (OSB) is engineered with multiple rectangular-like thin cut wood strands (or flakes), coated with thermoset adhesives and pressed at high temperature and pressure. OSB is similar to plywood in construction in that the core layers are oriented perpendicular to the surface layers. Currently, polymeric diphenylmethane diisocyanate (PMDI) and phenol formaldehyde (PF) adhesives are the major adhesives used in OSB production. pMDI has been used as a core resin and PF as surface resin in OSB production to accelerate curing as pMDI has a relatively low curing temperature requirement than PF in wood panels (Schwarzkopf et al., 2009). Interestingly,

pMDI has become a standard adhesive in OSB manufacturing supplanting phenol formaldehyde (PF). This is in part due to formaldehyde emission concerns from PF. However, pMDI is expensive. Modification of pMDI with low-cost bio-based polymers remains a challenge, as it ages within minutes of modification due to its high reactivity to other functional groups. Mao et al. blended pyrolysis bio-oil with pMDI for OSB production and the adhesive system was applied to the wood flakes within 8 minutes of mixing due to profuse bubbling (Mao et al., 2011). An alternative adhesive that has been modified with bio-based polymers to be used in OSB production is epoxy resins.

Epoxy (EP) resins are versatile thermosetting polymers used in construction, wood repairs, automobile parts, insulating, coatings and paints owing to their high strength properties, chemical resistance, good compatibility with other materials, good gap filling and high thermal stability (Celikbag et al., 2017; Blank et al., 2003). Nonetheless, EP resins remain as a minor wood adhesive in the wood composite industry. A major disadvantage of EP resin is cost and brittleness requiring improvement (Rowell, 2012; Pizzi et al., 2003). Recent studies have focused on utilizing bio-oil to either physically blend with epoxy or synthesized epoxy resin. The results from these findings suggest that the hydroxyl groups found in bio-oil react with the epoxide groups to form cross-linked copolymer network structures. Other functional groups like carboxyls have been reported to participate in the curing of epoxy resin. Comparative tensile-shear strength of bio-oil based epoxy to commercial epoxy has been reported. (Celikbag et al., 2017; Liu et al., 2017; Celikbag et al., 2015; Kuo et al., 2014; Sasaki et al., 2013; El Mansouri et al., 2011).

This study focused on the utilization of epoxy and epoxy modified pyrolysis bio-oil system in OSB production. To the best of our knowledge, this is the first study utilizing epoxy and epoxy substituted bio-oil in oriented strand board production. The study also characterized the hydroxyl groups (OH) of the bio-oil using quantitative ^{31}P NMR. The ratio of epoxy to OH groups is critical to optimizing epoxy crosslinking (Wei et al., 2014). The chemical interaction of the modified epoxy-bio-oil was studied using FTIR. The thermal and chemical stability of the cured epoxy system was also analyzed. Thus, the objective of this research was to produce OSB and characterize the effect of the epoxy, and epoxy-bio-oil resins on the mechanical and physical properties on the OSB panels.

4.3 Materials and Methods

4.3.1 Materials

Norbord Inc. in Alabama donated pre-screened pine wood of 8% moisture content. Epoxy resin (Epon 828) was obtained from Hexion Inc. Emulsified wax (Hexion Bord'N-Seal FMH-XD) and pMDI (MONDUR 541) were donated by J.M. Huber, Corp., and Commerce GA. Polypropylene glycol (PPG)-based polyetheramine as a curing agent (JEFFAMINE T-430) was donated by Huntsman Corporations. All chemicals were used as received and were of reagent grade.

4.3.2 Fast Pyrolysis Bio-oil Production

Pyrolysis bio-oil from loblolly pine wood was produced at Mississippi State University in a 7 kg h^{-1} auger-fed pyrolysis reactor similar to Li et al. (Li et al., 2013) without spraying of any chemicals. The auger speed was 10 rpm at applied pyrolysis temperature of 450 °C. The retention time was approximately 2 seconds. Methanol at a rate of 50% (v/v) was used to methylate the whole bio-oil and filtered to remove char and ash particles using #1 Whatman paper. The excess methanol was recovered using a rotary evaporator at 60 °C under 28" Hg vacuum. The water

content of the bio-oil was determined using volumetric Karl Fischer titrator (Mettler Toledo, model V20) with a hydranal-composite 5 solution (Sigma-Aldrich).

4.3.3 ATR-FT-IR

At room temperature (22 ± 1 °C), the attenuated total reflection Fourier Transform Infrared (ATR-FT-IR) spectra of EPON828, EPOIL resin, and FP bio-oil were acquired between 4000 and 650 cm^{-1} with an ATR-FT-IR spectrometer (Model Spectrum400, Perkin Elmer Co., Waltham, MA). The functional groups were determined at 64 scans with a 4.00 cm^{-1} resolution.

4.3.4 Epoxy/Pyrolysis Bio-oil Resin Formulation

Pyrolysis bio-oil and epoxy resin at various mixing levels (Table 2) were weighed into a beaker and a homogenous blend obtained using a magnetic stirrer and christened EPOil. Before mixing, the epoxy resin was heated to 60 °C on a water bath and the bio-oil added to ensure uniform mixing for 20 min at 2000 rpm. The mixture was kept at 45 °C. Epoxy resins and their physical blends at different substitution levels were hand-mixed with the calculated amount of Jeffamine T-403, W_J based on the epoxy equivalent weight (EEW). 10% acetone was added as a solvent-based on the epoxy solids to reduce the resin viscosity. The viscosity of the adhesives was measured by Fungilab rotary viscometer (Smart Series H, Model V210001). The adhesive specimens for characterization were prepared as described above and the resin was mixed with T-403 and transferred into an aluminum pan and heated in a conventional oven. The curing temperature was at 80 °C for 2 h followed by 120 °C for 1 hour and finally at 180 °C for an additional 1 hour. The samples were then allowed to cool to room temperature in the oven.

$$W_J = \frac{W_E \times AHEW}{EEW}$$

Where W_E is the amount of epoxy resin; AHEW is the amine hydrogen equivalent weight, the weight of amine hardener containing one equivalent of amine hydrogen.

4.3.5 Fabrication of Oriented Strand Board.

Oriented strand boards were manufactured following the material require parameters in Table 4.1. The screened wood strands were placed in a rotating blender sealed with vinyl covering with an aperture of 5cm by radius, cut in the middle to accommodate adhesive and wax. In a typical OSB batch fabrication, wax, followed by either pMDI or EPOil or Epoxy was sprayed unto the wood strands in a rotating blender equipped with a tumbler. Spraying was achieved using HVLP spray gun (HUSKY model # H4840GHVSG) powered by an air compressor. The coated strands were weighed and transferred unto a 43 x 43 cm frame placed on metallic platen covered with foil to prevent adhesion of the board to the platen. The strands were hand oriented. The platens were then hot pressed with Wabash hydraulic press (model 50-24-2TM) for 3 minutes (including closing and opening of the press) at constant temperature and pressure at 200°C and 2 MPa respectively. The desired board thickness of (11mm) was controlled with a distance bar placed at each side of the sandwiched platen. Panels made with pMDI adhesive only were used as control. The OSB panel had a 70% surface (EPOil or epoxy resin) to 30% core (PMDI) ratio. The target density was 641 kg/m³ (40 lbs/ft³). A total of 36 panels (six panels each for each adhesive treatment) were produced. Half of the panels were post-treated (hot-stacked) in an oven immediately after hot pressing at 160 °C for 2 hours. The moisture content for the wood strands were approximately 6 ± 1% at the time of adhesive loading.

Table 4.1: OSB manufacturing parameters

Item	Description
Adhesive loading	3% wt (oven dry wood basis)
Adhesive type used	Epon 828 substituted with pyrolysis bio-oil (top) and PMDI (core)
Wax	1% wt (on oven dry wood basis)
Press temperature	210°C
Post-Treatment	with and without post-treatment (hot-stack)
Panel format	3-layer: 70 wt % (face 35wt% each) and 30 wt % (core)
Panel dimension	41 cm x 41 cm x 11 cm
Target Density	641 kg/m ³
Press time	180 seconds (closing and opening of press inclusive)
Epoxy/bio-oil substitution	80/20, 70/30, 60/40, 50/50

4.3.6 Characterization of board properties

Panels were cooled to ambient temperature and were cut into test specimens in accordance with ASTM D1037-12. The test specimens were conditioned at 20 °C ± 2°C and relative humidity of 65% ± 2 in a conditioning chamber. Each sample was weighed, and the dimensions are taken for density determination. The modulus of elasticity (MOE), modulus of rupture (MOR), internal bond strength (IB), and thickness swell (TS) of the test specimens was carried out following ASTM D1037-12 (ASTM International, 2012) recommendations. Strand board samples referred to as wet boards were soaked for 24-hours continuously (method B) according to the ASTM D1037-12 standard.

4.3.7 Bending test (Modulus of Elasticity (MOE) and Modulus of Rupture (MOR))

For the MOE and MOR tests, sixteen samples of dimensions 30.5 x 7.6 by 1.1 cm were randomly selected from 6 panels (eight replicates were used in dry test condition and the other half in wet

test condition) for each formulation. Samples designated wet were soaked in water for 24 hours at $20\text{ }^{\circ}\text{C} \pm 1\text{ }^{\circ}\text{C}$. Three-point static bending test, carried on a universal testing machine (Zwick/Roell Z010), was used to determine the MOE and MOR. The MOE measures the stiffness of the panels under bending, while the MOR measures the maximum load carrying capacity of a member in bending. Load/deflection curve was obtained from tensile loading applied at a speed of $0.31\text{''}/\text{min}$ ($7.874\text{ mm}/\text{min}$). TestXpert® II software was used to compute the MOE (E) and MOR, and (R_b) respectively; where P_{max} is the maximum load (N), b is the width of the specimen (mm), d is the thickness of the specimen (mm), L is the length of span (mm), $\Delta P/\Delta y$ is the slope of the straight-line section of the load-deflection curve (N/mm), E is the modulus of elasticity (GPa), and R_b is the modulus of rupture (MPa).

$$E = \frac{L^3}{4bd^3} \frac{\Delta P}{\Delta y}$$

$$R_b = \frac{3PP_{max}L}{2bd^2}$$

4.3.8 Internal Bond Strength

Internal Bond Strength (IB), which measures the adhesive bond strength, was conducted in the dry condition according to the ASTM D1037-12 standard method. Ten replicates for the different adhesive types under investigation of dimensions $5.1 \times 5.1 \times 1.1\text{ cm}$ were used. The IB samples were glued with hot melt adhesive unto an aluminum alloy block and then loaded unto an IB fixture on the Zwick/Roell Z010 testing machine. The IB test, which measures the tensile loading perpendicular to the glued specimen surface, was calculated from the following equation

$$IB = \frac{\text{Maximum load(N)}}{(\text{mm}) \times \text{Width (mm)}}$$

4.3.9 Thickness Swelling (TS) and Water Absorption (WA)

Square specimens of dimensions 15.2 x 15.2 cm were prepared for the TS and WA tests. Eight replicates each of the different adhesive formulations panels were used. The weight of the samples was measured before and after soaking. Prior to soaking, the samples average dimensions were taken at the center, 2.54 cm inward from the edge of the four corners of the samples with a Vernier caliper. This process was repeated immediately after the soaking test. Samples were soaked in water maintained at 20 °C ± 3 °C for a 24-hr duration. Samples were drained and wiped with a paper towel and the weights and dimensions recorded as described above. The TS was evaluated as the difference in thickness expressed as a percentage between the average thickness before and after the 24-hr soak. WA was calculated as the weight difference in percentage before and after the 24-hr water soak.

4.3.10 Thermogravimetric Analysis

Thermal degradation behavior of the epoxy and epoxy substituted bio-oil samples was carried out by using thermogravimetric analyzer (Shimadzu, TGA-50/50H). Samples of 9 ± 1 mg were heated under an N₂ atmosphere at 20 mL/min from ambient temperature to 800 °C at a heating rate of 10 °C/min.

4.3.11 Differential Scanning Calorimetry (DSC) Analysis

The glass transition temperature (T_g) was established with a Differential Scanning Calorimetry (TA Instruments Q2000 DSC, TA Instruments, New Castle, DE, USA). For each scan, ~6 ± 1 mg of dried cured epoxy, or epoxy substituted bio-oil were added into an aluminum pan. The temperature schedule for the DSC was scheduled from ambient temperature to °C and then raised

from 20 to 210 °C. A 50 mL/min nitrogen flow was used at a heating rate of 10 °C/min. For polymers, glass transition temperature (T_g) is defined as the temperature at which the mechanical properties of a polymer radically changes from the glass state into a high elastic state due to the internal movement of the polymer chains.

4.3.12 Solvent Resistance of cured Epoxy and Epoxy Substituted Bio-oil

The cured epoxy and epoxy substituted bio-oil at different bio-oil content were grounded to 40 mesh by Wiley Mini Mill (Thomas Scientific, model no: 3383-L10, Swedesboro, NJ.) for acetone extraction. The soxhlet extractor was obtained from Ace Glass Incorporated (Vineland, NJ.). Extraction thimbles filled with the grounded resin samples (~2g) were placed into the soxhlet system, and then the extraction flask was filled with 150 mL acetone. The soxhlet systems were heated up and allowed to reflux for 6h. After extraction, acetone was evaporated and the solid residue was dried in an oven for 5h at 105°C. The mass loss (%) for each adhesive formulation was then calculated as a percentage by subtracting the weight of residue from the weight of starting grounded POBER resin.

4.3.13 Scanning Electron Microscopy Analysis of cured Epoxy and Epoxy/bio-oil Resin

Cross-sectional surface morphology of the notched impact fractured samples were observed using a scanning electron microscope. All samples were sputter-coated with gold before scanning electron microscopy (SEM) analysis.

4.3.14 Data Analysis.

The MOE, MOR, IB, TS and WA properties were analyzed by Minitab ® 19.1.1 (64-bit) software using a one-way analysis of variance (ANOVA) for the different adhesive formulation. The

different levels of pyrolysis bio-oil substitution and the effect of hot-stacking were compared using Tukey honestly significant difference test (Tukey's HSD) ($P < 0.05$).

4.4 Results and Discussion.

4.4.1 Viscosity

Adhesive spraying and distribution is a fundamental production process in OSB manufacturing and it is closely associated with adhesive viscosity. To aid in effective spraying and homogenizing of the adhesive ethylene glycol monomethyl ether was added to the adhesive mixtures except for the pMDI. The viscosities of the different adhesive formulation is shown in Table 4.2. The reduction in viscosity may be associated with the moisture in the bio-oil substituted in to the epoxy resin.

Table 4.2 : Adhesive formulations with associated viscosities, panel density and mat moisture content (MC)

Resin code	Resin Composition (%)		Viscosity (mPa s)	Panel density g/cm ³	Mat (%)
	Epoxy (%)	Bio-oil (%)			
PMDI	0	0	282	648 ± 3	7 ± 1
Epoxy	100	0	472	647 ± 3	7 ± 1
EP_B(20%)	80	20	457	648 ± 2	8 ± 1
EP_B(30%)	70	30	443	649 ± 2	8 ± 1
EP_B(40%)	60	40	431	648 ± 3	9 ± 1
EP_B(50%)	50	50	416	649 ± 2	10 ± 2

4.4.2 ATR-FT-IR

The IR spectra of pyrolysis bio-oil, epoxy resin (EPON 828), and epoxy substituted pyrolysis bio-oil are illustrated in Figure 4.2. Band assignments for other functional groups are summarized in Table 4.3. The broad peak at around 3363 cm^{-1} indicated the presence of O–H groups in the bio-oil. The ^{31}P -NMR analysis corroborated the FTIR results that bio-oil contains substantial aromatic and aliphatic type O–H groups. The band assignment at 1716 cm^{-1} was ascribed to carbonyl (C=O) groups in the bio-oil. The presence of carbonyl moieties in bio-oil is associated with the decomposition of cellulose and hemicellulose of the pine biomass (Uddin et al., 2018).

The band absorbance at 2968 cm^{-1} and 1460 cm^{-1} were C–H vibration and C–H deformation vibration, respectively. Aromatic species in the bio-oil, also confirmed by the GC-MS analysis, gave characteristic peaks at $1019\text{--}1180\text{ cm}^{-1}$, $1213\text{--}1297\text{ cm}^{-1}$, 1608 cm^{-1} , and 1508 cm^{-1} . A distinguishing characteristic peak for Epon was assigned at 913 cm^{-1} for the epoxide ring. Individual IR spectra of the substituted epoxy-bio-oil reveal that the reaction was complete. For instance, in Figure 4.1, pyrolysis bio-oil showed strong O–H peak at 3363 cm^{-1} . However, weaker peaks were observed in the EP-bio-oil spectra indicating that O–H groups in the pyrolysis bio-oil were consumed during curing as illustrated Figure 4.1.

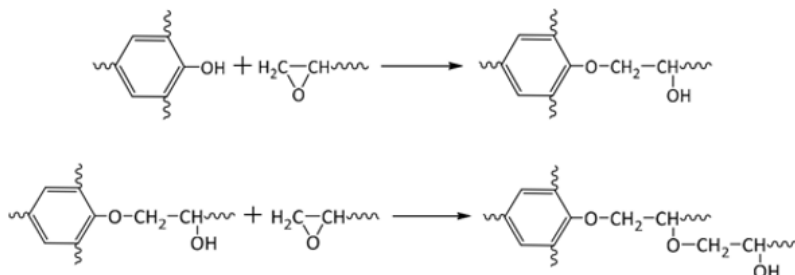


Figure 4.1: Reaction of hydroxyl groups of the bio-oil with the epoxide of Epoxy resin.

However, the cured EP-bio-oil spectra showed a slight increase in –OH peak with high levels of bio-oil substitution. This could be ascribed to the excess –OH functionalities that were not consumed during curing. Interestingly, the EPON 828 epoxide groups with band assignment at 913 cm^{-1} are completely removed from the cured EP-bio-oil spectra. This confirmed that the reaction between EPON 828 and pyrolysis bio-oil was completed, thus the disappearance of the epoxide signatures within the spectra.

The IR spectra also reveal that the carbonyl groups (1716 cm^{-1}) of the bio-oil also participated in the curing of EPON 828 and as the carbonyl peak was nearly removed from the spectra. This is demonstrated in the carbonyl cross-linking reaction with epoxy in equations Figure 4.3. It could be inferred from the FTIR spectra that the hydroxyl and carbonyl groups within the pyrolysis bio-oil took part in the curing of EPON 828.

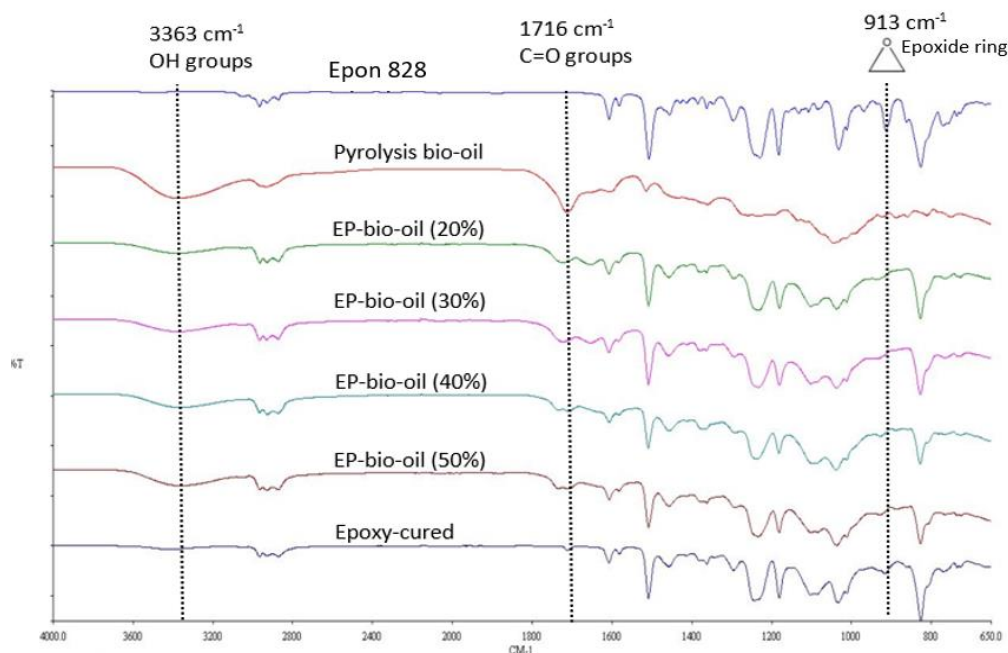


Figure 4.2: FTIR spectra of fast pyrolysis bio-oil, EPON 828 (unmodified commercial grade) and epoxy substituted bio-oil at different bio-oil content (EP-bio-oil).

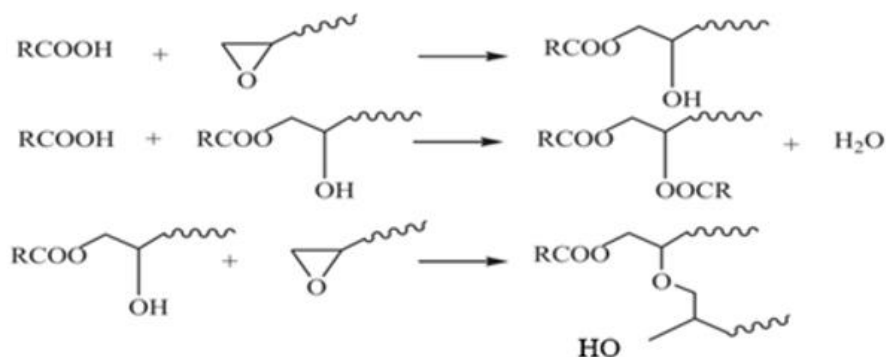


Figure 4.3: Reaction of carbonyl groups of the bio-oil with the epoxide of Epoxy resin.

Table 4.3: FTIR band assignment of pyrolysis bio-oil, EPON 828 (unmodified commercial grade) and Epoxy substituted bio-oil (EP-bio-oil).

Sample	Wavenumber (cm ⁻¹)	Band Assignment
Pyrolysis Bio-oil	3363	O–H stretching
EPON & Pyrolysis Bio-oil	2968-2936	Aromatic C–H stretching
Pyrolysis Bio-oil	1716	C=O stretch in conjugated carbonyls, ketones, and ester moieties
EPON, & pyrolysis Bio-oil, & EP- bio-oil	1608, 1508	in ring C-C stretch
EPON, & pyrolysis Bio-oil, & EP- bio-oil	1214-1233	C–C, C–O, and C=O stretching
Epoxy & EP- bio-oil	1000 - 1178	Deformation vibration of C–H bonds in benzene rings
Epon	1035	C–H bending
Epon	913	Epoxide
Epon	825	Aromatic ring bending

4.4.3 Bending properties

Three-point bending test (MOE and MOR) of the OSB panels produced from pMDI (control), epoxy and epoxy substituted pyrolysis bio-oil is illustrated in Figures 4.4 and 4.5. From Figure 4.4, the MOE of OSB panels made from 100% epoxy resin showed mean values of 49.55 ± 2 GPa and 50.99 ± 1 GPa (hot-stacked). Substituting epoxy resin with pyrolysis bio-oil up to 30% did not affect the MOE of the panels. It was interesting to observe an increase in MOE 50.36 ± 1 GPa and 52.99 ± 1 GPa (hot-stacked) at 20% bio-oil substitution.

However, a significant reduction in MOE at higher bio-oil substitution levels was noted. The retained or improved MOE properties at lower levels of bio-oil replacement in epoxy can be attributed to the optimal stoichiometric ratio of epoxy/bio-oil mixing. Auad et al illustrated that for optimum cross-linking density to occur, the precise molar ratio of epoxy to hydroxyl groups blend is critical before curing (Auad et al., 2006). It could be conjectured that the higher amount of bio-oil replacement (40% to 50%) may have deviated from the optimal stoichiometric ratio, leading to a reduction in cross-linking density. This was evident in the stiffness values from 50.36 ± 0.79 GPa at 20% bio-oil substitution to 33.52 ± 2 GPa at 50% bio-oil substitution (in the untreated samples).

It is apparent from Figure 4.5 that the MOR for the untreated and hot-stacked panels, and the wet MOE and MOR followed a similar trend of decreasing strength with higher bio-oil replacement. A possible elucidation is that pyrolysis bio-oil is replete with phenols and phenolic derivatives, as seen in the GC-MS analysis in Figure 3.5, which could impact the degree of polymerization and curing in-situ the wood panels during hot pressing. Higher molecular weights resulting from high bio-oil substitution levels may have shifted the curing time of the panels forward. This assumption agrees with Celikbag et al. findings on reacting epoxy with pyrolysis bio-oil using

triphenylphosphine catalyst without curing agent. They noted that lower levels of pyrolysis bio-oil substitution resulted in a low molecular weight resin system, which increased epoxy resin reactivity (Celikbag et al., 2017). El Mansouri et al, also found that a decreased molecular weight results in more hydroxyl groups accessibility for reaction during the cure of bio-based epoxy resin (El Mansouri et al., 2011).

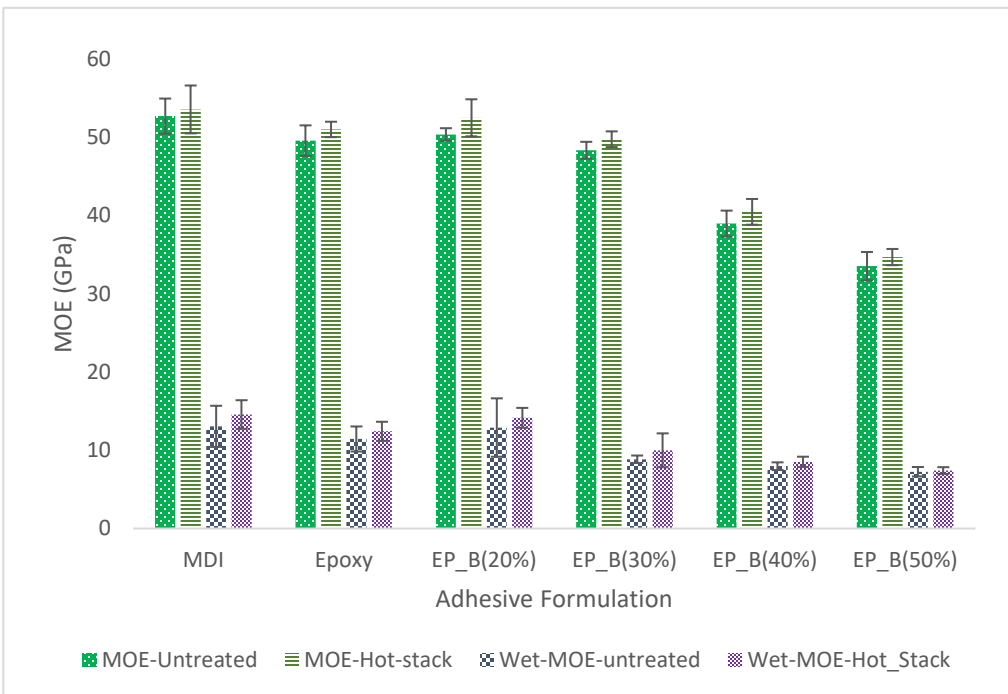


Figure 4.4: Modulus of Rupture of OSB bonded with the epoxy and epoxy substituted bio-oil adhesives with different bio-oil contents. B (20%) = 80% epoxy resin substituted with 20% bio-oil; B (30%) = 70% epoxy resin substituted with 30% bio-oil; B (40%) = 60% epoxy

Analysis of variance (ANOVA) of the untreated and hot-stacked samples for the MOE and MOR (in dry and wet conditions) were significantly different at $p < 0.05$. Further analysis by Tukey's HSD on the effect of hot-stacking on the bending properties within each adhesive formulation at

all conditions was not significant. Nonetheless, the hot-stacking improved the bending properties of OSB panel for all the adhesive formulations.

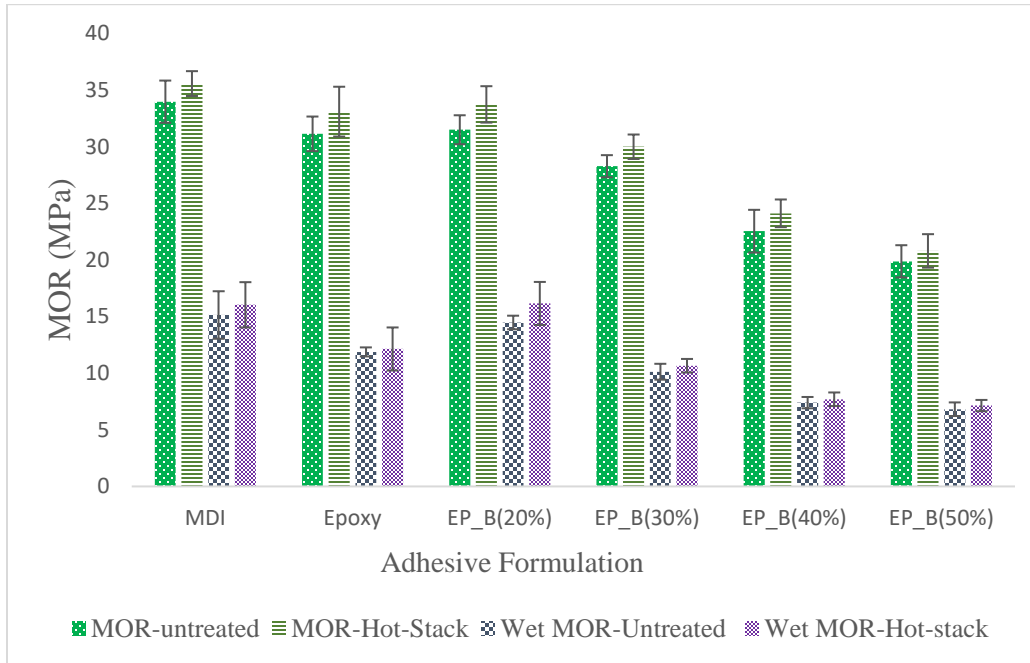


Figure 4.5: Modulus of Rupture of OSB bonded with the epoxy and epoxy substituted bio-oil adhesives with different bio-oil contents. B (20%) = 80% epoxy resin substituted with 20% bio-oil; B (30%) = 70% epoxy resin substituted with 30% bio-oil; B (40%) = 60% epoxy

For example, the MOR of the untreated 20% bio-oil substituted epoxy resin increased from 33.98 ± 2 MPa to 35.58 ± 1 MPa when hot-stacked, which is ~5% increase in flexural modulus. Furthermore, substituting epoxy resin with pyrolysis bio-oil up to 30% did not significantly affect the MOE and MOR of the panels. This is an interesting finding because (i) higher levels of bio-oil substitution at optimal panel bond strength translates into cost savings for manufacturers. (ii) fast pyrolysis bio-oil is sustainable to produce, promoting “green” chemicals utilization. It is worth mentioning that the MOE and MOR of the control OSB panels were higher than the epoxy and epoxy substituted bio-oil in all instances. However, it was not significantly different from the

epoxy and epoxy substituted bio-oil up to 30%. This indicates that epoxy resin modified bio-oil offers an alternative structural adhesive to pMDI.

4.4.4 Internal Bond Strength (IB)

The IB strength measures the strength of the adhesive in the OSB panels such that the tested samples are pulled apart axially with the load direction perpendicular to the horizontal axis of the boards. Figure 4.6 shows the results of the IB test. Hot-stacking did not significantly affect the IB properties of the individual adhesive binder system in the OSB panels. As the bio-oil content increased in the epoxy resin system, hot stacking effect on the IB also increased. For instance, the percentage increase in IB strength was ~6%, ~10 % and ~21 % for bio-oil content of 30%, 40% and 50 %, respectively. Conversely, high levels of bio-oil in the epoxy resin system reduced the IB strength of the panels. It could be speculated that the improvement in IB strength of the panels after prolonged heating may have aided the reaction of residual epoxy resin with unreacted large molecular weight compounds such as lignin derivatives in the bio-oil. Although a minimal increase in IB after hot-stacking was noted for pMDI, epoxy and 20% bio-oil substituted epoxy samples. Mao et al. expressed that longer hot-pressing time may be required to spread large bio-oil molecules on wood strand surfaces when they blended pMDI with pyrolysis bio-oil (Mao et al., 2011).

The pyrolysis bio-oil in this study had a substantial amount of water (19%). This could mean that at high substitution levels of bio-oil, the mat moisture increased, which could interfere with the adhesive bonding, thereby requiring longer pressing time. Chan et al observed a similar reduction in IB strength at high levels of pyrolysis bio-oil content with phenol formaldehyde resin (Chan et al., 2002). This may have caused a significant reduction in IB strength in the untreated IB samples at high bio-oil substitution.

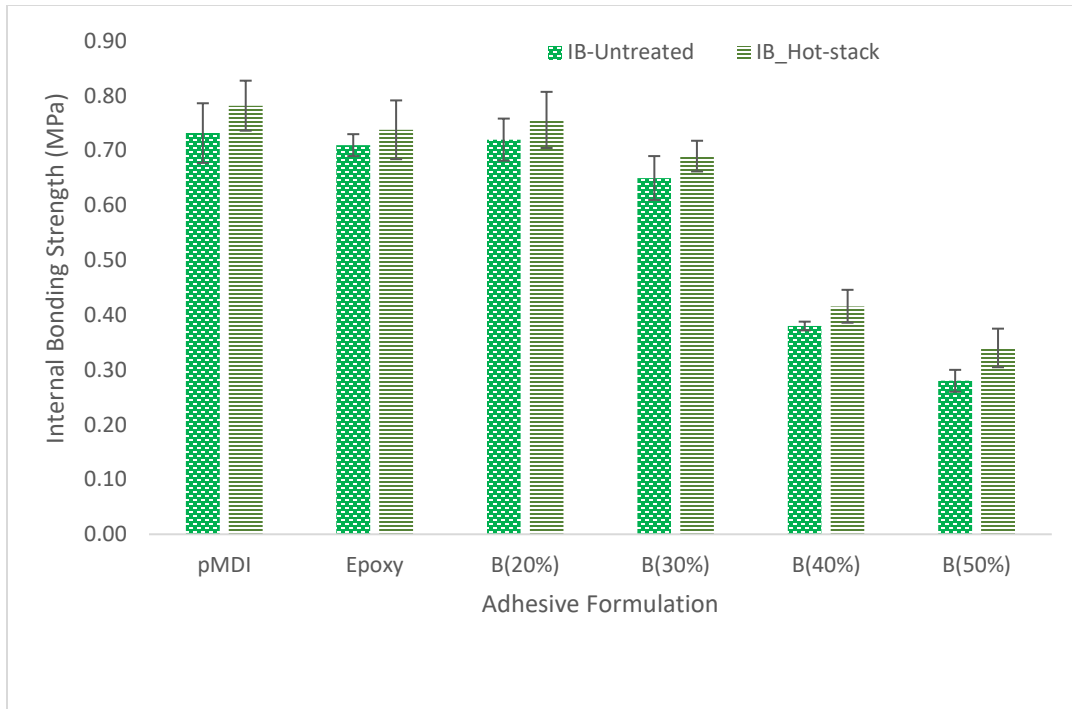


Figure 4.6: Internal bond strength of OSB bonded with the epoxy and epoxy substituted bio-oil adhesives with different bio-oil contents. B (20%) = 80% epoxy resin substituted with 20% bio-oil; B (30%) = 70% epoxy resin substituted with 30% bio-oil; B (40%) = 60%

4.4.5 Thickness Swell (TS) and Water Absorption (WA)

The 24-hour water soak test is depicted in Figure 4.7. High levels of bio-oil in the epoxy resin system increased the TS and WA properties of the OSB panels (in the untreated and hot-stack conditions) and were significantly different ($p < 0.05$). TS and WA increased by 68% and 75% for epoxy substituted bio-oil from 20% to 50%, respectively. The high TS and WA trends observed at high bio-oil content in the epoxy resin system are traceable to the increased wood strand moisture at high bio-oil substitution. Also, a more probable reason is the interaction between the polar functional groups in pyrolysis bio-oil like hydroxyls ($-OH$) and aldehydes ($-COOH$) with water. Polar functional groups are capable of forming hydrogen bonding with the $-OH$ groups in wood

(Mekonnen et al., 2014). The hydrogen bonds developed were severed in the presence of water; thus, the increased TS and WA.

Relatively, the hot-stack OSB panels were hydrophobic compared to the untreated samples. Reduced water uptake and swelling of wood cell walls by heat treatment reduce water intake, as the wood cell wall absorbs less water due to a decrease in the amount of hydroxyl groups (Inoue et al. 1993; Aro et al. 2014). The prolonged heating of the hot-stacked samples removed free water resulting from the bio-oil and, to some extent, bound water from the wood cell walls. This may have improved the TS and WA in the hot-stack panels.

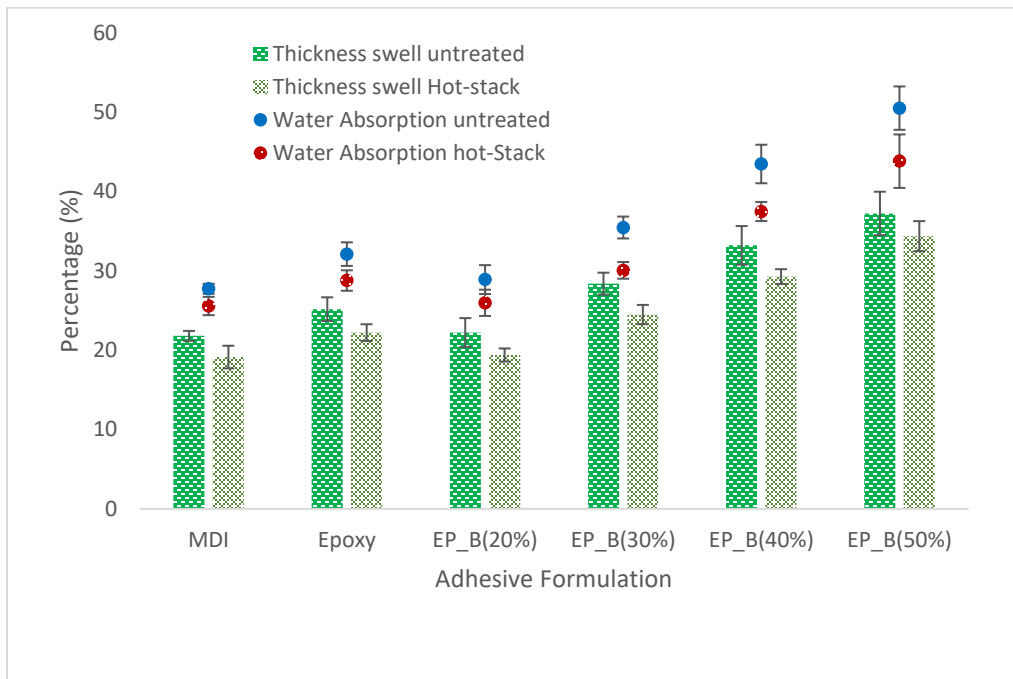


Figure 4.7: Thickness swell (TS) and water absorption (WA) bonded with the epoxy and epoxy substituted bio-oil adhesives with different bio-oil contents. B (20%) = 80% epoxy resin substituted with 20% bio-oil; B (30%) = 70% epoxy resin substituted with 30% bio-oil

4.4.6 Thermogravimetric Measurements of Epoxy and Epoxy substituted Bio-oil.

The TGA and DTG of epoxy (Epon 828), and epoxy substituted bio-oil resin are presented in Figure 4.8 and Table 4.4. The TGA thermographs for Epon 828, and epoxy substituted bio-oil samples exhibited a similar 3-stage degradation process. A similar second-stage degradation process was observed for all the adhesive types studied, out of which the unmodified epoxy resin (EPON 828) exhibited higher thermal stability. From Figure 4.5, Epoxy resin was found to be stable up to 320 °C. The thermal stability decreased at higher levels of bio-oil substitution in the epoxy resin (from 289 to 229 °C, respectively, for 20% to 50% bio-oil content). The reduction in thermal stability may be due to unreacted low molecular weight compounds in the bio-oil. The weight loss reached a maximum of 67% in the temperature range from 320 to 510 °C for the epoxy resin, while the maximum weight loss was 68% for epoxy substituted bio-oil (20%) at a temperature range from 276 to 520 °C. This could have resulted from the degradation of the ether and ester groups formed by the ring-opening reactions between the amine groups of the curing agent and epoxy-bio-oil groups (Mailhot et al., 2005).

The statistic heat-resistance index (T_s) temperature is a characteristic of the thermal stability of the cured resin in the physical heat tolerance limit. The T_s value was estimated from the temperature at 5% weight loss (T_{d5}) and 30% weight loss (T_{d30}) of the specimens obtained from the TGA as in equation (1) (Chiu et al. 2008) and summarized in Table 4.4 .

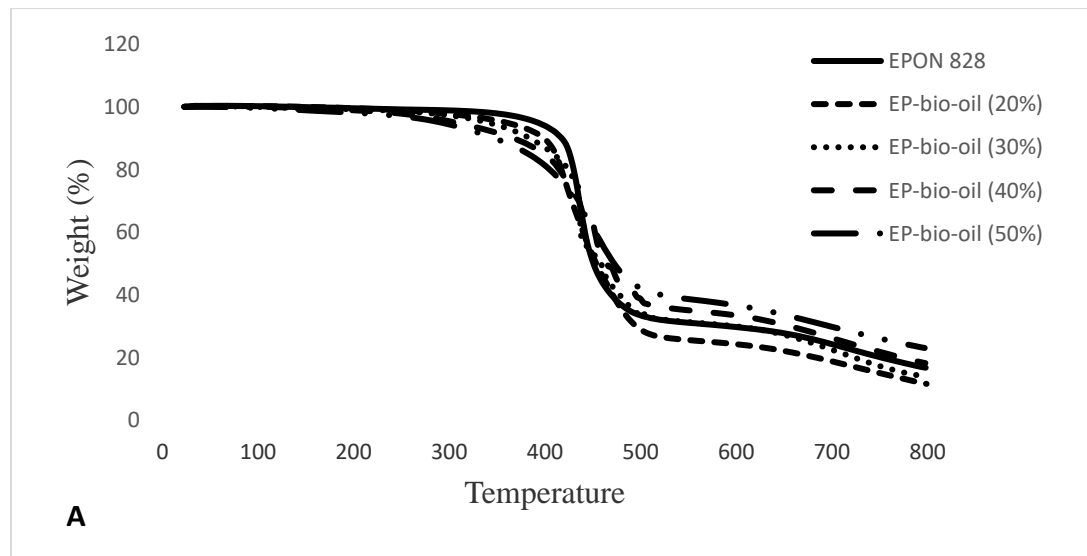
$$T_s = 0.49 [T_{d5} + 0.6 (T_{d30} - T_{d5})] \quad \text{equation} \quad (1)$$

The T_s value for the blended bio-oil epoxy resin generally was low relative to that of the neat epoxy resin. However, the T_s value was comparable up to 30% bio-oil substitution at 197 °C, and 202 °C for the neat epoxy resin, respectively. These index values are considered as medium-range index

values (Hafiezal et al., 2019) and it is also critical to the curing of the OSB during hot pressing at 200 °C.

The DTG thermographs showed a maximum decomposition rate temperature at 437 °C for neat epoxy, and could be ascribed to the pyrolysis of the cross-linked network (Sahoo 2018). A similar degradation took place in the epoxy substituted bio-oil, which showed two degradation peaks. However, the first peaks align with the degradation of epoxy to the left. The second degradation shoulder peaks of the epoxy substituted bio-oil, for example, 20% bio-oil content, showed maximum decomposition temperature at 471 °C, and may be attributed to macromolecular compounds such as aromatic phenolic hydroxyls which crosslinked with the epoxide groups of Epon 828. Thus, improving the thermal stability of the modified epoxy resins.

Also, the improved stability may have been influenced by the presence of unreacted lignin in the resin system that requires higher temperatures exceeding 380 °C for degradation (Rowell 2005).



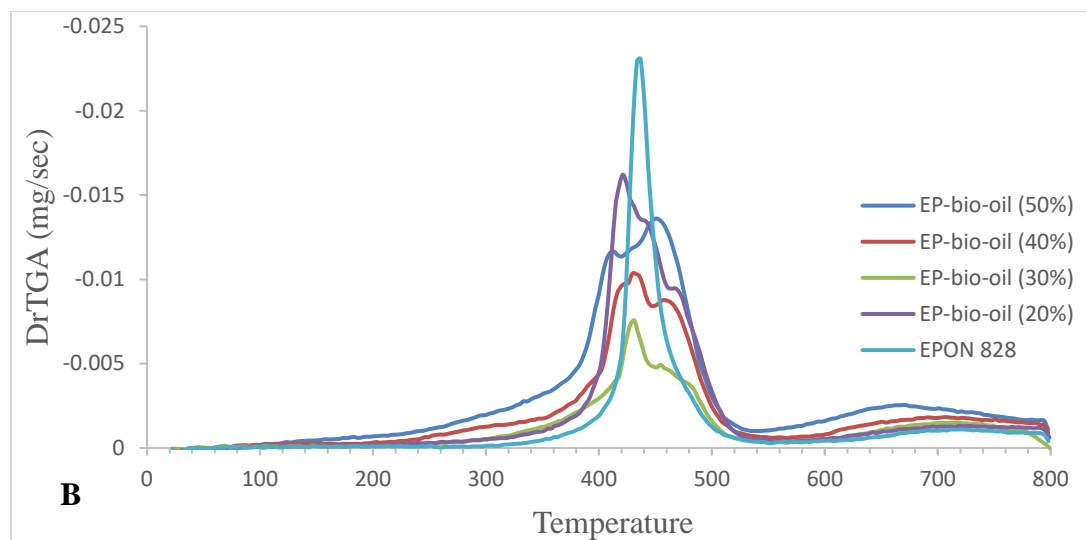


Figure 4.8: Thermogravimetric (TGA) and (B) Derivative weight loss (DTG) thermograms of Epon 828 (commercial neat epoxy), and epoxy substituted bio-oil at different bio-oil content.

Table 4.4: TGA data of the cured epoxy resins and epoxy bio-oil resins.

Samples	T _{d onset} (°C)	T _{d max} (°C)	T _{d5} (°C)	T _{d30} (°C)	T _s (°C)
Epoxy	314	437	385	433	202
EP-bio-oil (20%)	276	471	361	428	198
EP-bio-oil (30%)	266	451	341	438	197
EP-bio-oil (40%)	260	453	306	436	188
EP-bio-oil (50%)	229	447	293	433	185

EP = epoxy resin.

4.4.7 DSC analysis

The glass transition, T_g , of all the cured samples (epoxy, and epoxy substituted bio-oil at various bio-oil contents) determined using DSC is illustrated in Figure 4.9. The thermograms suggested that the epoxy/bio-oil resin systems utilized the curing agent and as a result, no crystallization or

melting transitions were observed. High bio-oil substitution levels into the epoxy resin system apparently reduced the T_g of the cured resin system. This low glass transition could be attributable to the free volume within the cured sample and unreacted part of the resin and excess bio-oil (Sahoo 2018). The higher T_g for the 20% and 30% bio-oil substituted epoxy resins is suggestive of better cross-linking density as demonstrated by the consumption of phenolic hydroxyls ($-OH$), and carboxyl moieties ($C=O$) with the complete removal of the epoxied functional groups signature in the IR spectra (Figure 4.2).

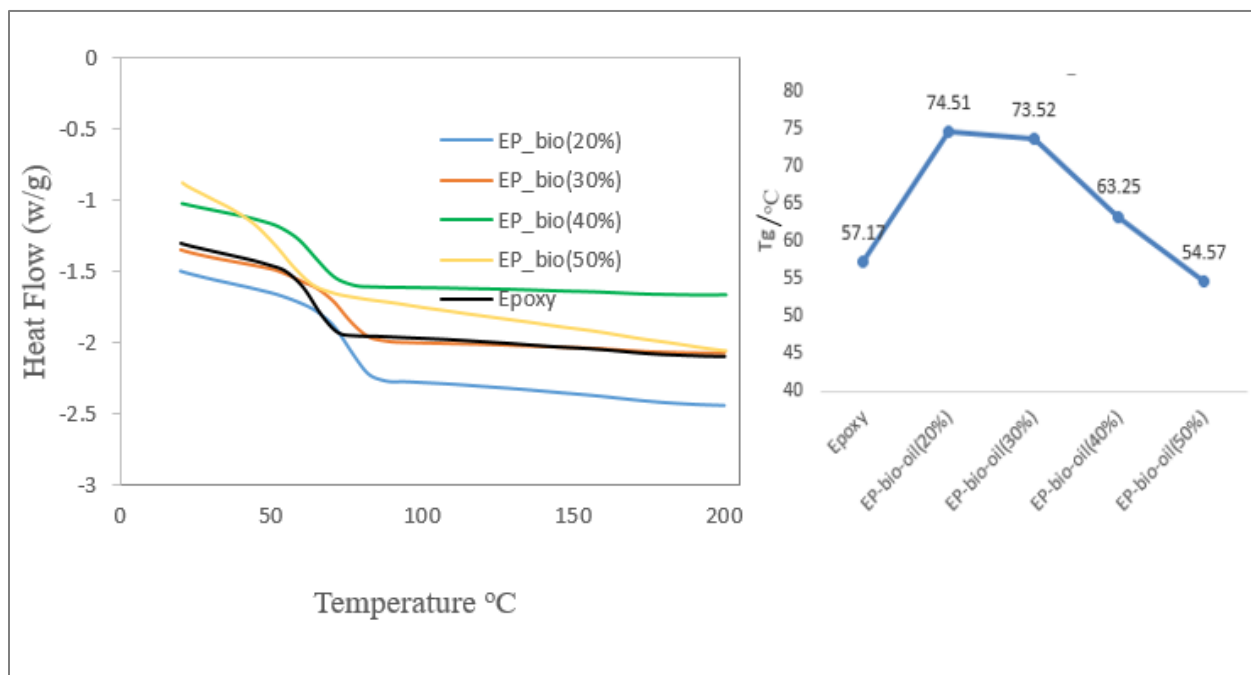


Figure 4.9: Thermal transitions of differential scanning calorimetry (DSC) of Epon 828 (commercial neat epoxy), and epoxy substituted bio-oil at different bio-oil content.

4.4.8 Solvent Resistance of Epoxy and Epoxy substituted Bio-oil

Figure 4.10 shows the mass loss of cured epoxy and epoxy substituted bio-oil at different bio-oil content. The solubility of the adhesive systems and the minimum epoxide content for the stability

of the final product were determined by acetone extraction. Acetone is an effective solvent for fast pyrolysis bio-oil (Mao et al., 2011), and epoxy and therefore, could dissolve unreacted bio-oil, and epoxy from the polymer matrix. A decrease in mass loss from 39% to 6% was observed as the bio-oil replacement content in the epoxy resin decreased. This reveals that the epoxy/bio-oil polymer became more completely reacted and, thus, the less soluble product. Celikbag et al, agreed with this observation and found that higher mass loss was associated with high levels of bio-oil incorporation into epoxy resin system when epoxy was cross-linked with pyrolysis bio-oil using triphenylphosphine as a catalyst (Celikbag et al., 2015). The increase in insolubility at 20% bio-oil substitution into the epoxy resin system suggests that a near stoichiometric ratio was reached and a highly cross-linked network dominated the cured resin structure.

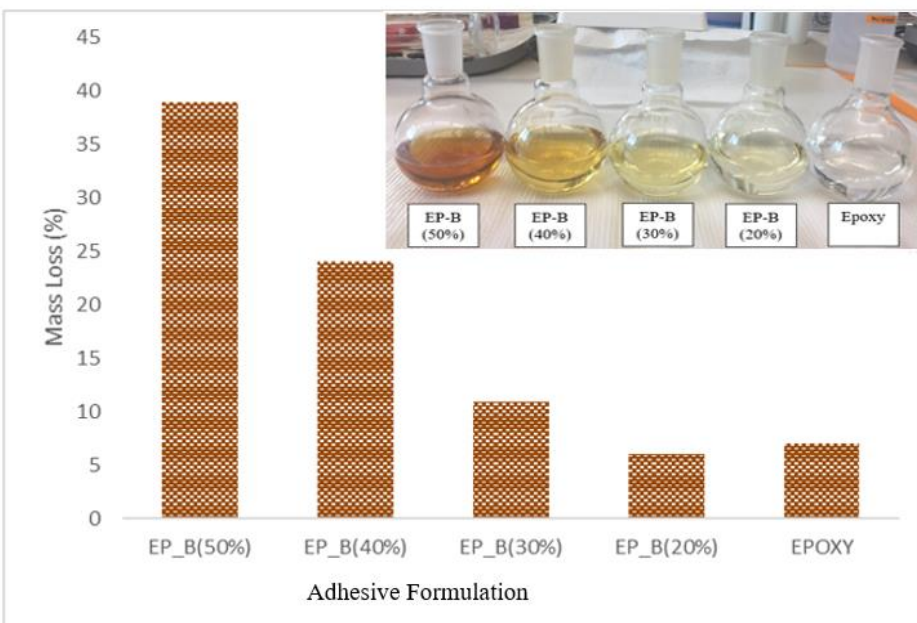
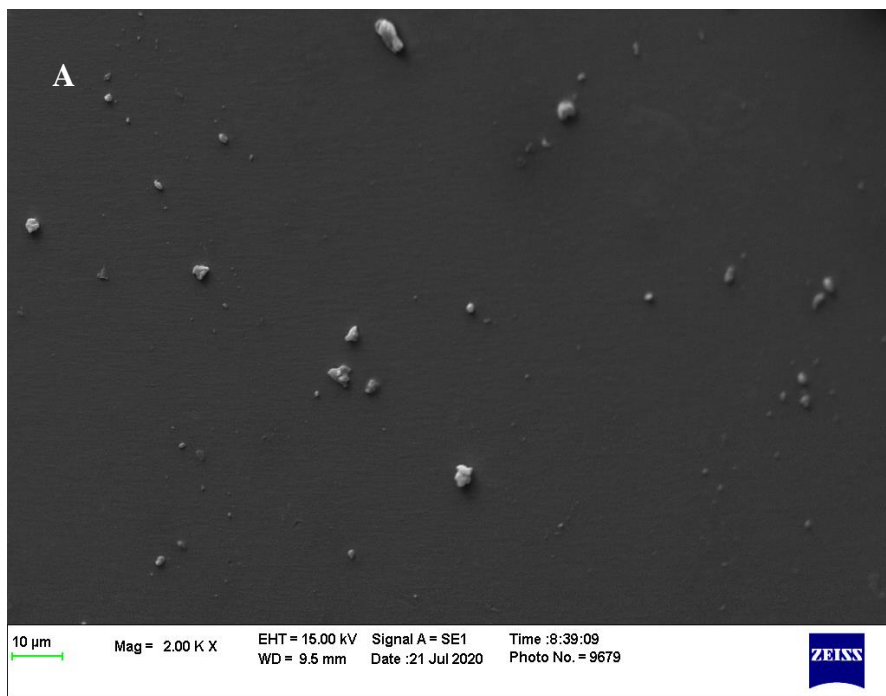


Figure 4.10: Mass loss (wt %) of Epon 828 (commercial neat epoxy), and epoxy substituted bio-oil resins system under acetone for 6 h. EP_B = epoxy resin substituted bio-oil; B (20%) = 80% epoxy resin substituted with 20% bio-oil; B (30%) = 70% epoxy resin substitution.

4.4.9 Epoxy and Epoxy substituted with Bio-oil Morphology

The SEM analysis of the cured epoxy and epoxy/bio-oil is shown in Figure 4.11. Morphology of the epoxy/bio-oil resin was found to be homogeneous. The epoxy indicated similar homogeneity. Fractured surface of epoxy was smooth, indicating high brittleness, whereas epoxy/bio-oil revealed random degree of fracture with a low extent of brittleness. Furthermore, the fractured surface of epoxy/bio-oil is suggestive of a more diverse system due to the possibility of the formation of bio-epoxy from several aromatic substituted compounds.



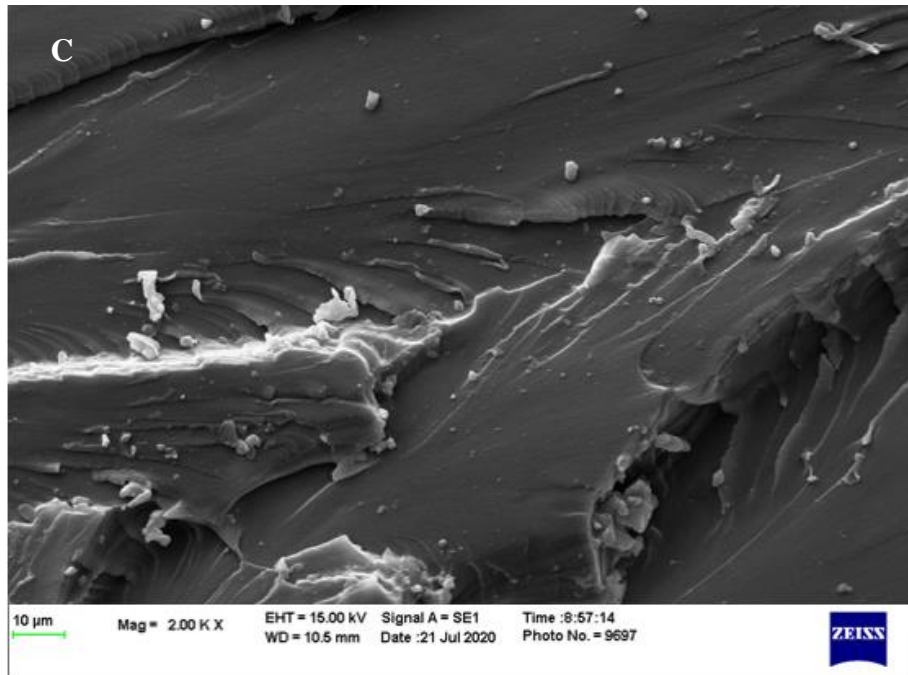
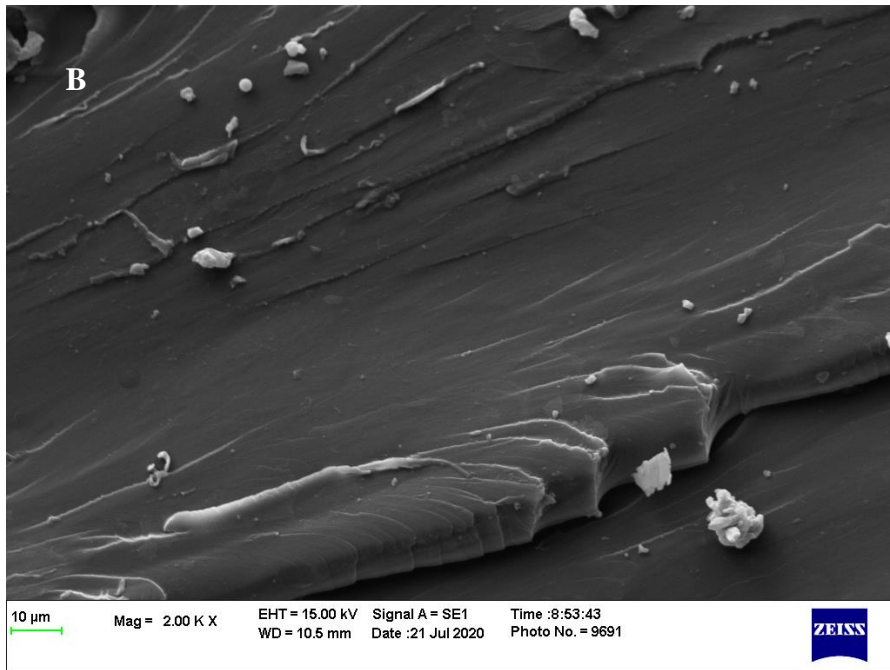


Figure 4.11: Morphology by scanning electron microscopy (a) neat Epoxy (EPON 828); (b) Epoxy/Bio-oil (80:20); (c) Epoxy/Bio-oil (780:30).

4.5 Conclusion

Epoxy resin and epoxy substituted bio-oil resins at different bio-oil contents were successfully incorporated into the wood strands and OSB boards were fabricated. The strength properties of the OSB from the epoxy resin systems revealed that lower dosage of bio-oil up to 30% substitution is feasible without significantly reducing the OSB strength properties. Improvement in the ‘hot stacking’ samples of the OSB panels indicated that the epoxy resin system has a high-temperature requirement for complete resin cure. However, the ‘hot stacking’ effect was not significant within the same resin formulation. 20% bio-oil substitution was shown to improve the wet properties of the OSB panels. The OH and C=O functional groups contributed to the curing mechanism of the epoxy resin system. The TGA work demonstrated that overall the bio-oil substitution in epoxy exhibited mass loss events due to the different chemical functionalities in the bio-oil. The Tg of the bio-oil epoxy resin system performed by DSC also confirmed higher thermal stability at lower bio-oil substitution levels. This study is an industrially novel for the wood composite manufacturing sector.

4.6 Acknowledgements

This work was supported by the Agriculture and Food Research Initiative – “Hydrophobic Bio-Oil-Epoxy Binders for Wood Composites” (Project Award Number 2017-67021-26134). The Auburn University Intramural Grants Program (Auburn, AL, United States) is recognized for startup funding for part of this project. Furthermore, Regions Bank provided partial support, and the Forest Products Development Center (Auburn University, Auburn, AL, United States) is acknowledged for supplementary funding of materials and supplies. The Center for Bioenergy and Bio products (Auburn University, Auburn, AL, United States) is acknowledged for the use of their

facilities. The Center for Polymers and Advanced Composites (Auburn University, Auburn, AL, United States) is also recognized for the use of their facilities.

4.7 References

1. Aro, M., B. Brashaw, and P. Donahue. 2014. Mechanical and physical properties of thermally modified plywood and oriented strand board panels. *Forest Prod. J.* 64(7–8):281–289.
2. ASTM: D1037, “Standard Test Methods for Evaluating Properties of Wood-Base Fiber and Particle Panel Materials,” Current, pp. 1–8, 2012.
3. Auad, M. L., Nutt, S. R., Stefani, P. M., & Aranguren, M. I. (2006). Rheological study of the curing kinetics of epoxy-phenol novolac resin. *Journal of Applied Polymer Science*, 102(5), 4430–4439. <https://doi.org/10.1002/app.24674>
4. Bardalai, M., & Mahanta, D. (2015). A Review of Physical Properties of Biomass Pyrolysis Oil (Vol. 5, Issue 1).
5. Blank, W. J., He, Z. A., & Picci, M. (2003). Catalysis of the epoxy-carboxyl reaction. www.wernerblank.com
6. Bridgwater, A. V. (2012). Review of fast pyrolysis of biomass and product upgrading. *Biomass and Bioenergy*, 38, 68–94. <https://doi.org/10.1016/j.biombioe.2011.01.048>
7. Celikbag, Y., Meadows, S., Barde, M., Adhikari, S., Buschle-Diller, G., Auad, M. L., & Via, B. K. (2017). Synthesis and Characterization of Bio-oil-Based Self-Curing Epoxy Resin. *Industrial and Engineering Chemistry Research*, 56(33), 9389–9400. <https://doi.org/10.1021/acs.iecr.7b02123>
8. Celikbag, Y., Robinson, T. J., Via, B. K., Adhikari, S., & Auad, M. L. (2015). Pyrolysis oil substituted epoxy resin: Improved ratio optimization and crosslinking efficiency. *Journal of Applied Polymer Science*, 132(28), 1–9. <https://doi.org/10.1002/app.42239>
9. Chan, F., Riedl, B., Wang, X. M., Lu, X., Amen-Chen, C., & Roy, C. (2002). Performance of pyrolysis oil-based wood adhesives in OSB. *Forest Products Journal*, 52(4), 31–38.
10. Chiu, Y.; Chou, I.; Tseng, W.; Ma, C.M. Preparation and thermal properties of diglycidylether sulfone epoxy. *Polym. Degrad. Stab.* 2008, 93, 668–676.
11. Demirbaş, A. (2000). Mechanisms of liquefaction and pyrolysis reactions of biomass. *Energy Conversion and Management*. [https://doi.org/10.1016/S0196-8904\(99\)00130-2](https://doi.org/10.1016/S0196-8904(99)00130-2)
12. El Mansouri, N. E., Yuan, Q., & Huang, F. (2011). Synthesis and characterization of kraft lignin-based epoxy resins. *BioResources*, 6(3), 2492–2503. <https://doi.org/10.15376/biores.6.3.2492-2503>

13. Hafiezal, Mohd Radzi Mohd, Abdan Khalina, Zainal Abidin Zurina, Md Deros Mohd Azaman, and Zin Mohd Hanafee. 2019. "Thermal and Flammability Characteristics of Blended Jatropha Bio-Epoxy as Matrix in Carbon Fiber-Reinforced Polymer." *Journal of Composites Science* 3(1):6.
14. Inoue, M., M. Norimoto, M. Tanahashi, and R. Rowell. 1993. Steam or heat fixation of compressed wood. *Wood Fiber Sci.* 25(3):224–235.
15. Kuo, P. Y., Sain, M., & Yan, N. (2014). Synthesis and characterization of an extractive-based bio-epoxy resin from beetle infested *Pinus contorta* bark. *Green Chemistry*, 16(7), 3483–3493. <https://doi.org/10.1039/c4gc00459k>
16. Li, Q., Steele, P. H., Yu, F., Mitchell, B., & Hassan, E. B. M. (2013). Pyrolytic spray increases levoglucosan production during fast pyrolysis. *Journal of Analytical and Applied Pyrolysis*, 100, 33–40. <https://doi.org/10.1016/j.jaap.2012.11.013>
17. Liu, Y., Gao, J., Guo, H., Pan, Y., Zhou, C., Cheng, Q., & Via, B. K. (n.d.). Interfacial Properties of Loblolly Pine Bonded with Epoxy/Wood Pyrolysis Bio-oil Blended System.
18. Liu, Y., Via, B. K., Pan, Y., Cheng, Q., Guo, H., Auad, M. L., & Taylor, S. (2017). Preparation and characterization of epoxy resin cross-linked with high wood pyrolysis bio-oil substitution by acetone pretreatment. *Polymers*, 9(3). <https://doi.org/10.3390/polym9030106>
19. Mailhot, Bénédicte, Sandrine Morlat-Thérias, Mélante Ouahioune, and Jean Luc Gardette. 2005. "Study of the Degradation of an Epoxy/Amine Resin, 1 Photo- and Thermo-Chemical Mechanisms." *Macromolecular Chemistry and Physics* 206(5):575–84.
20. Mao, A., Shi, S. Q., & Steele, P. (2011). Flakeboard bonded with polymeric diphenylmethane diisocyanate/ bio-oil adhesive systems. *Forest Products Journal*, 61(3), 240–245. <https://doi.org/10.13073/0015-7473-61.3.240>
21. Mekonnen, T. H., Mussone, P. G., Choi, P., & Bressler, D. C. (2014). Adhesives from waste protein biomass for oriented strand board composites: Development and performance. *Macromolecular Materials and Engineering*, 299(8), 1003–1012. <https://doi.org/10.1002/mame.201300402>
22. Pan, S., Pu, Y., Foston, M., & Ragauskas, A. J. (2013). Compositional Characterization and Pyrolysis of Loblolly Pine and Douglas-fir Bark. *BioEnergy Research*, 6(1), 24–34. <https://doi.org/10.1007/s12155-012-9223-1>
23. Pizzi, A., Mittal, K., & Dunky, M. (2003). Adhesives in the Wood Industry. In *Handbook of Adhesive Technology, Revised and Expanded (Issue August 2003)*. <https://doi.org/10.1201/9780203912225.ch47>

24. Rowell, R. M. (2012). Handbook of wood chemistry and wood composites, second edition. In *Handbook of Wood Chemistry and Wood Composites, Second Edition*. <https://doi.org/10.1201/b12487>
25. Rowell, R.M. *Handbook of Wood Chemistry and Wood Composites*; CRC Press: Boca Raton, FL, USA, 2005
26. Sahoo, S. K., Khandelwal, V., & Manik, G. (2018). Development of completely bio-based epoxy networks derived from epoxidized linseed and castor oil cured with citric acid. *Polymers for Advanced Technologies*, 29(7), 2080–2090. <https://doi.org/10.1002/pat.4316>
27. Sasaki, C., Wanaka, M., Takagi, H., Tamura, S., Asada, C., & Nakamura, Y. (2013). Evaluation of epoxy resins synthesized from steam-exploded bamboo lignin. *Industrial Crops and Products*, 43(1), 757–761. <https://doi.org/10.1016/j.indcrop.2012.08.018>
28. Schwarzkopf, M., Huang, J., & Li, K. (2009). Effects of adhesive application methods on performance of a Soy-based adhesive in oriented strandboard. *JAOCS, Journal of the American Oil Chemists' Society*, 86(10), 1001–1007. <https://doi.org/10.1007/s11746-009-1437-9>
29. Uddin, M. N., Techato, K., Taweekun, J., Rahman, M. M., Rasul, M. G., Mahlia, T. M. I., & Ashrafur, S. M. (2018). An overview of recent developments in biomass pyrolysis technologies. *Energies*, 11(11). <https://doi.org/10.3390/en11113115>
30. Vispute, T. (2011). *Pyrolysis Oils: Characterization, Stability Analysis, and Catalytic Upgrading to Fuels and Chemicals*. http://scholarworks.umass.edu/open_access_dissertations/349
31. Wei, N., Via, B. K., Wang, Y., McDonald, T., & Auad, M. L. (2014). Liquefaction and substitution of switchgrass (*Panicum virgatum*) based bio-oil into epoxy resins. *Industrial Crops and Products*, 57, 116–123. <https://doi.org/10.1016/j.indcrop.2014.03.028>
32. Zhang, Q., Chang, J., Wang, T., & Xu, Y. (2007). Review of biomass pyrolysis oil properties and upgrading research. *Energy Conversion and Management*, 48(1), 87–92. <https://doi.org/10.1016/j.enconman.2006.05.010>

Chapter 5

Bond Durability of Polymeric Diphenylmethane Diisocyanate (PMDI) Substituted with Defatted Soy Flour in Oriented Strand Board Production

5.1 Abstract

Polymeric Diphenylmethane Diisocyanate (PMDI) used in the manufacture of OSB can be partially substituted with soy flour without degrading the bond integrity of the wood panels. Soy flour is about one-third of the cost of pMDI and can yield cost savings. Properties such as an internal bond, wet MOE and MOR, and thickness swelling are unaffected by soy flour substitution of up to 20%. Adding soy flour to the regular dose of pMDI can enhance board properties.

5.2 Introduction

Soy flour and soy protein are commercially used in adhesive formulations in products such as decorative veneers where exposure to water is relatively low (Li 2010, Li et al. 2004). Being hydrophilic, soy products tend to retain water, which potentially causes board distortion or structural failure in a moist environment. The advantage of soy flour over an adhesive such as methylene diphenyl diisocyanate (PMDI) is principally cost; it is about one-third the cost of PMDI. Hence, 20% soy flour substitution in PMDI would lower total adhesive costs by 13%. There is also a green value attached to the use of soy products. Soy protein is more expensive than pMDI; as a result, the extensive literature (Vnučec et al. 2017) on adhesive formulations with soy protein has yet to find commercial application. This study defines the acceptable range of soy flour substitution in PMDI for OSB applications and discusses some of the operational factors that must be understood and taken into account before commercial use can be considered. The chemistry of

the interaction of soy flour components and PMDI have been discussed elsewhere (Hand 2018, Mhike 2014).

5.3 Materials

Wood strands from southern yellow pine of moisture content 7-8% were provided by Norbord Corporations, J.M. Huber, and Louisiana- Pacific. Defatted soy flour (7B) was donated by Archer Daniels Midland. PMDI (MONDUR 541) and emulsified wax (Hexion Bord'N-Seal FMH-XD) were provided by Huber Corp.

5.3.1 Attenuated Total Reflection -Fourier Transform-Infrared (ATR-FT- IR)

The FT- IR spectra of PMDI, defatted soy flour, and cured PMDI substituted soy flour (10%) resins were obtained between 4000 and 650 cm^{-1} with an ATR-FT-IR spectrometer (Model Spectrum 400, Perkin Elmer Co., Waltham, MA) at 64 scans with a 4.00 cm^{-1} resolution. The cured PMDI substituted soy flour (10%) resin was conducted at 80 °C for 2 hours and the temperature ramped to 120 °C for 1 hour, 160 °C for 30 minutes and 200 30 minutes. After curing, the samples were left in the oven to cool to 25 °C.

5.3.2 Viscosity

The viscosities of the PMDI and PMDI substituted with 10% defatted soy flour were measured using Fungilab rotary viscometer (Smart Series H, Model V210001) with spindle L2 at 30 rpm at room temperature and at 40 °C.

5.3.3 OSB Production

Wax was first sprayed on the wood strands at 1% loading. PMDI or mixtures of PMDI and soy flour were sprayed on the wood strands at 2 and 4% loading with a paint sprayer powered by an air compressor. However, PMDI was first heated to 40 °C before the soy was added. Mats were

formed in a 43 x 43 cm frame and then hot pressed for 3 minutes at 213 °C and 2 MPa for boards with 2% adhesive. The pressure and temperature were held constant for the entire 3 minutes. A distance bar was added to reach the target thickness during pressing. Shorter press times were used for boards prepared with 4% adhesive. The nominal thickness of the board was 11 mm. The target density was 641 kg/m³ (40 lbs/ft³) for OSB. The OSB had a 50% surface to core ratio unless indicated otherwise. Internal bond (IB), water absorption (WA) and thickness swelling (TS) were measured according to ASTM D1037-12 (2012).

5.3.4 Moisture Cycle Test for Board Delamination (Adhesive Bond Performance) and Strength Retention Test

The adhesive durability performance of the OSB panels was assessed by the 6-cycle test following the recommendation of the APA PS10 (2011) for small static bending test. Thirty samples, each of dimensions 11 mm x 25.4 mm x 127 mm, were matched in two groups – half for the moisture cyclic test and the other as control (unexposed). PMDI bonded panels were the control specimen. The cyclic samples were soaked in water at 66 °C for 30 minutes under 506 mbar. The vacuum was released after 30 minutes and the samples were kept soaked at atmospheric pressure for an additional 30 minutes. Afterward, the samples were removed and dried at 82°C in an oven supplied with air circulation of 46 air changes per minute for 6 hours. The samples were then returned to the pressure oven and the vacuum-soak cycle repeated as described above. Following this, samples were dried for 15 hours at 82 °C. This completed two cycles and the entire vacuum-soak cycles and drying regimes repeated for two more days until 6 cycles completed.

The specimens were tested dry for strength retention from the static bending test. The specimens were tested as a beam across a 100 mm clear span. Specimen was oriented such that the cut dimension of 25 mm (1 inch) acts as specimen depth and the panel thickness acts as the specimen

width as specified in PS-10. The load was applied at mid-span at a rate of 0.25 mm/minute until sample failed. The average breaking load (N) for each adhesive treatment for the panels was estimated and used for the strength retention determination. Bond integrity of the specimen was tested dry for strength retention using the relation:

$$RS = \frac{P_t}{P_c} \times 100$$

Where %RS =Percent retained strength of the sample

P_t = Average of fifteen-specimen breaking load (N) after cycling

P_c = Average of fifteen-unexposed sample breaking load (N)

The minimum percent retained strength is 50%. Following the 6-cycle test, the samples were dried to $\pm 2\%$ moisture content (MC) with reference to the unexposed samples mc.

5.4 Results and Discussion

5.4.1 FT-IR Analysis of PMDI substituted Soy Flour

The FT-IR spectra for the soy flour, PMDI and PMDI substituted soy flour is illustrated in Figure 5.1. There was evidence from the IR spectra that the soy flour crosslinks with the PMDI. The characteristic absorption peak for the isocyanate of the PMDI was assigned at the wavelength of 2245 cm^{-1} . The broad absorption band observed between $3,600\text{-}3,077$ ($3,275\text{cm}^{-1}$) was ascribed to the free and bounded O–H and N–H groups, respectively, for the soy flour. The O–H and N–H groups in soy protein and the O–H in absorbed water could form hydrogen bonding with the carbonyl groups of the peptide linkage in the protein structure (Nanda et al. 2007). The C–H stretching vibration of the methyl (CH_3) and methylene (CH_2) moieties ranged from 2924 and 2855

cm^{-1} . The narrow peak at 1744 cm^{-1} was attributed to the C=O stretching vibration of the residual fatty acid ester group. Typical absorption bands of the peptide linkages were associated with C=O stretching vibration at 1633 cm^{-1} (amide I), and N–H bending at 1536 cm^{-1} (amide II). The absorption band at 1240 cm^{-1} (amide III) contributed to the C–N stretching, and N–H bending vibration (Schmidt 2005). The peak at 1394 cm^{-1} resulted from protein side-chain COO- and the band absorption at 1049 cm^{-1} indicated –C–NH₂ bending vibration.

FTIR of the cured PMDI substituted with soy (10%) showed evidence of crosslinked structures of soy flour with the PMDI: the reduction of the N=C=O peak intensity at 2267 cm^{-1} coupled with the consumption of the O–H/N–H at 3265 cm^{-1} . Moreover, the formation of hydrogen bonding between N–H and C=O group at 1706 cm^{-1} and was attributed to the urethane linkage signal resulting from the isocyanate reaction with O–H groups. A similar band was observed at 1709 cm^{-1} in the formation of hydrogen bonding of hard segments in segmented poly (urethane urea) copolymer (Ning et al., 1996). Socrates defined the absorption due to the CHN group in the range of $1600\text{-}1500 \text{ cm}^{-1}$ as associated secondary urethanes (amide II band) (Socrates 2001). The band was observed at 1593 cm^{-1} and 1507 cm^{-1} .

Urea linkage in the cured polymer was observed at 1670 cm^{-1} as monodentate urea, which denoted a single hydrogen bonded amine from a urea group to a carbonyl from another urea group (Ning 1996). The complete removal of the –C–NH₂ bending vibration signature at 1049 cm^{-1} of the soy flour IR in the cured PMDI/Soy (10%) resin spectrum suggested that soy flour crosslinked with the PMDI resin.

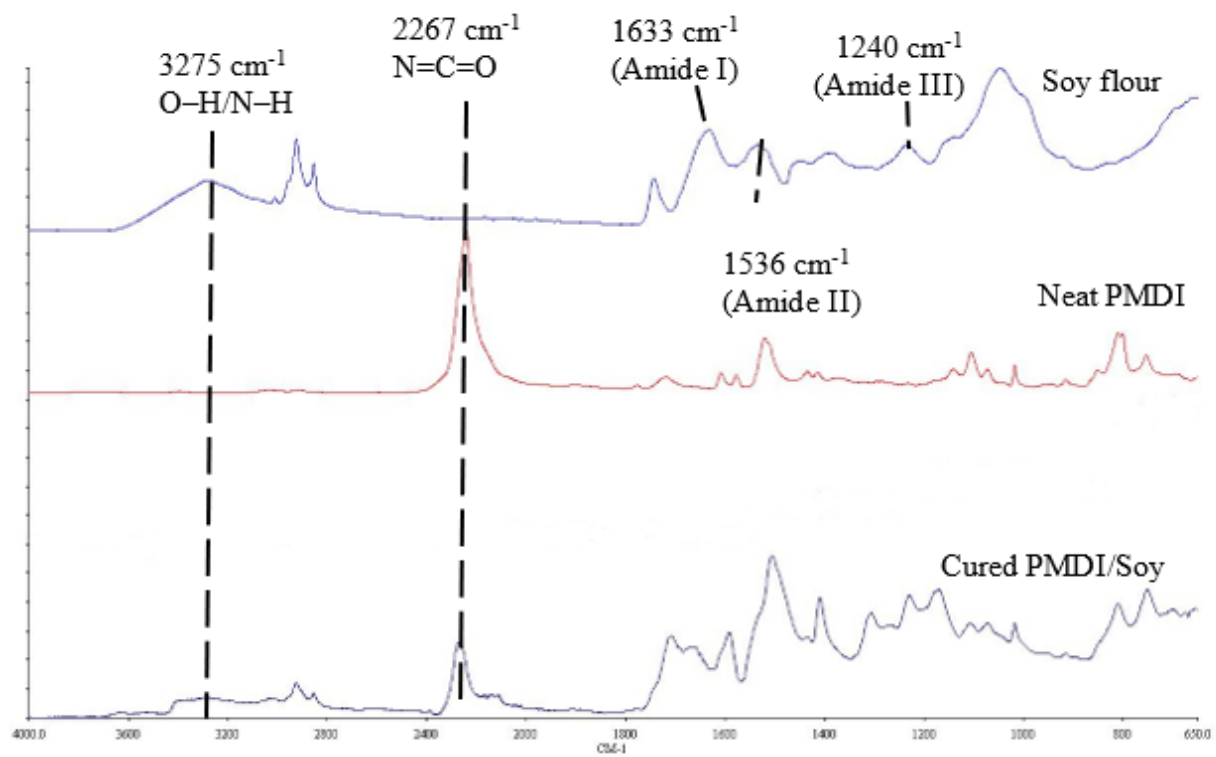


Figure 5.1: FTIR spectra for PMDI, Soy and cured PMDI (90%)/Soy (10%)

5.4.2 5.3.2. Effect of Soy Flour substitution on Adhesive Viscosity

The viscosities of PMDI and PMDI substituted with 10% defatted soy flour is presented in Figure 5.2. The initial viscosity of the PMDI alone was 248 mPa s at room temperature and 162 mPa s at 40 °C, respectively. The substituted soy flour in PMDI at 40 °C increased the viscosity by 2.5 % (166 mPa s). When the adhesive mixture was cooled to room temperature, for 60 minutes, the viscosity doubled (359 mPa) relative to that at 40 °C. This implies that PMDI substituted with soy flour should be kept above room temperature. The viscosity of the PMDI/soy mixture increased to 553 mPa s when the PMDI and soy were mixed at 25 °C and kept for 60 minutes. This has a negative practical implication on adhesive spraying, spreading and penetration into the wood of the wood. A probable reason for the high viscosity at 25 °C is bubble entrapment. The reaction of the isocyanate of PMDI and H₂O or OH groups in the soy generates CO₂ bubbles. Since the

viscosity of PMDI alone at room temperature is relatively high, the generated bubbles were trapped in the resin, which increased the viscosity of the adhesive mixture. PMDI viscosity falls at 40 °C, which accelerates the evolution of the CO₂ bubbles. Much more froth was associated with the adhesive mixture at 40 °C, which coincides with the greater bubble release from the adhesive. The presence of bubbles is known to increase viscosity (Abivin et al. 2008, ACC 2012, Albartamani 2000) because of flow line distortion around the bubbles (Llewelin et al. 2002).

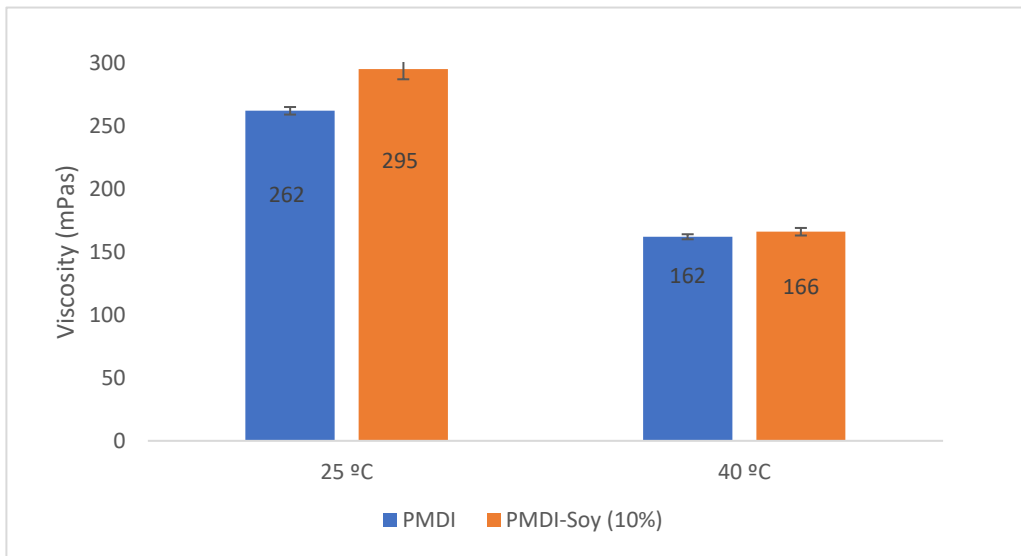


Figure 5.2: Viscosity of PMDI and PMDI/soy mixture (9:1) at 5 minutes of mixing.

5.4.3 5.3.3. Soy flour substitution effect on OSB properties

Our initial studies in the production of strand board were carried out with soy flour and PMDI applied separately onto the furnish. However, the wet properties were compromised in the presence of soy flour. It is likely that free soy particles on the surface of the wood attracted and retained water. The problem was not observed when the adhesive and soy flour were mixed before application because of the soy flour bonded with the PMDI (Hand et al. 2018). The results

presented below were all obtained with premixed soy flour and PMDI. In some instances, soy flour was only substituted in the face adhesive.

5.4.3.1 2% Adhesive loading

The effect of substituting PMDI adhesive with soy flour on wet properties is shown in Table 5.1. Measurements were made with (a) soy flour present only in the face adhesive and (b) in both face and core. Up to 20% soy substitution can be tolerated in the face-treated boards. No statistical difference in properties between control and soy-treated was evident for condition (b) where the soy was substituted in both face and core layers. However, soy flour substitution was limited to 10% in this case.

Table 5.1: (a) Soy substitution only in face adhesive

Soy (%)	Wet MOR (MPa)	Wet (MPa)	MOE TS (%)
0	12 ± 2	1,450 ± 300	41 ± 6
10	11 ± 2	1,400 ± 300	40 ± 4
20	12 ± 1	1,350 ± 200	41 ± 3

Table 5.1: (b) Soy in face and core adhesive

Soy (%)	Wet MOR (MPa)	Wet (MPa)	MOE TS (%)
0	12 ± 2	1,400 ± 370	42 ± 5
10	11 ± 3	1,250 ± 320	38 ± 6

5.4.3.2 4% Adhesive loading

Panels are normally produced under conditions that go beyond minimum specifications to keep a safety margin. A small substitution of soy flour may not significantly affect the measured properties. Runs were made at press times of 1.5 and 1.75 min., which were well below the 3 min press time used in the rest of the study. It was anticipated that the effect of soy would be more apparent under the shorter press times, where the boards would be weaker. The internal bond results illustrated in Figure 5.3 shows that, as expected, the strength decreased when the pMDI load was reduced from 4% to 3.6% pMDI. However, the addition of soy flour to 3.6% pMDI restored the strength back to the value obtained at 4% pMDI.

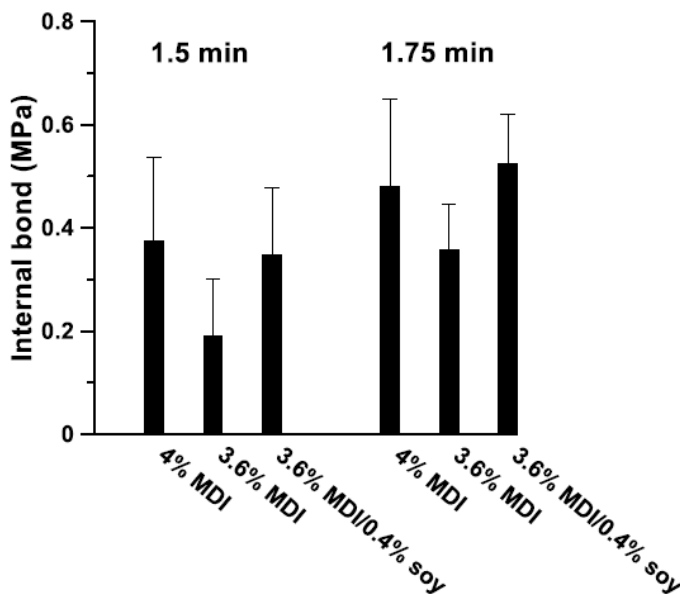


Figure 5.3: Internal bond strength of PDMI and PMDI substituted with soy flour.

The edge swelling is of importance because it is a critical property for panels with potential exposure to moisture. Results from Fig. 5.4 demonstrate that soy flour can be used to partially substitute pMDI adhesive to reduce cost or be added to the regular adhesive dose to improve board performance. The edge swelling values in Figure. 5.5 are quite similar; evidently, edge swelling is

insensitive to small changes in soy flour substitution. However, panel delamination at the 1.5 minutes pressing time was observed in some of the OSB panels (Figure 5.6). The soy flour substituted boards (3.6% pMDI + 0.4% soy) performed almost as well as the 4% pMDI boards, whereas the 3.6% pMDI samples pressed for 1.5 minutes delaminated to a greater extent.

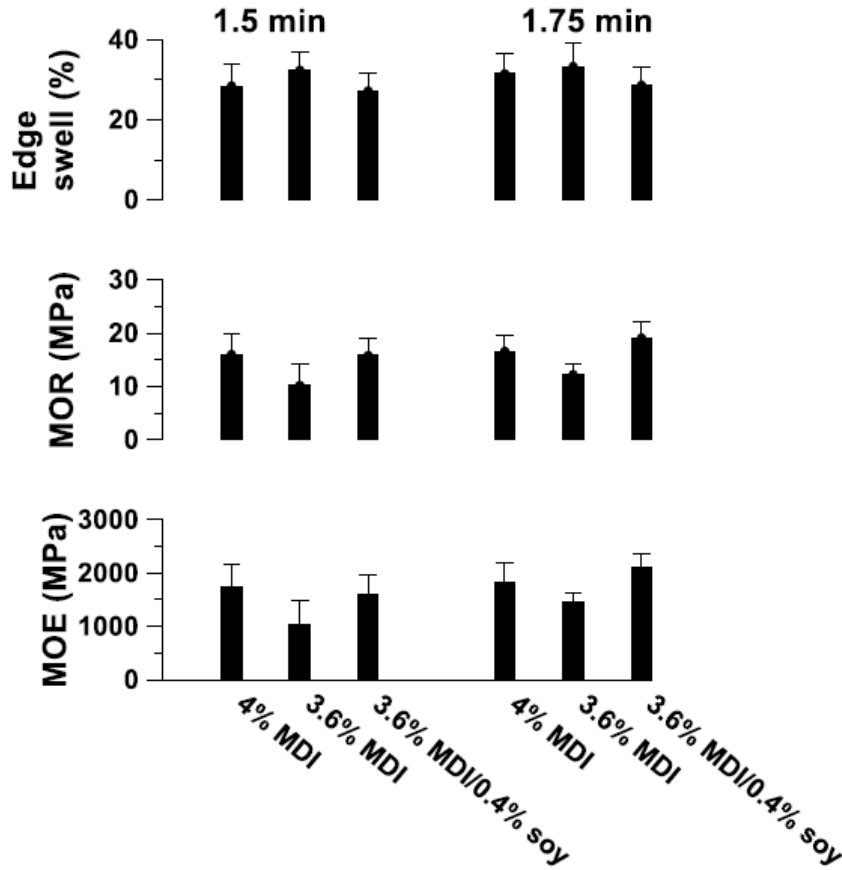


Figure 5.4: Effect of soy flour substitution on the modulus of elasticity and modulus of rupture and edge swell of OSB panels at 1.5 minutes and 1.75 minutes of hot pressing.



Figure 5.5: Delaminated OSB panel pressed for 1.5 minutes.

5.4.4 Six cycle water-vacuum soak test and strength retention test

The PMDI amended with soy flour exhibited similar bond integrity as the PMDI alone (Figures 5.3. and 5.4.). This is interesting because newly developed or modified adhesives must exceed the bond integrity of the delamination test and retain 50% of the initial strength of the panel before it could be commercialized for wood panel production. It is evident that the substitution of soy flour in the PMDI resin improves the wet strength of the OSB, which is consistent with the 24 hour water soak test result.

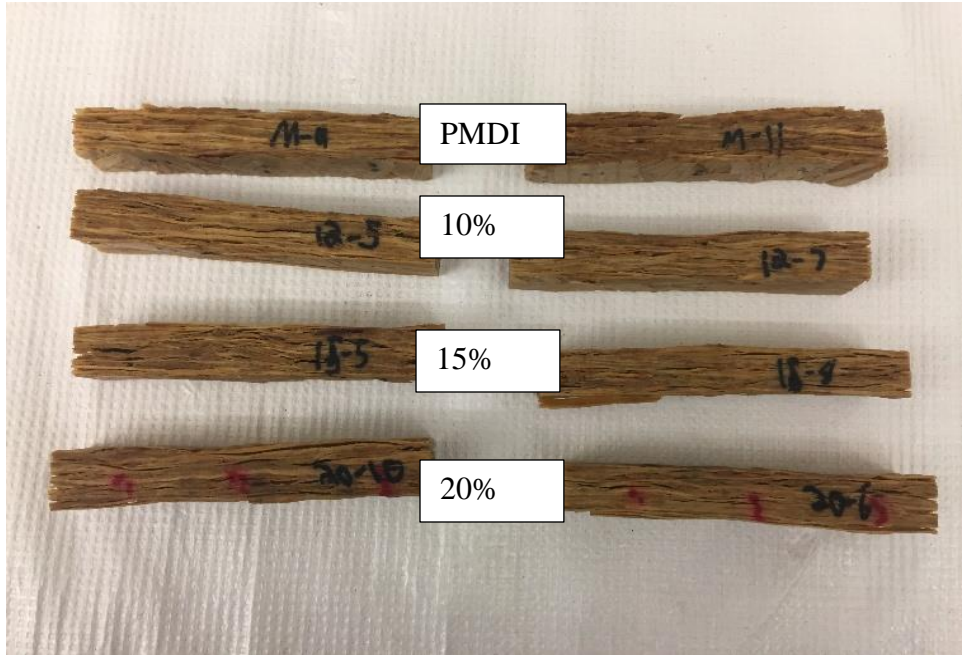


Figure 5.6: Delaminated OSB panel after the 6 cycle water- vacuum soak test.

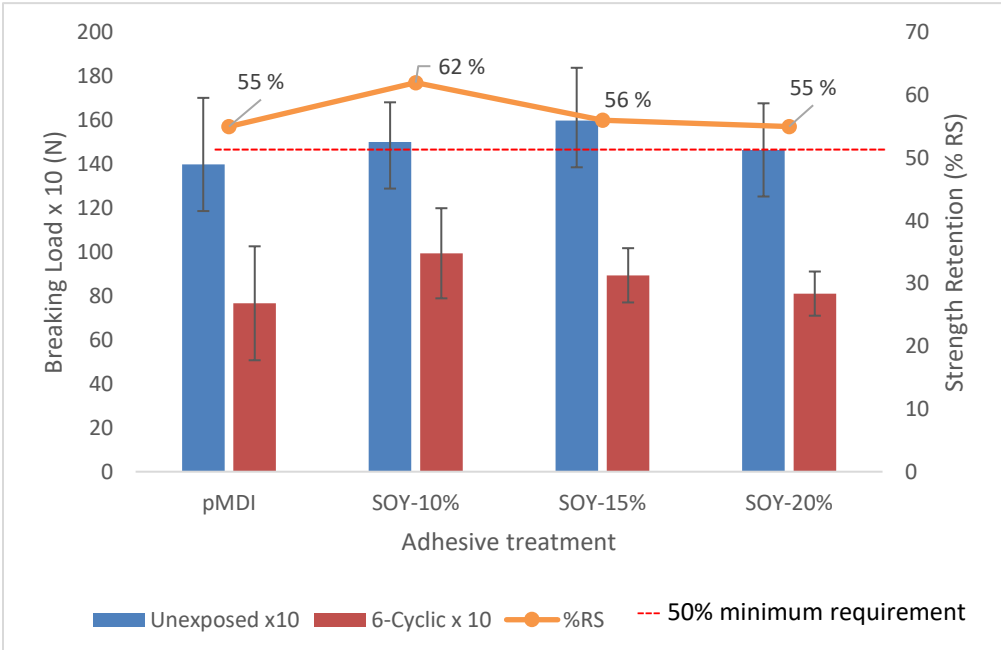


Figure 5.7: Strength retention test for the different adhesive formulations from the breaking load

5.5 Conclusions

Up to 20% of pMDI adhesive can be substituted by soy flour in OSB. Board properties deteriorate at higher levels of substitution and the adhesive mixture increase in viscosity, so maintaining PMDI and soy mixture at about 40 °C is critical to the pot life of the resin. The addition of soy flour to the regular dose of PMDI can improve board performance.

5.6 Acknowledgements

This study was funded by the United Soybean Board and the Alabama Farmers Federation.

5.7 References

1. Abivin, P., I. Hénaut, J-F. Argillier, and M. Moan. 2008. Viscosity behavior of foamy oil: experimental study and modeling. *Petroleum Sci. Technol.* 26:1545-1558.
2. Albartamani, N. S. 2000. Experimental studies on “foamy oil” phenomena, Ph.D. thesis. University of Alberta, Alberta, Canada.
3. American Chemistry Council, Guidance for working with pMDI and polymeric pMDI: things you should know. 2012. <https://polyurethane.americanchemistry.com/Resources-and-Document-Library/11364.pdf>
4. APA-The Engineered Wood Association, PS2-04 Performance standards for wood-based structural-use panels, 2004.
5. ASTM D1037 – 12, Standard test methods for evaluating properties of wood-base fiber and particle panel materials, 2012.
6. Hand, W. Defatted soy flour substitution in phenol formaldehyde and methylene diphenyl diisocyanate wood adhesives and their curing kinetic behavior. 2018. Ph.D. thesis, Auburn University.
7. Hand, W., G. Cheng, B. Via, and S. Banerjee 2017. Soy-substituted liquid phenol formaldehyde binders for flakeboard. *Eur. J. Wood Wood Prod.* 75:135-138.
8. Hand, W. G., W. R. Ashurst, B. Via, and S. Banerjee 2018. Mechanism of interaction of soy flour with phenol-formaldehyde and isocyanate adhesives. *Int. J. Adhes. Adhes.* 87:105-108.
9. Llewellyn, E. W., H. M. Mader, and S. D. R. Wilson, 2002. The rheology of a bubbly liquid, *Proc. R. Soc. Lond. A* 458:987–1016.
10. Li, K. US. Formaldehyde-free adhesives and lignocellulosic composites made from the adhesives. US patent 7,722,712, 2010.
11. Li, K., S. Peshkova, and X. Geng 2004. Investigation of soy protein-kymene adhesive systems for wood composites. *J. Am. Oil Chem. Soc.* 81:487-491.
12. Mhike, M. 2014. Characterization of methylene diphenyl diisocyanate protein conjugates. Ph.D. thesis, Portland State University.
13. Nanda, P.K., Rao, K.K. and Nayak, P.L. (2007), “Biodegradable polymers. XI. Spectral, thermal, morphological and biodegradability properties of environment-friendly green plastics of soy protein modified with thiosemicarbazide”, *Journal of Applied Polymer Science*, Vol. 103 No. 5, pp. 3134-42.

14. Ning, L., De-Ning, W. and Y. Sheng-Kang, "Crystallinity and hydrogen bonding of hard segments in segmented poly (urethane urea) copolymers," *Polymer.*, vol. 37, no. 16, pp. 3577–3583, 1996.
15. Schmidt, V., Giacomelli, C., & Soldi, V. (2005). Thermal stability of films formed by soy protein isolate-sodium dodecyl sulfate. *Polymer Degradation and Stability*, 87(1), 25–31. <https://doi.org/10.1016/j.polymdegradstab.2004.07.003>
16. G. Socrates, *Infrared and Raman characteristic group frequencies: tables and charts*. John Wiley & Sons, 2001.
17. Via, B., W. Hand, and S. Banerjee 2019. Use of soy flour in adhesive formulations used to manufacture engineered wood composites, US patent allowed.
18. Vnučec D., A. Kutnar, and A. Goršek. 2017. Soy-based adhesives for wood-bonding – a review. *J. Adhes. Sci. Technol.* 31(8):910-931.

Chapter 6

Increasing Cold Tack of pMDI resin with Partial Soy Flour Substitution

6.1 Abstract

Partial substitution of pMDI resin with soy flour increases the cold tack of the resin to the level achieved by UF resin. The increase is caused by the reaction of the isocyanate resin with the water contained in soy flour. The higher cold tack should increase the stability of pre-mats, especially in particleboard manufacturing.

6.2 Introduction

Urea formaldehyde (UF) resins are typically used in the manufacture of particleboard. Concerns with formaldehyde emissions from these resins have prompted a switch to binders such as polymeric methylene diphenyl diisocyanate (pMDI). However, the low cold tack of pMDI reduces the structural integrity of the pre-mat (Solt et al. 2019). Cold tack is also important for veneer, where low cold tack can distort layer orientation. Attempts to increase the cold tack of pMDI, *e.g.*, by adding a combination of polyols and monols to pMDI have been reported by Moriarty (2017). In previous work, partial (~15%) substitution of soy flour in pMDI resin for the manufacture of OSB leads to significant cost benefits without compromising wet or dry board properties (Cheng et al. 2019). In this study, an additional benefit of soy flour substitution – an increase in the cold tack of pMDI resin, which improves the pre-press integrity of a mat was demonstrated and the fabrication of particleboards at higher levels of soy flour substitution studied.

6.3 Materials and Methods

6.3.1 Materials

Defatted soy flour (7B) was provided by Archer Daniels Midland; its moisture content was 5.91%. The pMDI resin was MONDUR 541 from Covestro. Different batches of pMDI were used for the various measurements, so the results should only be compared within each set. UF resin was obtained from Arauco Wood Products. Wood sawdust particles were provided by West Fraser and dried to 6-7% MC. Emulsified wax (Hexion Bord'N-Seal FMH-XD) was obtained from Huber Corp. The soy/resin adhesives were prepared by adding the soy into the resin in small batches and stirring until the mixture was uniform. Ensuring that the mixture is uniform is very important for maintaining wet strength, as will be discussed in the next chapter.

6.3.2 Cold Tack of PMDI substituted soy

The tack of the various resin formulations was measured with a modified ASTM technique (ASTM 2017). Metal coupons were coated with resins at a density of 0.65 g over 26 cm² at 40°C. This temperature is optimum for mixing pMDI with soy flour (Via et al. 2019). The plates were angled at 30° and a steel bolt (2.2 cm wide, 1.34 cm in diameter, 13.14 g) was rolled down each plate and its travel distance averaged from four measurements.

6.3.3 Particle Board Production

For the particle board fabrication, the wax was first sprayed on the wood particles at a loading of 1% of the particle weight. PMDI or mixtures of MDI and soy flour were then sprayed on the furnish with a paint sprayer powered by an air compressor. Particle board was made with a resin load of 4% of wood weight. The resin was applied to both the face and core layers.

Mats were formed in a 43 x 43 cm frame without orientation and then hot pressed for 3 minutes at 210 °C and 2 MPa. The nominal thickness of the board was 1.1 cm. The particleboard target density was 689 kg/m³ (43 lbs/ft³).

6.3.4 Soy flour substitution in MDI mitigates platen sticking

MDI tends to stick to press platens, which increases maintenance downtime. Various release agents are used to partially control the problem, but they add to cost and labor. It was reasoned that because soy flour reacts with MDI it might inhibit the bonding of MDI to the platens and thereby reduce sticking. Particle mats were pressed at 200 °C and 2 MPa for 4 minutes. Aluminum platens were used to sandwich the particles for hot pressing. The adhesive and wax loadings were 4% and 1%, respectively. Three conditions were used: i) MDI coated particles; ii) One half of the mat made with MDI with the other made with 25% soy substituted MDI; iii) MDI coated particles with one side layered with soy powder as a barrier coating.

The soy flour level of 25% was higher than the 10-15% level that has been typically used in order to magnify any changes observed.

6.4 Results and Discussion

6.4.1 Cold Tack

Figure 6.1 shows the effect of resin tack on the distance traveled by the various bolts. The distance is longest for the MDI-treated plate (reflecting its low tack) and is about equal for the UF- and 10%-soy substituted plates. The travel distance falls linearly with soy flour substitution, as illustrated in Figure 6.2, reflecting a corresponding increase in tack. It is likely that the tack increase results from the reaction of water contained in the soy flour (5.9%) with MDI. It follows

that adding water to pMDI should also increase the tack of pMDI in our “inclined plate” measurements.

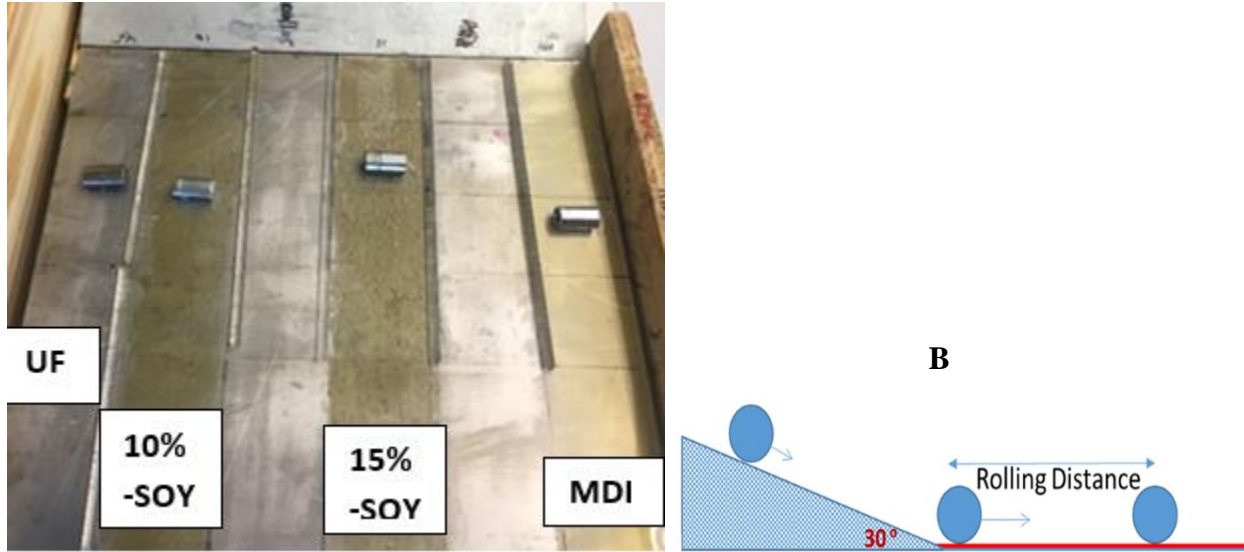


Figure 6.1: Images of bolts after rolling down inclined resinated plates. B= is schematic setup of the tack test.

Water (1% by weight of pMDI) was added to pMDI and the resin was filmed on a metal coupon as above. The travel distance of a bolt on the control and water-modified resins was 18.5 ± 0.3 and 13.7 ± 0.8 cm, respectively, *i.e.* a drop of 26%. If water is solely responsible for the tack increase induced by soy flour, then a similar drop should be obtained from Figure 6.2. Substituting 15% soy flour in pMDI adds the equivalent of 1% water to the resin. The corresponding decrease in travel distance is 32%. Substituting 20 percent soy flour in pMDI adds the equivalent of 1.2 percent water to the resin. The corresponding decrease in travel distance is 52 percent, which is twice the value obtained from adding water alone. The difference is probably due to the hydroxyl and other groups present in soy flour components that can also react with pMDI. The likely reason for the increase in cold tack is that water increases the polarity of the pMDI resin by adding amine and

derived functionalities to the pMDI structure. The increased polarity would allow the resin to better wet the surface of the wood.

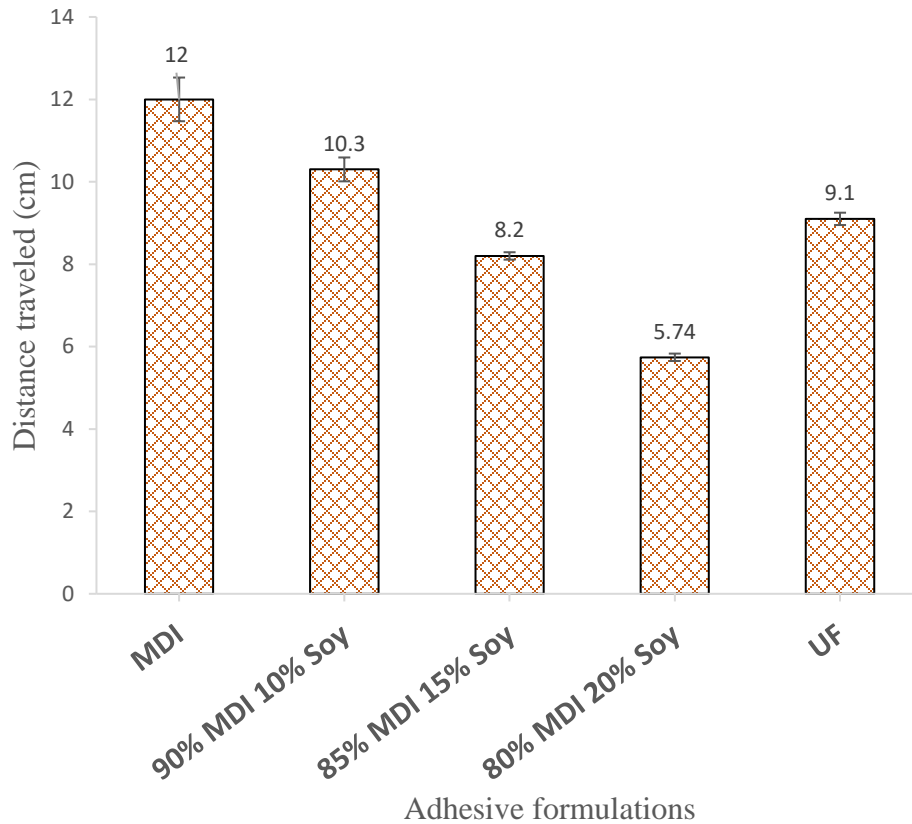


Figure 6.2: Effect of soy flour substitution on distance down an inclined surface.

6.4.2 Particleboard Applications

Results from the soy-treated particleboard are shown in Figure 6.3. There was no statistical difference between the control and soy-treated boards. Hence, in the absence of spraying issues, at least 20% of soy flour can be substituted for particleboard. However, as described earlier, the main benefit of soy flour is its ability to increase the cold tack, which is important for both particleboard and plywood (Hogger et al. 2018). At 12% soy flour substitution, the cold tack approximates that provided by UF resin. Higher soy flour substitution may lead to excessive tack.

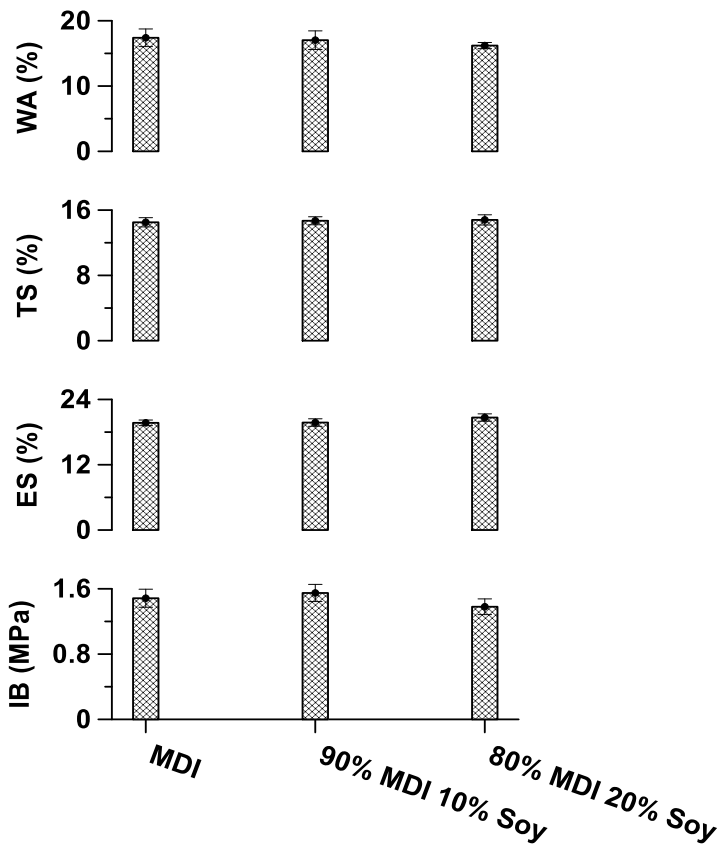


Figure 6.2: Effect of soy substitution on particleboard properties; n (number of samples tested per treatment) =12; ES =Edge swell; TS= thickness swell; WA= water absorption and IB = Internal bond strength.

The increase of pMDI tack by the addition of water has been noted by (Moriarty 2017, a, b), but there was no discussion of the effect of board properties. Zhang et al. (2018) has reported a fivefold increase in lap shear strength when water is added to pMDI at a level of 30%. However, the lap samples were cured at 160 °C for 5 hours under 50 kPa pressure, which bears no resemblance to industrial practice. Also, wet properties, which are especially sensitive to changes in resin formulation, were not reported.

Tack is defined as the adhesive failure energy of adhesive joints formed with low contact pressure during a short contact time (Zosel 1985). PMDI is known to over-penetrate wood cell lumen (Kamke, 2007), resulting in no tack. It is probable that the higher tack of the soy-modified resin improves resin spread at the bond line, thereby increasing the interfacial contact area and hence the slightly improved dry and wet properties of the particle board panels with soy.

6.4.3 Soy flour substitution in MDI mitigates platen sticking

The aluminum platens released easily from the pressed boards in all instances. Wood particles and fibers were pulled off the board and attached to the platen when unmodified PMDI is used as the resin; these particles are largely absent with the soy-modified resin.

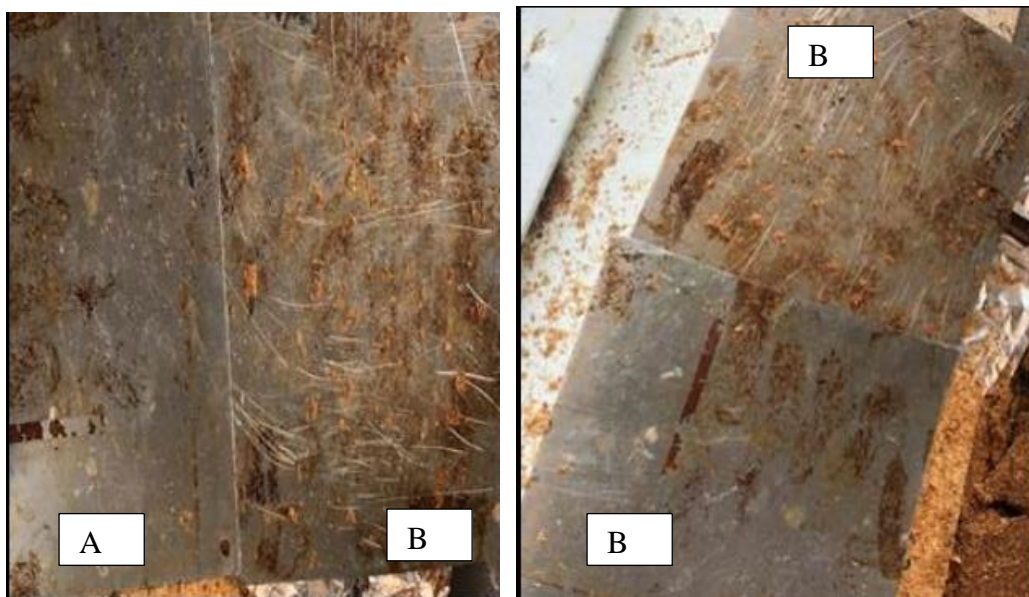


Figure 6.3: Platens coded B was placed on MDI resinated particles, and A and C were placed on either MDI substituted with soy or soy powder sprinkled on top of MDI coated particles.

Relatively clean surfaces were observed for both soy substituted PMDI or soy powder treated surfaces (Figure 6.4 and 6.5). It follows that the soy barrier coating is not necessary as the platens

used for the soy-PMDI mixture are equally clean. Clearly, soy decreases the attraction of MDI to aluminum and reduces the pull-off of fiber. Of course, the reduction in PMDI dose because of the presence of soy flour also reduces deposits. This finding will be very significant if it also applies to the steel plates used in the industry.

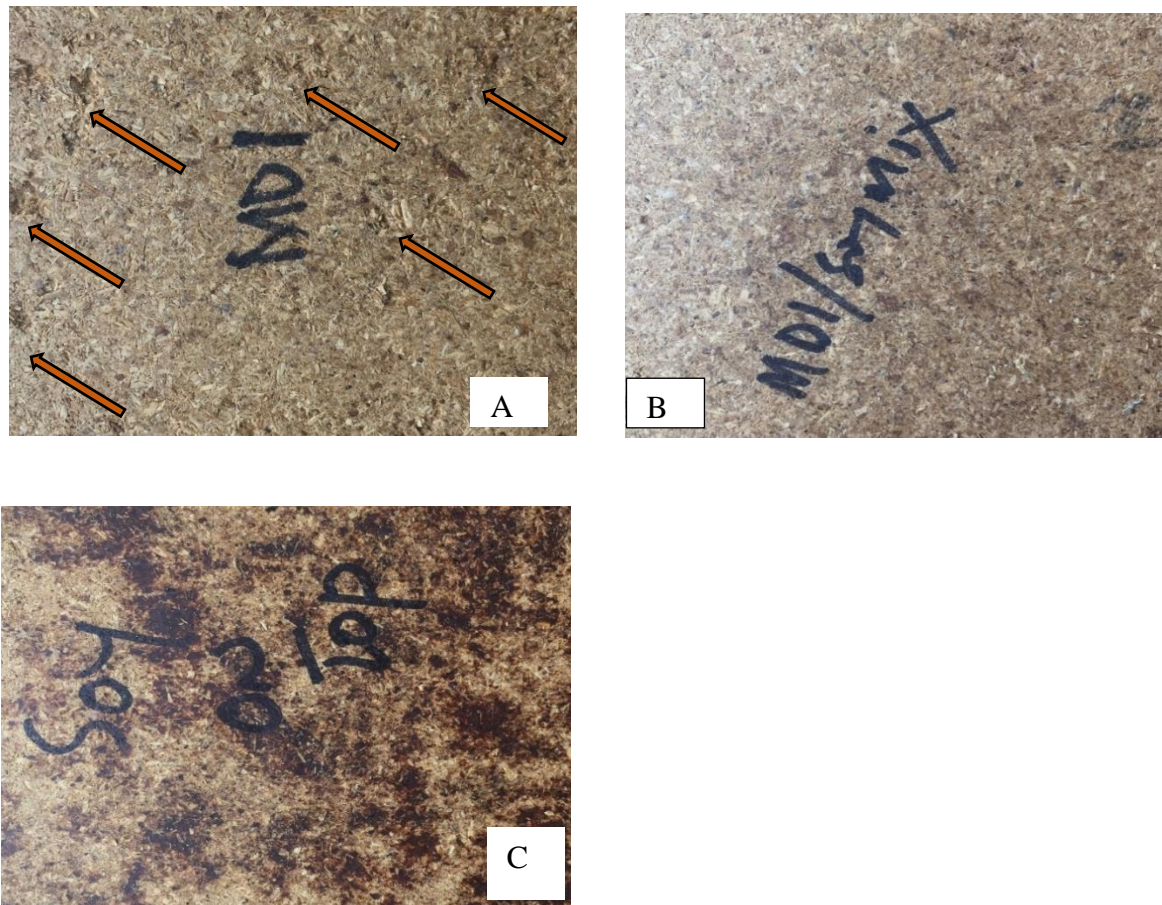


Figure 6.4: Surface appearance of particle boards with MDI (A) only and MDI (either mixed with soy (B) or surface sprinkled with soy (C)).

6.5 Conclusions

The cold tack of pMDI resin increases by partial substitution with soy flour to the same level obtained with UF resins. The increase is caused by the reaction of the isocyanate resin with the water contained in soy flour. Soy flour is much cheaper than PMDI resin and provides the same wet and dry strength properties when substituted in PMDI at or about 15%. For particleboard, the soy-flour provides the added benefit of increased cold tack. Between 15% and 20% substitution level of soy is probably a practical maximum because higher levels could lead to excessive cold tack as well as to higher resin viscosity. The added benefit of cold tack provides a compelling economic and technical justification for its use in engineered wood.

6.6 Acknowledgement

This project was funded by the United Soybean Board.

6.7 References

1. ASTM Designation: D3121-17. 2017. Standard test method for tack of pressure-sensitive adhesives by rolling ball, ASTM International, West Conshohocken, PA.
2. ASTM International. 2012. Standard test methods for evaluating properties of wood-base fiber and particle panel materials. ASTM D1037. ASTM International, West Conshohocken, Pennsylvania.
3. Cheng, Q., Essien, C., Via, B., Banerjee, S. Cost savings from soy flour substitution in MDI resin for bonding flakes and particle, *Forest Prod. J.* in press.
4. Hogger, E. M., H. W. G. van Herwijnen, J. Moser, W. Kantner and J. Konnerth. 2018. Cold tack of urea formaldehyde resins as an important factor in plywood production. *Eur. J. Wood Prod.* 76:1391-1398.
5. Solt, P., J. Konnerth, W. Gindl-Altmutter, W. Kantner, J. Moser, J. Mitter, and H. W. G. Herwijnen. 2019. Technological performance of formaldehyde-free adhesive alternatives for particleboard industry, *Int. J. Adhes. Adhes.* 94, 99-131.
6. Moriarty, C. J., 2017. Method of applying a binder composition to a lignocellulosic substrate, US patent 9,771,460.
7. Moriarty, C. J. 2017. Method of adjusting the tack value of a binder composition, US patent 981, 6007.
8. Solt, P., Konnerth, J., Gindl-Altmutter, W., Kantner W., Moser, J., Mitter, J., van Herwijnen, H. W. G. 2019. Technological performance of formaldehyde-free adhesive alternatives for particleboard industry, *Int. J. Adhes. Adhes.* 94, 99-131.
9. Via, B., Hand, W., Banerjee, S. 2019. Use of soy flour in resin formulations used to manufacture engineered wood composites, US patent 10,266,694.
10. Zhang, C. L. Yu, F. Ferdosian, S. Vijayaraghavan, J. Mesnager, V. Jollet and B. Zhao. 2018. *Ind. Eng. Chem. Res.* 57, 16318–16326.
11. Zosel, A. 1985. Adhesion and tack of polymers: Influence of mechanical properties and surfacetensions, *Colloid Polym. Sci.* 263, 541–553.

Chapter 7

Soy Flour Substitution in pMDI Resin for Composite Panel Applications

7.1 Abstract

Partial substitution of pMDI resin by 10-15% soy flour for the manufacture of strand boards, improves board properties while decreasing cost. For MDF the soy-substituted resin performs as well as the control pMDI. The reaction of soy flour with pMDI occurs over several hours as tracked by CO₂ evolution. The soy-amended resin must be used within about thirty minutes of formulation. Uniform mixing of soy flour with pMDI is critical because unreacted soy flour tends to retain water, which degrades the wet properties of the board. The soy flour increases the tack of pMDI resin, which increases the surface coverage and the relative bonded area at the glue line.

7.2 Introduction

In previous work, partial substitution of soy flour in pMDI resin for the manufacture of strand board and particleboard improves cost-benefits without deteriorating board properties. These properties have a strong dependence of how the soy flour and pMDI are mixed and applied. At room temperature, the soy flour raises resin viscosity to the point where it impedes spraying. This increase does not occur if the mixture is prepared at 40 °C (Via et al. 2019,) Also, soy flour increases the cold tack of pMDI, which is especially useful for particleboard where the mats tend to disintegrate while being conveyed to the press (Asafu-Adjaye et al. 2020). The interaction of soy flour and pMDI resin at press temperatures have been detailed (Hand et al. 2018). This paper examines the mechanism of interaction of soy flour with MDI resin and illustrate the effect of uniform mixing of resin and soy flour on board properties. We also identify situations where partial soy flour substitution improves product performance.

7.3 Materials and Methods

Defatted soy flour was provided by Archer Daniels Midland (Chicago, IL); its dry-basis moisture content was 6.2%. The pMDI resin was MONDUR 541 from Covestro. Screened wood strands (moisture content: 7-8%) were donated by J.M. Huber, Louisiana-Pacific and Norbord Corporations. Fiber for MDF boards was obtained at a moisture content of 9% from Kronospan. Emulsified wax (Hexion Bord'N-Seal FMH-XD) was obtained from Huber Corp.

7.3.1 Methods

Wax was first sprayed on the wood stands at a loading of 1% for flakeboard and 0.2% for MDF. MDI or mixtures of MDI and soy flour were then sprayed on the furnish with a paint sprayer powered by an air compressor. The strand board and MDF was made with a resin load of 3% of wood weight. The resin was applied to both face and core layers. Mats were formed in a 43 x 43 cm frame without orientation and then hot pressed for 3 minutes at 213 °C and 2 MPa. The nominal thickness of the board was 1.1 cm. The target density was 641 kg/m³ (40 lbs/ft³), and 650 kg/m³ (41 lbs/ft³) for strand board and MDF, respectively.

For MDF, there was a challenge of blending the resin with the fiber. In industry the resin is added at the blow line, a procedure that is not possible to easily reproduce in the lab. These difficulties were resolved by using a cement mixer-like blender with the orifice covered with clear plastic. A 3-cm diameter hole was cut out from the center of the plastic to accommodate the spraying gun. Aggregated fibers were dispersed by hand and mat-forming procedure was similar to the strand boards (Figure 7.1). Internal bond (IB), water absorption (WA) and thickness swell (TS) were measured according to ASTM D1037-12 (2012).



Figure 7.1: 1 Medium density fiber board mat (A); hot press with MDF mat (B); trimmed MDF panels (C); Tested specimen for MOR and MOE (wet from left (dark colored) and dry) (D).

The moisture cycle test for bonding performance (single cycle or D4 test), was run according to APA PS2 (2004). Specimens (152 x 152 mm) were soaked in 66 °C water under about 506 mbar. The vacuum was released after 30 mins and the samples were kept soaked at atmospheric pressure for an additional 30 minutes. They were then dried at 80°C for 15 hours. Internal bond (IB), water absorption (WA) and thickness swell (TS) were measured according to ASTM D1037-12 (2012).

CO₂ measurements were made with a Neulog NUL-260 instrument (Figure 6.2). Mixtures of MDI (30 g) and either soy flour (3 g) or water (190 μ l) were stirred at a Reynolds number of about 47 and the headspace CO₂ measured. The amount of water added was equivalent to the water contained in 3 g of soy flour. The stirring speed \sim 1000 rpm was kept constant across all the measurements.



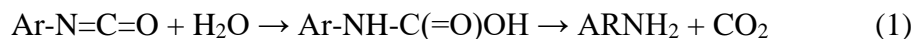
Figure 7.2: CO₂ measurement set up with a thermometer and CO₂ sensor housed in the cover.

The contact angle was measured on a metal coupon with the sessile drop method using Dataphysics Optical Contact Angle Measuring and Contour Analysis System (OCA-50) equipped with a 6.5-fold zoom lens. Measurements were taken after 30 seconds of application.

7.4 Results and Discussion

7.4.1 Mixing Soy Flour and MDI resin: CO₂ evolution

PMDI resin can react with the water contained in soy flour and/or with functional groups in components of the flour. The reaction of PMDI with water proceeds, according to eq. (1) (Yakabe 1999).



PMDI and water do not mix well; they tend to form two layers, and the rate of reaction is partly governed by physical processes such as mixing efficiency. Allport et al. (2003) have reported that the half-life for the reaction of water and pMDI is less than two hours, although this value is very approximate. Because the reaction of pMDI with either water or soy flour releases CO₂, the measurement of CO₂ evolution over time can provide insight into the reaction.

CO₂ emission profiles measured under various conditions are illustrated in Figure 7.3. The “water only” curve corresponds to the amount of water contained in the two “soy” curves. The maximum CO₂ that would be evolved if all the water were to react with pMDI is 8,150 ppm over and above the baseline value of 360 ppm. The terminal value for the “water only” curve in Figure 7.3 is 2,800 ppm, which represents 31% conversion. Hence, the reaction should continue slowly for several hours. However, water is not the only source of the CO₂. The “dry soy” curve where bone-dry soy flour was mixed with pMDI also reflects appreciable CO₂ release. Also, some of the CO₂ was trapped as bubbles or dissolved in the resin and was released slowly.

The rates of all the processes in Figure 7.3 are quite similar. Their interpretation is difficult because CO₂ evolution depends on both the pMDI reaction rate and the rate of CO₂ release from the resin. The CO₂ values are higher at 40 °C than at 22 °C because the reaction should be faster at 40 °C,

and also because the viscosity of pMDI is almost three times lower at 40 °C than at 22 °C (Cheng et al. 2019). The lower viscosity at 40 °C facilitates the escape of CO₂ bubbles trapped in the resin. The rate for “dry soy” is higher than that for “water only” which implies that the functional groups in soy flour react faster than does water. He et al. (2005) reported the opposite situation for PMDI reaction with wood of varying moisture content. They found the rate to double from going from dry wood to 7% MC wood. However, the water in wet wood is bound to water at these low levels, which is different from our case where the water added to MDI is free water. Nevertheless, both studies indicate that the reaction rate of pMDI with water or soy flour is quite similar.

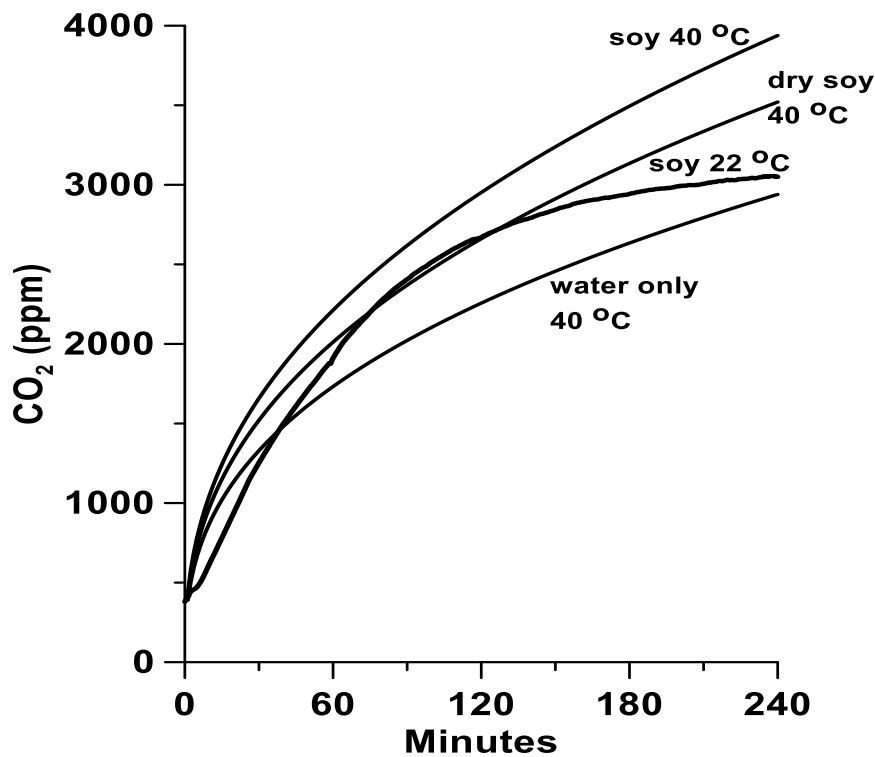


Figure 7.3: CO₂ evolution from the reaction of MDI resin with soy flour or water.

This results seemingly conflict with those of Yakabe et al. (1999) who found the reaction of MDI with water to take several hours. However, Yakabe et al. (1999) noted that the reaction was mass transfer limited because the two liquids are effectively immiscible. In our measurements water was stirred into excess MDI, where mass transfer limitations would be less severe. The practical aspect of our findings is that gas is evolved for an extended period from soy/MDI mixtures. The viscosity increases as a result so the mixture must be used within about 30 minutes at 40° C before spraying is impeded. However, this issue may be moot if inline mixers are utilized (Thakur *et al.* 2003).

7.4.2 Strand Board Applications

Previous work, our lab noted that wet properties degraded when soy flour substitution exceeded 10%. The average edge swell increased, but this was caused by high values in a small subset of the samples; most of the samples were unaffected by the soy (Cheng et al. 2019). This would be the outcome if the soy flour was not fully dispersed; small clumps of soy flour present in just a few samples would tend to attract moisture. It follows that more uniform mixing should reduce edge swell. Two modes of blending were used to evaluate the importance of uniform mixing: stirring soy flour into pMDI by (a) hand with a glass rod, and (b) with a blender with a whip fixture at 2000 ± 200 rpm. About 0.3-0.5 g of the soy powder was added at a time to the pMDI over 5 minutes.

Results from D4 tests are presented in Table 7.1. Blender mixing gives better results than hand mixing ($p < 0.05$), and all the soy values are low than those of the control pMDI. Strength properties (both dry and wet) are illustrated in Figure 7.4. While the dry properties are relatively unaffected by the mode of mixing, there is a clear improvement in wet strength. For MOE and MOR the values from the blended soy resin are better than those from pMDI alone. These results have been confirmed in industrial pilots.

Table 7.1: Edge swell results of MDI and substituted with 12% and 15% soy flour with different blending techniques

OSB Sample	Edge Swell
pMDI	50 ± 6
12% soy hand	43 ± 3
12% soy blender	35 ± 2
15% soy hand	33 ± 4
15% soy blender	30 ± 2

¹n=6

An operational concern with the use of soy is its potential effect onboard quality if the production line goes down and the resinated flakes need to be stored prior to pressing. The effect of storage was measured by resonating the flakes and pressing immediately and after a delay of 6 hours. The results are provided in Table 7.2. As expected, the properties of the control boards (pMDI only) degrade upon storage, but surprisingly, the properties of the soy-treated boards are, for the most part, better than those of the pMDI controls.

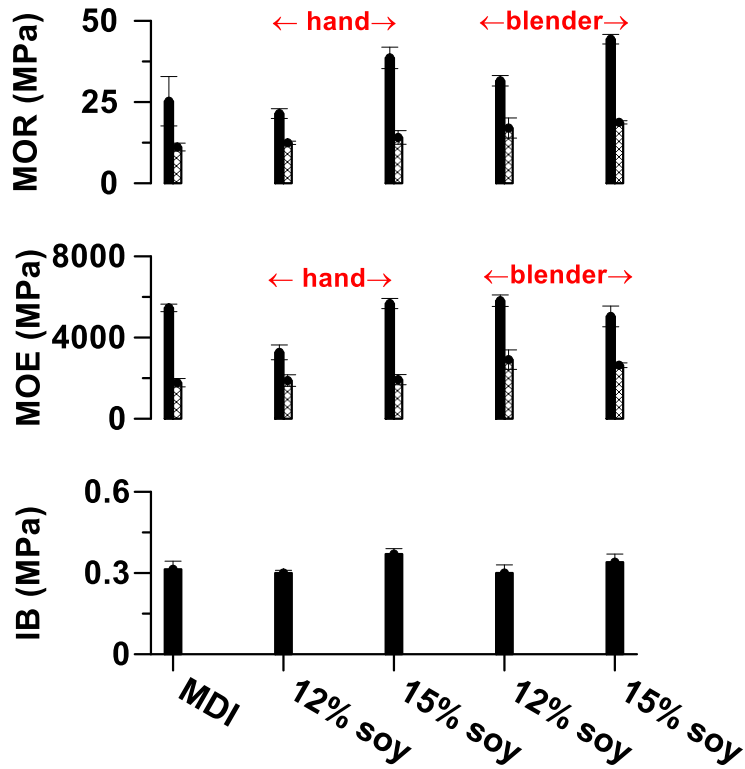


Figure 7.4: Effect of soy substitution on strand board properties. The hatched bars represent wet properties; n=8.

Table 7.2: Properties of boards made from flakes prepared immediately after resination and after 3 and 6 hours.

	TS ² Inner (%)	TS ² Edge (%)	WA ³ Inner (%)	Dry MOE (MPa)	Wet MOE (MPa)	Dry MOR (MPa)	Wet MOR (MPa)	IB (MPa)
Control-0 hrs.	15 ± 1	21.2 ± 0.4	30 ± 7	5400 ± 900	1500 ± 60	40 ± 5	15 ± 2	0.77 ± 0.03
Soy-0 hrs.	14 ± 1	20 ± 1	22 ± 1	6200 ± 700	1550 ± 50	43 ± 5	16 ± 1	0.9 ± 0.1
Control-3 hrs.	11 ± 2	17 ± 1	22 ± 4	7400 ± 900	1900 ± 300	53 ± 9	19 ± 2	0.8 ± 0.1
Soy-3 hrs.	13 ± 1	19 ± 1	22 ± 3	6500 ± 300	1960 ± 60	45 ± 3	21 ± 2	0.9 ± 0.2
Control-6 hrs.	17 ± 2	20 ± 2	30 ± 1	3000 ± 100	1000 ± 100	24 ± 3	12 ± 1	0.6 ± 0.1
Soy-6 hrs.	13 ± 1	21 ± 2	23 ± 3	3300 ± 200	1120 ± 60	27 ± 2	12 ± 1	0.7 ± 0.1

¹3% resin loading, 10% soy flour substitution, n=6 ²thickness swell; ³water absorption

7.4.3 Soy Flour in MDF Application

Boards were prepared with various resin formulations and tested for various strength properties. The results from two separate runs (a and b) are shown in Figure 7.5. The properties of boards from run (b) are better than those from run (a) because of the higher density used in the run (b). The properties of the soy-treated and control (MDI) boards are broadly equivalent. There appears to be a trend for the soy flour to slightly improve dry properties while degrading wet properties to a small extent, but these differences are in the neighborhood of the 1σ uncertainty.

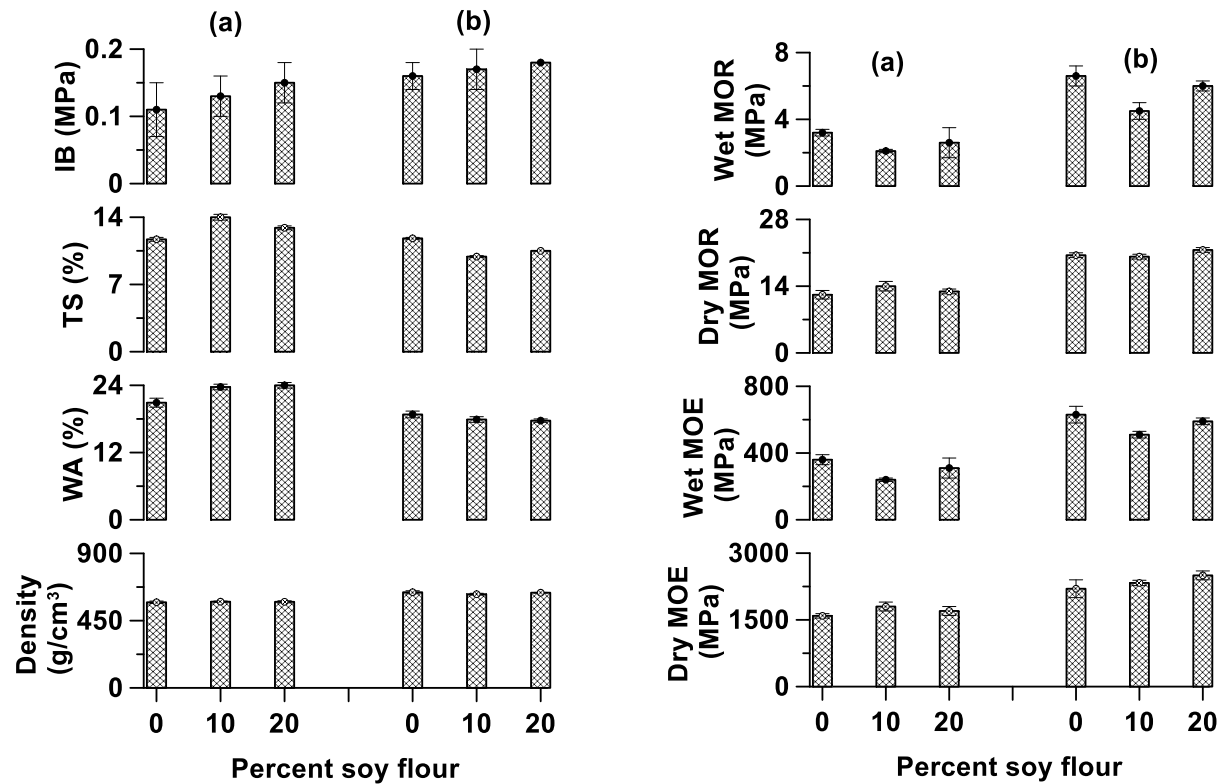


Figure 7.5: Effect of soy substitution on MDF properties at two different densities; n=8.

7.4.4 Mechanism

The effect of soy flour substitution on strand board and MDF are similar in that the wet and dry properties either improve or remain unchanged. Kowalski et al. (2013) have noted that an effective adhesive immediately wets a surface upon contact. Wetting increases surface coverage and

promotes surface penetration, which fills in microscopic surface irregularities. Tack is defined as the adhesive failure energy of adhesive joints formed with low contact pressure during a short contact time (Zosel 1985). It is likely that the higher tack of the soy-amended resin improves resin spread at the bond line, thereby increasing the interfacial contact area. The contact angle measurements support this position. The contact angle of pMDI on a metal surface is 42.5°; the corresponding value for the soy-amended MDI lower at 32.6°. Thus, a single mechanism is proposed for increasing the pre-press stability of particle mats and for strength enhancement in OSB panels.

7.5 Conclusions

The wet and dry properties for 10-15% soy flour substituted boards are equivalent or superior to those of control (pMDI only) boards for both strand board, and MDF. Mixing is central to the overall panel properties, hence homogenized well-dispersed soy in PMDI should be considered a primary manufacturing target. The 15% substitution level is probably a practical maximum because higher levels could lead to excessive cold tack as well as to higher resin viscosity. The higher tack of the soy-treated resin likely increases the relative bonded area at the glue line.

7.6 Acknowledgment

This project was funded by the United Soybean Board.

7.7 References

1. Allport, D. C., D. S. Gilbert and S. M. Outterside. 2003. MDI and TDI: Safety, Health and the Environment: A Source Book and practical guide. p.240,
2. Asafu-Adjaye, O., B. Via and S. Banerjee. 2020. Increasing cold tack of pMDI resin with partial soy flour substitution, *Forest Prod. J.*, in press.
3. ASTM D1037 – 12. 2012. Standard test methods for evaluating the properties of wood-base fiber and particle panel materials.
4. Hand, W. G., W. R. Ashurst, B. Via, and S. Banerjee 2018. Mechanism of interaction of soy flour with phenol-formaldehyde and isocyanate resins. *Int. J. Adhes. Adhes.* 87:105-108.
5. He, G. and N. Yan, 2005. *Int. J. Adhes. Adhes.* Effect of moisture content on curing kinetics of pMDI resin and wood mixtures. 25, 450–455.
6. Hogger, E. M., H. W. G. van Herwijnen, J. Moser, W. Kantner and J. Konnerth. 2018. Cold tack of urea formaldehyde resins as an important factor in plywood production. *Eur. J. Wood Prod.* 76:1391-1398.
7. Kowalski, A., Z. Czech and L. Byczyński, 2013. How does the surface free energy influence the tack of acrylic pressure-sensitive adhesives (PSAs) *J. Coat. Technol. Res.* 10: 879–885.
8. Moriarty, C. J. 2017. Method of applying a binder composition to a lignocellulosic substrate, US patent 9,771,460.
9. Moriarty, C. J. 2017. Method of adjusting the tack value of a binder composition, US patent 981,6007.

10. Solt, P., J. Konnerth, W. Gindl-Altmutter, W. Kantner, J. Moser, J. Mitter, and H. W. G. Herwijnen. 2019. Technological performance of formaldehyde-free adhesive alternatives for particleboard industry, *Int. J. Adhes. Adhes.* 94, 99-131.
11. Thakur, R. K., Ch. Vial, K. D. P. Nigam, E. B. Nauman and G. Djelveh. 2003. Static mixers in the process industries-a review, *Trans IChemE, Vol 81, Part A*, 787-827.
12. Via, B., W. Hand, and S. Banerjee, S. 2019. Use of soy flour in resin formulations used to manufacture engineered wood composites, US patent 10,266,694.
13. C. Zhang, L. Yu, F. Ferdosian, S. Vijayaraghavan, J. Mesnager, V. Jollet and B. Zhao. 2018. *Ind. Eng. Chem. Res.* 57, 16318–16326.
14. Weaver F. W. and N. L. Owen. 1995. Isocyanate-wood adhesive bond, *Appl. Spectrosc.* 48, 171-176.
15. Yakabe, Y., K. M. Henderson, W. C. Thompson, D. Pemberton, B. Tury and R. E. Bailey. 1999. Fate of methylenediphenyl diisocyanate and toluene diisocyanate in the aquatic environment, *Environ. Sci. Technol.* 33, 2579-2583.
16. Zosel, A. 1985. Adhesion and tack of polymers: Influence of mechanical properties and surface tensions, *Colloid Polym. Sci.* 263, 541–553.

Chapter 8

General Conclusions and Recommendations

8.1 General Conclusions

The first section of this dissertation discussed the properties of bio-oil as an adhesive feedstock. The effect of fast pyrolysis (FP) and hydrothermal liquefaction (HTL) on the quality of bio-oil was investigated to enhance the utilization of bio-oil in epoxy resin formulation and PMDI modification. Consequently, partially substituted epoxy resin with bio-oils, and PMDI amended bio-oils were used to produce wood composites such as oriented strand boards. Although research has been performed on bio-oil and epoxy substitution with various formulations and curing agents, there was no published work on the performance of epoxy resin substituted bio-oil, and epoxy resin in comminuted wood composites like OSB. Major findings from this section are summarized as follows:

- FP process, and HTL in water/ethanol process from the same loblolly biomass was studied for the first time employing GC-MS (volatile chemical compounds present <300 °C), FTIR (chemical functional groups), TGA (volatile chemical decomposition), ³¹P-NMR (hydroxyl number distribution) to understand the physical and chemical effect on the resultant bio-oil produced.
- The physical properties analyzed revealed that HTL process utilizing water/ethanol at subcritical conditions resulted in bio-oil yield of about 67% while the FP bio-oil was about 35%. Improved bio-oil yield was attributed to the hydrogen donation capability of ethanol which stabilizes the free radicals generated during HTL.

- FTIR and GC-MS analysis suggested that the FP and HTL bio-oils have similar chemical functional groups but different chemical composition. Esterified chemical compounds characterized the HTL bio-oil. FP bio-oil had a substantial amount of phenols and phenolic derivatives.
- High concentration of aliphatic and phenolic OH moieties was demonstrated via quantitative ^{31}P -NMR from the FP and HTL bio-oils. FP bio-oil OHN was 10.3 mmol/g and that of HTL was estimated to be 9.25mmol/g. The seemingly low OHN of the HTL was attributed to the consumption of OH groups in the esterification reaction.
- FP bio-oil substituted in epoxy resin (EPON 828) was cured in-situ wood strands to manufacture oriented strand board (OSB). The mechanical properties (MOE, MOR and IB) and physical properties (thickness swell (TS) and water absorption (WA)) of the panels decreased with higher bio-oil substitution. TS and WA increased by 68% and 75% for epoxy substituted bio-oil from 20% to 50%, respectively. This was ascribed to the rupture of hydrogen bonds formed between the polar functional groups in pyrolysis bio-oil like hydroxyls ($-\text{OH}$) and aldehydes ($-\text{COOH}$) with the $-\text{OH}$ groups in wood.
- 20% bio-oil replacement level revealed improved mechanical properties and hydrophobicity of the OSB panels in contrast to the epoxy resin only.
- FT-IR analysis showed that OH groups and carbonyl groups in bio-oil opened the epoxide ring in epoxy resin and created crosslinked structure. The crosslinked structure of bio-oil cured epoxy resin system was confirmed by DSC analysis used to calculate the Tg. The Tg was 57 °C and 74.5 °C respectively, for epoxy resin unmodified and 20% bio-oil substituted epoxy.

- TGA analysis of the epoxy substituted bio-oil resins showed increased thermal stability at low levels of bio-oil substitution (i.e., 20% bio-oil substitution level was stable up to 276 °C).
- Bio-oil cured epoxy resins presented only 5.7 wt.% mass loss when extracted with acetone for 64 hours, which indicated that the resulting bio-oil-epoxy based resin had a superior chemical resistance.
- 30% bio-oil amended epoxy resin system was suggested to be practical optimum to achieve acceptable mechanical and physical properties of OSB panel production

The second section of the dissertation's overall objective was to advance the understanding of resultant wood composite panels produced from blending defatted soy flour and PMDI. Though research has been performed on soy and their substitution into PMDI as a wood adhesive, limited published work existed involving utilizing whole defatted soy flour without chemical pre-modifications substituted into PMDI in the production of oriented strand board (OSB), particle board and medium density fiber board (MDF). Understanding of the blending mechanism and the production process of OSB could be leveraged to meet the technological and engineering challenges related to the integration of soy/PMDI resin system in the wood composite industry. Apart from this bio-based adhesive been cost-effective, additional benefits of soy amended PMDI were explored to make the resin system more competitive to PDMI alone. Consequently, the following findings were concluded from the dissertation:

- PMDI be heated to 40 °C before soy flour is substituted to avoid flour aggregation and promote good dispersion. Constant stirring eliminated frothing.

- The cold tack of soy amended PMDI was accessed to benefit pre-mat stability in particle board production as PMDI alone has limited tack limiting its utilization in particle board production. Soy amended PMDI showed increased cold tack at higher soy flour replacement levels. The tack achieved with the soy/PMDI was about equal for the UF- and 10%-soy/PMDI resin system. The increase in tack was attributed to the reaction of water and OH groups in the soy flour.
- Particle boards produced with the soy/PMDI resin system exhibited similar wet mechanical and physical properties with no statistically significant difference. Excessive tack may result from high soy substitution levels and could limit adhesive spread; hence the slightly increased in edge swell of the 20% soy amended PMDI.
- The soy amended PMDI resin system had an additional benefit of decreasing the attraction of MDI to aluminum platens. This is very significant as PMDI stick to press plated and releasing agents are employed to expedite production. Soy amended PMDI could reduce the total amount of releasing agents used in the composite panel production.
- Blending mechanism of soy substituted PMDI studied with effervescing of CO₂ revealed that, PMDI reacts with water contained in soy flour and/or with functional groups in components of the flour. This was verified when the bone dried soy flour released appreciable CO₂. CO₂ values were higher at 40 °C than at 22 °C because the reaction was faster at 40 °C, and also because the viscosity of PMDI was low. For effective mixing, the PMDI should be heated be at 40 °C first before mixing the soy and the soy/PMDI mix should be applied with thirty minutes of mixing.

- Small clumps of soy flour present in soy/PMDI mix will cause increased edge swell, TS and WA as the soy will retain water. Mixing of soy powder should be added at a time to the PMDI to achieve a homogenized uniform mixture. The blender mix at ~2000 rpm gave a better strand board mechanical and physical properties relative to the hand rod mixing.
- The effect of soy flour substitution on strand board and MDF were similar relative to the PMDI only in that the wet and dry properties either improve or remain unchanged. This was likely due to the higher tack of the soy-amended resin which improved the resin spread at the bond line, thereby increasing the interfacial contact area. The contact angle measurements supported this position.
- The contact angle of pMDI on a metal surface was 42.5°; the corresponding value for the soy-amended MDI was lower at 32.6°. Thus, a single mechanism was proposed for increasing the pre-press stability of particle mats and for strength enhancement in OSB panels.
- The 15% substitution level is probably a practical maximum because higher levels could lead to excessive cold tack as well as to higher resin viscosity.
- The moisture cycle test reveals that soy amended PMDI as resin produced a durable bond with wood strands.

8.1.1 Future Work

- Bio-deterioration and biodegradability are very central to the service life of many wood composites, especially when the panels are used as either a construction material or as a

packaging. Insects like termites and wood decay fungi affinity to composites made with bio-oil based epoxy resin could limit the acceptability of such panels.

- It is recommended that the 6 moisture-vacuum soak cycle test recommendations of Performance Standard for wood base structural use (PS-2 -10, 2011) be conducted to assess the bio-oil based epoxy resin adhesive bond durability.
- Apart from OSB, different wood composites like plywood could be explored where high bio-oil substitution levels will yield competitive mechanical and physical properties.
- A comprehensive cost-benefit analysis of bio-based epoxy resins is critical and could be investigated. Cost performance analysis would provide an insight into the future of bio-based epoxy resins.
- It is recommended to investigate the rheological properties of soy amended pMDI and soy flour adhesives to characterize the behavior of the wood/resin interface.
- It is also recommended that the soy amended PMDI bond line in wood composite be investigated using microscopy analysis.

8.2 Appendix A

GC-MS Analysis

Table S1. GC-MS Analysis of Hydrothermal liquefaction bio-oil (HTL)

RT	% Peak	Phenols & Phenol Derivatives
12.06	1.000943	Phenol
12.25	2.19633	Phenol, 2-methoxy-
13.43	0.856751	Phenol, 4-methyl-
13.91	0.730954	Phenol, 2-methoxy-4-methyl-
14.98	0.717065	2H-1-Benzothiopyran, octahydro-, trans-
15.14	0.682765	Phenol, 4-ethyl-2-methoxy-
15.61	0.709284	1-Phenyl-1-heptyne
15.91	0.33338	3-Amino-4-methoxybenzamide
16.34	0.96016	Phenol, 2-methoxy-4-propyl-
17.14	1.107595	Phenol, 2-methoxy-4-(1-propenyl)-
17.37	2.02417	Phenol, 2-methoxy-4-(1-propenyl)-, (E)-
17.83	0.764034	Benzenemethanol, 3-fluoro-
18.30	2.279731	Vanillin
18.82	0.861616	1,4-Benzenediol, 2-methyl-
18.99	0.751206	Phenol, 2-methoxy-4-propyl-
19.16	0.440079	Ethanethioamide, N-phenyl-
19.40	0.745238	Benzenamine, 2,4-dichloro-
19.52	0.437084	Allenyl o-nitrophenyl sulfide
19.78	0.71996	2,4-Dimethoxybenzylamine
19.90	0.996468	Homovanillyl alcohol
20.04	1.085992	1,1'-Biphenyl, 4-nitro-
20.25	0.371865	3,7-Benzofurandiol, 2,3-dihydro-2,2-dimethyl-
20.66	0.877579	Phenylacetylformic acid, 4-hydroxy-3-methoxy-
21.51	1.052246	Ethyl 3,4-dihydroxybenzoate
23.29	0.628988	(1,1,2-Trichloro-3-ethylallyl)benzene
25.40	0.367291	1-Benzyl-4-methyl-3,6[1H,2H]-pyridazinedione
26.14	0.560382	Trichloroacetic acid, phenyl ester
27.11	0.310	8-Chloro-5-quinolinecarboxylic acid
27.84	0.517423	p-Dimethylaminobenzylidene p-phenetidine
28.74	0.396213	2(3H)-Furanone, 4,5-dihydro-5-bromo-3-methyl-4-(phenylthio)-
29.74	0.347794	3,7-Dihydroxy-3-phenyl-4-chromanone
30.35	0.468496	1,4-Cyclohexandione-2-[(3,4-methylenedioxy)phenyl]propionic acid
26.29922		

RT	% Peak	Esters
6.45	7.01	Acetic acid, hydroxy-, ethyl ester
6.69	5.66	Propanoic acid, 2-hydroxy-, ethyl ester
8.22	2.39	Butanoic acid, 2-hydroxy-, ethyl ester, (./-.)-
10.79	2.26	Formic acid, 1-methylpropyl ester
11.74	2.59	Pentanoic acid, 4-oxo-, ethyl ester
13.17	1.16	Butanedioic acid, diethyl ester
13.58	0.34	Hexanoic acid, 5-oxo-, ethyl ester
11.74	0.80	Tetradecanoic acid, ethyl ester
22.55	1.57	Hexadecanoic acid, ethyl ester
24.51	0.72	Octadecanoic acid, ethyl ester
24.51		

RT	% Peak	Ketone
4.84	1.818	2-Propanone, 1-hydroxy-
8.77	0.941	2-Cyclopenten-1-one, 2-methyl-
9.85	1.447	2,5-Hexanedione
10.56	0.571	2-Cyclopenten-1-one, 3-methyl-
13.02	0.903	2-Cyclopenten-1-one, 3-ethyl-2-hydroxy-
14.35	0.548	2-Hydroxy-3-propyl-2-cyclopenten-1-one
15.37	0.384	11-Oxadispiro[4.0.4.1]undecan-1-one
15.77	0.982	2-Cyclohexen-1-one, 4-(1-methylethyl)-
17.00	0.549	2-Cyclohexen-1-one, 6-methyl-3(1-methylethyl)-
8.142		

RT	% Peak	Acid
4.51	1.586	Acetic acid
24.42	1.175	Ethyl Oleate
2.761		

RT	% Peak	Aldehydes
18.68	0.263	Acetaldehyde, (3,3-dimethylcyclohexylidene)-, (E)-
23.10	0.633	4-Hydroxy-2-methoxycinnamaldehyde
0.896		

RT	% Peak	Furans
7.73	1.235	Furfural
10.25	1.112	2-Furancarboxaldehyde, 5-methyl-
11.25	0.536	2-Furancarboxylic acid, ethyl ester
11.64	2.760	Furazan-3-carboxamide, 4-amino-N-(2-tetrahydrofurfuryl)-
16.64	2.819	2-Furancarboxaldehyde, 5-(hydroxymethyl)-
8.463		
RT	% Peak	Others
3.33	2.036342	Ethylidenecyclobutane
6.93	0.524228	2-Propanol, 1-ethoxy-
7.15	0.301032	Ethane, 1-isothiocyanato-2-methoxy-
8.06	2.05067	2-Butanol, 3-methyl-
9.37	0.395024	Silane, triethyl-
12.78	0.579486	Hexane, 1,1-diethoxy-
14.55	0.361391	7-Methylxanthopteridine
14.70	1.876136	2-Acetyl-3-methylthiophene
17.63	0.64247	Tricyclo[4.2.1.1(2,5)]decan-9-one oxime
21.40	0.455002	1,2-Ethanediamine, N,N,N'-trimethyl-N'-(1,2,3,4-tetrahydro-2-naphthalenyl)-
24.78	0.412645	[2-Aminoethylamine]-N-carbothioic acid, 2-[1-[2-pyridyl]ethylidene]
25.19	0.424158	Chrysene, 1,2,3,4,4a,7,8,9,10,11,12,12a-dodecahydro-1-Oxa-2-sila-5-boracyclopent-3-ene, 4,5-diethyl-2,2-dimethyl-3-(1-methylethenyl)-
26.34	0.25497	
10.31355		

8.3 Appendix B

Table S1. GC-MS Analysis of Fast Pyrolysis bio-oil (HTL)

R.T	Area%	Phenols
11.94	1.110129	Phenol
12.25	2.476085	Phenol, 2-methoxy-
13.276	0.891825	Phenol, 4-methyl-
13.876	2.535085	2-Methoxy-5-methylphenol
14.896	0.758864	Benzaldehyde, 2-hydroxy-5-methoxy-
15.136	0.656472	Phenol, 4-ethyl-2-methoxy-
15.491	0.667786	Durohydroquinone
15.575	1.052508	3-Ethoxy-4-methoxybenzaldehyde
15.779	0.922575	1,4-Dimethoxy-2,3-dimethylbenzene
16.0127	0.755	Benzeneacetaldehyde, 2-methoxy-
16.337	1.40235	Phenol, 2-methoxy-4-(1-propenyl)-, (Z)-
16.664	1.473031	2,5-Dimethoxyethylbenzene
17.85	1.907463	Phenol, 2-methoxy-4-(1-propenyl)-, (E)-
17.708	0.591132	2-Benzothiazolamine, 4-methoxy-
18.308	2.161355	Vanillin
19.133	0.319179	(E)-Stilbene
19.354	1.351806	Ethanone, 1-(3-hydroxy-4-methoxyphenyl)-
19.716	1.366539	2,4-Dimethoxybenzylamine
19.909	1.221825	Propan-2-one, 1-(4-isopropoxy-3-methoxyphenyl)-
20.5	0.485745	Phenol, 4-(3-hydroxy-1-propenyl)-2-methoxy-
20.631	0.354287	Benzonitrile, 2-chloro-6-methyl-
20.788	0.499405	Benzenamine, 2-fluoro-5-(5-tetrazolyl)-
20.903	0.320946	Benzaldehyde, 4-[(trimethylsilyl)oxy]-
22.293	0.806702	Eugenol
22.667	2.386471	Silane, trimethyl(3-phenoxypropoxy)-
22.72	0.598898	2,3-Dimethoxybenzyl isothiocyanate
23.099	1.045489	4-Hydroxy-2-methoxycinnamaldehyde
23.372	0.448908	Tricyclo[4.2.1.0(2,5)]nona-3,7-diene, 9-methoxy-1-phenyl-
23.773	0.967387	Phenanthrene, 9,10-dihydro-1-methyl-
26.148	0.640674	1,3-Pentadiene, 1,1-diphenyl-, (Z)-
27.373	0.265465	(E)-2-Hydroxy-4'-dimethylamino-stilbene
28.756	0.495771	Benzaldehyde, 3-(4-fluorobenzyloxy)-4-methoxy-
32.93716		

R.T	Area%	Ketones
-----	-------	---------

4.812	4.630877	2-Propanone, 1-hydroxy-
8.259	0.289175	2-Cyclopenten-1-one, 2-methyl-
11.097	0.99496	2H-Pyran-2-one, 5,6-dihydro-
11.576	2.787799	2-Cyclopenten-1-one, 2-hydroxy-3-methyl-
12.508	0.331053	2-Cyclopenten-1-one, 3,4,4-trimethyl-
13.624	0.281597	1-Methoxy-3-keto-4-methyl-1,4-pentadiene
13.731	0.323069	4-Cyclopentene-1,3-dione, 4-propyl-
15.278	1.982063	4(1H)-Pteridinone, 5,6,7,8-tetrahydro-6-methyl-
21.908	0.774421	3(2H)-Thiophenone, dihydro-2-methyl-
12.39501		
R.T	Area%	Furans
5.461	0.982744	D-Fructose, 1-O-methyl-
7.731	1.400548	Furfural
10.241	0.431115	2-Furancarboxaldehyde, 5-methyl-
10.738	1.978224	2(5H)-Furanone
9.072	0.411936	Furan, 2-ethyl-5-methyl-
5.204566		
R.T	Area%	Acids
4.344	4.41345	Acetic acid
6.208	0.421622	Propanoic acid
20.114	0.460265	4-Fluorocinnamic acid
22.079	1.097622	Tetradecanoic acid
23.462	0.744113	Butanoic acid, 2-(aminocarbonyl)-2-ethyl-
7.137072		
R.T	Area%	Esters
9.943	0.571598	2-Propenoic acid, 3-(dimethylamino)-, ethyl ester
21.044	1.558417	Hexanoic acid, 3-hydroxy-, ethyl ester
24.402	0.896367	2-Trifluoromethylbenzoic acid, 2-methyl ester
3.026382		
R.T	Area%	Aldehydes
20.364	0.752246	2-Ethoxy-4-anisaldehyde
0.752246		
R.T	Area%	Sugars
21.6	8.975794	1,6-Anhydro-.beta.-D-glucopyranose (levoglucosan)
8.975794		

R.T	Area%	Others
3.343	1.367817	trans-1,4-Hexadiene
5.299	0.372863	2-Hydroxyethyl vinyl sulfide
14.065	4.027004	1,3-Propanediamine, N-methyl-
14.641	0.506526	Silane, 1,3-butadiynyltrimethyl-
18.824	0.747136	5-Acetoacenaphthylene
22.667	2.386471	Silane, trimethyl(3-phenoxypropoxy)-
24.583	0.974356	5-Chloro-2-methylquinoxaline
	10.38217	